Fall 2021

Identification of Structural Signature Responses From Response Time Histories Using B-Spline Impulse Response Techniques

Shadhan Ahmed AL Kharusi

Identification of Structural Signature Responses from Response Time Histories Using B-Spline Impulse Response Techniques

by

Shadhan Ahmed AL Kharusi

Bachelor of Science in Engineering
University of South Carolina 2019

Submitted in Partial Fulfillment of the Requirements

for the Degree of Master of Science in

Civil Engineering

College of Engineering and Computing

University of South Carolina

2021

Accepted by:

Rizos Dimitris, Director of Thesis

Yu Qian, Reader

Robert Mullen, Reader

Tracey L. Weldon, Vice Provost and Dean of the Graduate School

Dedication

To my Parents: your sincere care is beyond limitation.

To my brothers and sisters: your endless support and encouragement is beyond description.

To the mummeries of my brother Abu albayan: your moments and laughs will last forever.

Acknowledgments

I would like to express my sincere gratitude to my advisor and director of the thesis professor Dimitris C. Rizos for funding my project and for his constant guidance and support throughout the duration of my study in University of South Carolina. I would like to thank him for encouraging and giving me the opportunities since I was undergraduate student to involve, engage and participate in the AREMA(American Railway and Maintenance-of-Way Association) and ART groups. His great mentorship and valuable insights helped me to achieve this research objectives. His care, patience, and understanding were the main reason to complete my Master degree. Also, I would like to thank Dr. Yu Qian, Dr. Robert Mullen for being part of the thesis committee and for their guidance, support, and feedback. In addition, I would like to thank Professors Vitzilaios Nikos, and Austin Downey for their help during the course of this work. My appreciation is also extended to my collages Ahmed Al-zubaidi, and Datta Arya for their continues support. Also, I would like to thank Oman Research Council for their financial support. Finally, I would like to thank each and every member in the ART (Advance Railway Technology) group for the support they provide.

Abstract

Structure Health Monitoring (SHM) is an essential practice for ensuring the safety of people and the structures itself. For this purpose, variety of global and local damage detection methods have been used to investigate damages. Global damage detection focus on identifying damage in early stages while local damage detection related to damage location, severity, and prediction of the remaining of the structure. Any damage in structure leads to a change to the properties and characteristics of the dynamic response.

Existing methods uses modal-based and response-based for damage detection. Both have several shortcoming associate with sensitivity of the damage and measurement error, false damage detection, extensive test requirement, and time consuming. In this thesis, B-spline Impulse Response Function (BIRF) algorithm is used for extracting the Dynamic Signature Response (DSR) which represent the current condition of the structure and are independent of the loading. In addition, DSR is used to for prediction of the response for any arbitrary force. Analytical verification through computer simulation is presented followed by a feasibility study of the proposed method and examine by an experimental lab work. Furthermore, the method have been implemented in Drone-based vibration and monitoring and assessment of structure.

Table of Contents

List of Tables

List of Figures

Chapter 1

INTRODUCTION

1.1 Problem Statement

Structures in the built environment deteriorate due to different causes such as ageing, overuse, and extreme events. If the structural degradation process and damage accumulation go unnoticed, structures cease prematurely to serve the purpose they are designed for and become at high risk of catastrophic failures. Loss of functionality with, or without structural collapse, has significant economic, environmental, and societal impacts stemming from loss of property and productivity, disruption of services, personal injuries and even loss of human lives. Implementing robust structural monitoring, inspection, and maintenance protocols prevents premature failures, prolongs structural life and minimizes the impacts. Over the years, a variety of resources, ways, methods, and algorithms, known in a broad sense as Structural Health Monitoring (SHM), have been developed to establish practical, reliable, efficient, and economic ways to detect early-stage changes in the core integrity of structures, to monitor damage progression, and in structural prognostics. Capturing early-stage damage, or the potential for damage development, in HSM poses great challenges and has been the focus of vast research efforts.

1.2 Motivation

Vibration-based SHM methods assume that modal structural parameters change in the presence of damage that directly affects the structural stiffness, mass and damp-

ing. Vibration-based methods typically employ analytical modeling techniques and computer simulations along with vibration measurements. Typical shortcomings of existing techniques reported in the literature include one or more of the following: the need for extensive instrumentation and testing resources, techniques are computationally intensive and expensive, insensitivity of modal parameters to damage, and damage masked by noise, among others. Current research focuses on the alleviating the shortcomings and improving the reliability of the SHM techniques. On the other hand, less attention is given to the use of Impulse Response Techniques in SHM. An Impulse Response Function (IRF) is regarded as a characteristic response of the structure that depends on the physical structural parameters, i.e., stiffness mass damping and boundary conditions, and not the external loading. The research hypothesis is that the IRF is altered in the presence of structural damage, and thus, damage can be identified through IRF change detection. A special case of an Impulse Response Function is the B-Spline Impulse Response Function (BIRF) that was first introduced within a Boundary Element Method framework as a fundamental solution in elastodynamics [37][35], and subsequently used in Soil-Structure Interaction analysis [34][36][33][47], dynamic interaction of deformable bodies [29] [12], and railroad track dynamics and train track interaction [24][12]. The purpose of this research is to study the feasibility of using the BIRF for structural identification and damage detection and investigate the sensitivity of the BIRF to changes of the structural condition. To this end, the following objectives are identified:

1. Study impulse response function techniques, in general, and the B-Spline Impulse Response Function (BIRF), in particular, as reported in the literature in Boundary Element Method development in elastodynamics and soil-structure interaction.

2. Investigate the BIRF from a system identification perspective and develop the procedure to extract the associated Dynamic Signature Response (DSR) from time history records collected from experimental measurements.

3. Verify and validate the proposed DSR extraction procedures through computer simulations and experimental investigations, respectively.

4. Investigate the hypothesis that the development and accumulation of structural damage leads to measurable changes of the DSR of the structure.

5. Introduce a DSR-based Level-1 damage detection procedure and demonstrate its implementation through experimental testing and computer simulations.

6. Identify the advantages and limitations of the proposed approaches compared to the current state of practice.

1.3 Organization of the thesis

This thesis organized as follows: Chapter 1 introduces the problem, discusses the motivation for research and sets the objectives for this work. Chapter 2 presents a literature review on structure health monitoring, impulse response techniques, and damage detection and identification. Chapter 3 discusses the fundamentals of the B Spline polynomial and presents the mathematical background of the B Spline Impulse Response Function (BIRF) and its implementation in the prediction of the transient response of a dynamic system subjected to arbitrary excitation. Chapter 4 introduces the BIRF-based Dynamic Signature Response (DSR) within a system identification framework and presents the formulation of the inverse problem. In addition, it presents verification studies through computer simulations. Chapter 5 presents experimental validation for the proposed method in a laboratory setup and testing sequence with data analysis and result interpretations. Chapter 6 proposes

the procedure for adapting the B-DSR in Level-1 damage detection and demonstrates the implementation in a laboratory setup. Chapter 7 discusses concluding remarks and provides recommendation for future work.

Chapter 2

Literature Review

This chapter presents a review of the literature in Structural Health monitoring and damage detection, as well as on Impulse Response Techniques and the B-Spline Impulse Response Function.

2.1 Structural Health Monitoring

Civil Engineering structures deteriorate due to several effects such as ageing, overloading and overuse, inadequate maintenance, and extreme events, including earthquakes, floods, hurricanes and acts of terrorism. Structure Health Monitoring (SHM) has become an essential practice in ensuring the human safety and structural reliability [46].SHM refers to a group of activities for diagnosing the state and integrity of structures over time. SHM defines damage as changes in the material properties and/or their boundary conditions which affect the structural performance [2]. SHM can be thought of as the diagnostic tools in a patient-doctor relationship; as doctors need diagnostic tools to diagnose the patient's health, so do engineers, who use monitoring and assessment tools to check on the integrity of structural systems. The main purpose of SHM is to monitor, test for, and identify any underlying structural issues that may lead to loss of function and failure. The monitoring and diagnosis may be conducted either continuously, or on demand, or as part of a periodic inspection schedule. SHM can be used to validate structure performance, for instance, once a structure is designed for a specific service life, the performance of the structure can be tracked, as needed, especially after extreme load events. In addition, SHM can be

used to find the root cause of structural problems that may lead to different type of failures. Furthermore, information gathered from SHM activities can be used for the development and implementation of more efficient maintenance protocols. Monitoring and inspections are conducted through Nondestructive testing (NDT) procedures while Destructive testing used to evaluate specimen performance. NDT procedures are more favorable in SHM and they are performed using methods such as Visual test, this is not limited using naked eye, but includes using borescope in tight locations such as pipes [21], and unmanned aerial vehicles on large structures [19].Radiographic tests, Ultrasonic test, as an example, x-ray radiography and ultrasonic used for detecting damage in small specimens of composite material [23].Magnetic particle tests which applicable usually for iron and steel material, for instant, it's been used in the automotive industry for testing the drive shaft [51], among others, that are non-invasive and, in certain cases, do not interfere with operations.

2.2 Damage Detection and Identification

Damage in structure can be understood as the undesirable weakening that affects the structure behavior and can potentially alter the structure's original geometry. Damage identification methods categorize damage as local and global. Global damage detection focuses on the overall structure condition whereas local damage detection provides details about the location of the damage and the severity of it. Damage detection is classified in five different levels, i.e., (i) Level-1 detects the presence of global damage in the structure. Level 1 damage identification can be achieved using structure properties such as natural frequencies and mode shapes. (ii) Level 2 detects the location of the damage in the structure. For level 2 damage identification Ultrasonic testing can be used to locate the damage. (iii) Level 3 damage detection quantifies the severity of the damage, in addition to its location. This can be obtained by combining level 1 and level 2 damage identification with the structure model. (iv)

Level 4 damage identification predicts the remaining service life of the structure and can be used to indicate the needs for structure maintenance and repairs [17].(v) Level 5 damage identification is associated with smart structures with self-evaluating, self-healing or control capabilities.

Levels 1-3 are relevant to system identification, modeling and signal processing techniques. Levels 4 and 5 are based heavily on reliability and statistical analysis [48]. Figure 2.1 depicts the damage identification levels for SHM [49].

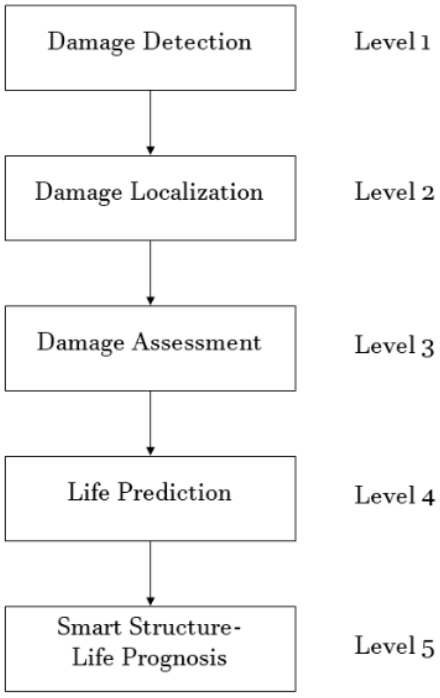

Figure 2.1: Main levels of SHM procedure for detecting a damage

Structural damage is currently detected by either visual inspection or localized experimental and testing methods [38]. Dynamics/Vibration-based damage detection is considered an effective technique to detect both global and local damage due to the relative simplicity of implementation. These methods aim to detect damage by analyzing vibration measurement data to evaluate changes in the structural vibration features such as means, variances, maximum, and minimum values of modal

frequencies, and modal shapes, among others. Current practice and research developments in early damage detection are broadly grouped into "Physics-Based" and "Data Driven" techniques [7]. Both methods identify changes in the system parameters since structural damage alters the structural damping, stiffness, mass and/or boundary conditions. Physics-based methods use computational models (e.g. the Finite Element Method FEM) of the structure and update the model parameters based on response data collected from the physical structure [7, 14]. Data-Driven methods use in situ testing measurements to identify changes in the dynamic response and other dynamic characteristics and correlate these changes to the severity of damage and its location [7, 3, 32]. All methods can be computationally intensive, may require extensive testing and instrumentation and are time consuming and they are not suitable for the rapid assessment of structural damage [33]. A discussion of these methods is presented in the following sections and summarized in Table 2.1.

Modal Frequency

Modal frequencies are a global property of a structure that can be used for detecting damage since the structure frequency expected to remain the same if its characteristics did not change. The frequency shift in a structure is used to detect the damage where the shift can be measured. The measured shift indicates that a change to the structure occurred, but it does not provide information about the location of the damage. According to Doebling [14] this technique has limitation on detecting damage because the natural frequency has low sensitivity to damages. Therefore, very precise measurements or large level of damage required for damage detection [14]. For a better reliable performance in terms of defect localization, modal frequency curve along with squared residual wavelet coefficients-based damage indicator is used [21].

Modal Force Residual

Residual force vectors, derived from the natural frequencies and mode shape of the intact and damaged structures, can be used for damage identification purpose [25]. For this method, finite element simulation used for calculating structure eigenvalues and eigenvector, and a real structure measurement used for extracting the eigenvalues and eigenvectors [53, 18, 54]. This method based on capturing the change in the mass and stiffens of the structure due to the damage. The residual modal force for the associated mode shape will be calculated and will be used for locating the damage [53].This method, can be combined with response sensitivity analysis for improving the accuracy and the efficiency of the damage identification [53].

Direct Mode Shape

Direct mode shape methods identify damage by comparing two sets of mode shapes using either "Modal Assurance Criteria" (MAC) or "Coordinate Modal Assurance Criterion" (COMAC). MAC investigates the similarities between two modes before and after damage. MAC values close to 1 indicates similarities of the mode shape and values close to 0 means that the two modes are dissimilar which indicate a damage in the structure [4]. COMAC gives a pointwise measure between the two sets of the mode shapes, provides local information and it combines information in different modes. A low value of COMAC represents a discordance at point which can be used to locate the damage in the structure [20].

Mode Shape Curvature Methods

Mode shape curvature methods use central difference approximation to derive the curvature for the mode shape function where the mode shape, mode number, and the distance between them should be known. To localize the damage, the absolute between the mode shape curvature before and after damage is calculated. The largest

absolute difference value provides information about the location of the damage. Mode shape curvature is more sensitive than the mode shapes method for identifying the damage location. However, damage localization detection is sensitive to high noise levels [15, 5].

Modal Strain Energy-Based Methods

Modal strain energy-based methods compare two sets of modal strain energy to locate the damage for beam-like structure and plate-like structures. This approach divides the structure into elements and estimates the modal strain energy before and after damage. For each load path, the mode shape would store an amount of energy. Once damage accrue to the structure, the amount of the stored energy in the mode shape in the load path will change. Measuring the change in the stored energy for a specific load path in a specific element would be used for localizing the damage [50, 8].

Modal Flexibility/Stiffness Matrix

Flexibility matrix is known as the inverse of stiffness matrix. Stiffness matrix relates force applied on the structure to the displacement produces anywhere on the structure. Each column on the flexibility matrix represents the displacement of the structure due to a unit force applied at the associated degree of freedom whereas each column on the stiffness matrix represents the amount of force that must be applied to the modal to maintain a unit displacement at the corresponding degree of freedom. Damage is detected using modal values to compute the flexibility or stiffness matrix of structure before and after damage[20].

Damping based method

Using the damping parameter to detect damage in structures has not been investigated as much compared to other dynamic properties such as natural frequencies

and mode shapes due to the complexities of the damping measurement and analysis. Theoretically, once the structure is damaged, the damping ratio will increase [10],e.g. a crack in concrete beam was observed to cause an increase of the damping [31]. Moreover, [9] stated using damping-based damage detection can detect small cracks that resulted in small or no frequency change. Lately, different studies have demonstrated that using damping-based-method can be more sensitive to detect damage, in some application, comparing with other parameters. However, using damping-based-method still in progress. Overall, using damping based method for detecting damage still under research and development [52].

Time Domain Methods

Time domain methods are routinely used in control and automation theory and often require smoothing and filtering of the time series to filter noise in the data. The time history of the response of structure subjected to an external load is used to identify damage. Any damage in the structure can be led to a change in the structural acceleration. An example is reported in [43] where a cantilever beam is loaded by a vertical impulse load at its free end the time history of the acceleration response is obtained through computer simulations. A subsequent analysis simulated damage by reducing the stiffness in selected elements while all other parameters were kept the same and the beam was loaded by the same impulse at the same location. Comparison of the acceleration time histories showed that the acceleration response has changed due to the damage that was introduced.

Frequency Domain

Force vibration and/or response function measurements can be used directly for damage identification purposes with no need to extract the modal parameters of the structure. Damage is detected directly from Frequency Response Function (FRF)

equation which not only can identify there is a damage, but also locate the damage [27, 16]. Overall, the biggest advantage in using FRF is that global quantities can be measured by placing response sensors at any point in the structure. For example, a simply supported aluminum beam experiment reported in [27] has been used in damage identification using FRF method. First, FRF is computed for the beam along with the natural frequencies and the corresponding model shapes. Then a damage was introduced to the model by a deep cut in the beam. The FRF was computed again and the two cases before and after damage are compared. A frequency shift indicates there is a damage in the beam However, the method is not sensitive for small damage cases and is highly dependent on the selected frequency. Choosing frequencies near a natural frequency provides results that are less effected by the noise, however it is less sensitive to damage.

Table 2.1: Summary of Damage Identification Techniques

Methods	Basic principles	Disadvantages	Reference
Eigenfrequency and mode shape residuals	• Using resonant frequencies. A characteristic shift of the eigenfrequency spectrum would result due to a stiffness change	• Dose not indicate the reason of the Eigenfrequency change, so a model must be available where the relation between frequency and stiffness change are known.	[18]
Model force Residual	• Using measurement data into eigenvalue problem. Damage would be located by the node residual force vector.	• The method is sensitive to the measurement error.	[18, 54]
Mode shape	• Using Mode shape of the Structure to detect damage. different techniques are used such as MAC and COMAC. • Mac(modal assurance Criterion) • COMAC (coordinate Modal Assurance Criterion)	• Series of sensors are required "sensor at each mass point". • Expensive/ limited in large structure. • Sensitive to location. • False damage detection	[10, 28]
Modal curvature	• It is an expansion to Mode shape theory. They are the second derivative of the modal shape.	• May sensors are required to define higher mode. • Performance of the method depends on the number of mode. • Attains error observed during using vibration data. • Higher frequency increase variance. • Using large sampling signals cause truncation error.	[28, 40]
Modal Flexibility/stiffens	• Modal values used to compute flexibility or stiffness matrix. Obtained values compared with undamaged state original structure	• Flexibility Sensitive to change in the lower frequency modes. • Stiffness matrix is sensitive to highest frequencies.	[20]
Damping-based-method	• Damping ratios are sensitive to cross-section internal force.	• It can be limited when the vibration data have large stander deviations. • Failure type should be considered because it may rise or fall the damage ratio.	[20]
Time Domain	• Using time-dependent parameter (e.g period of structure) for detecting damage.	• Using Periodogram analysis, it has been noted that Using FDPA(frequency domain periodogram analysis) provide better result comparing with TDPA.	[55]
Frequency Domain	• Using Fourier transform to detect damage. Change in vibration response indicate damage in the structure. • There are more than one approach FRF(Frequency Response Function) DFT(Discrete Fourier Transform)	• FRF and FRF with fuzzy clustering fails in detecting minor damages.	[1, 11, 44]

2.3 Impulse Response Techniques

Impulse Response

The impulse response is one of several ways of uniquely describing the behavior, or characteristics, of a Linear Time Invariant (LTI) system. The impulse response is the output, of an LTI system when the input is a unit impulse. Impulse response techniques are powerful since system response to given arbitrary input are computed through convolution techniques.

Discrete-time signal vs Continuous-time signal

Discrete time unit impulse function is also known as the unit sample function, is defined by a series of discrete points as

$$\delta_m(n) = \delta(n-m) = \begin{cases} 1, & n = m \\ 0, & n \neq m \end{cases}, n = 1, 2, ... \tag{2.1}$$

An example of applying a unit impulse as an input and the response/output due to the unit impulse presented in Figure 2.2. The output due to the unit impulse is called the impulse response.

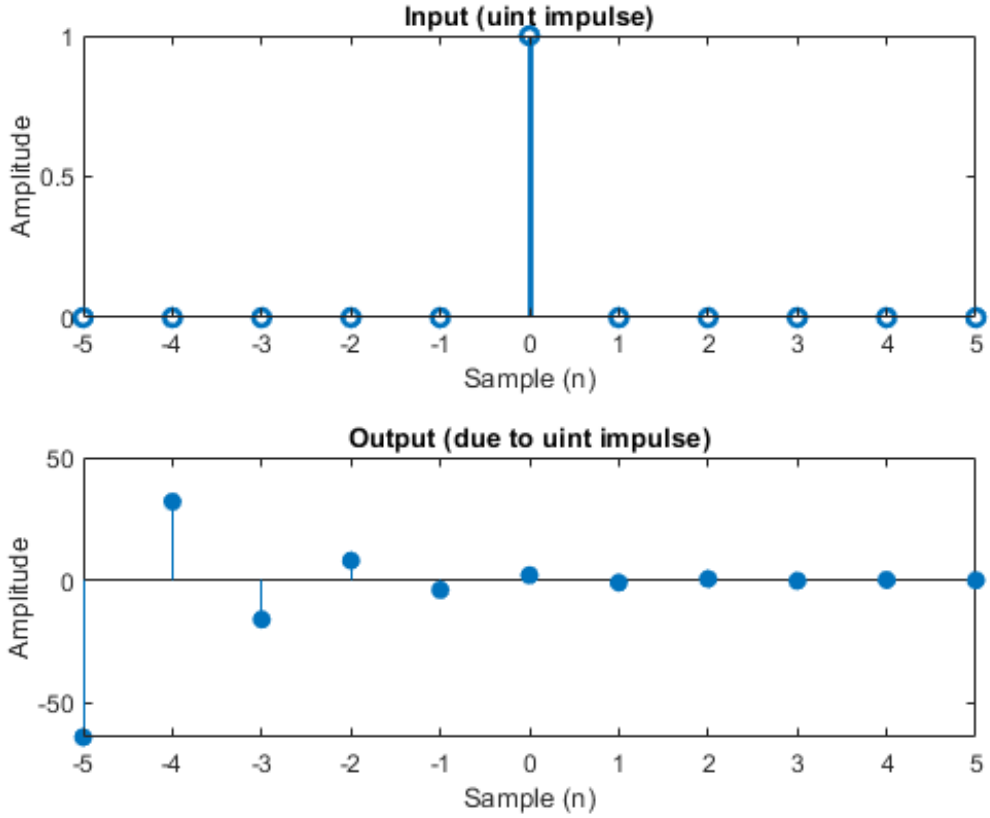

Figure 2.2: Input and Output of a Unit Impulse in discrete time

Once input unit impulse $\delta(n-m)$ is applied on the LTI system and the impulse response $h(n-m)$ is known, the response of the system to an arbitrary input,$x(n)$ is obtained through convolution with the impulse response as

$$y[n] = h(n) * x(n) = \sum_{k=-\infty}^{\infty} h(k)x(n-k) = \sum_{k=-\infty}^{\infty} x(k)h(n-k) \tag{2.2}$$

In the continuous time signal the impulse function is the Dirac delta function that is defined as the value of a step pulse $P(t) = 1/\Delta t$ as ΔT approaches zero. Figure 2.3 shows the schematic representation of the unit impulse in the continuous time. A characteristic property is that its integral over time is one.

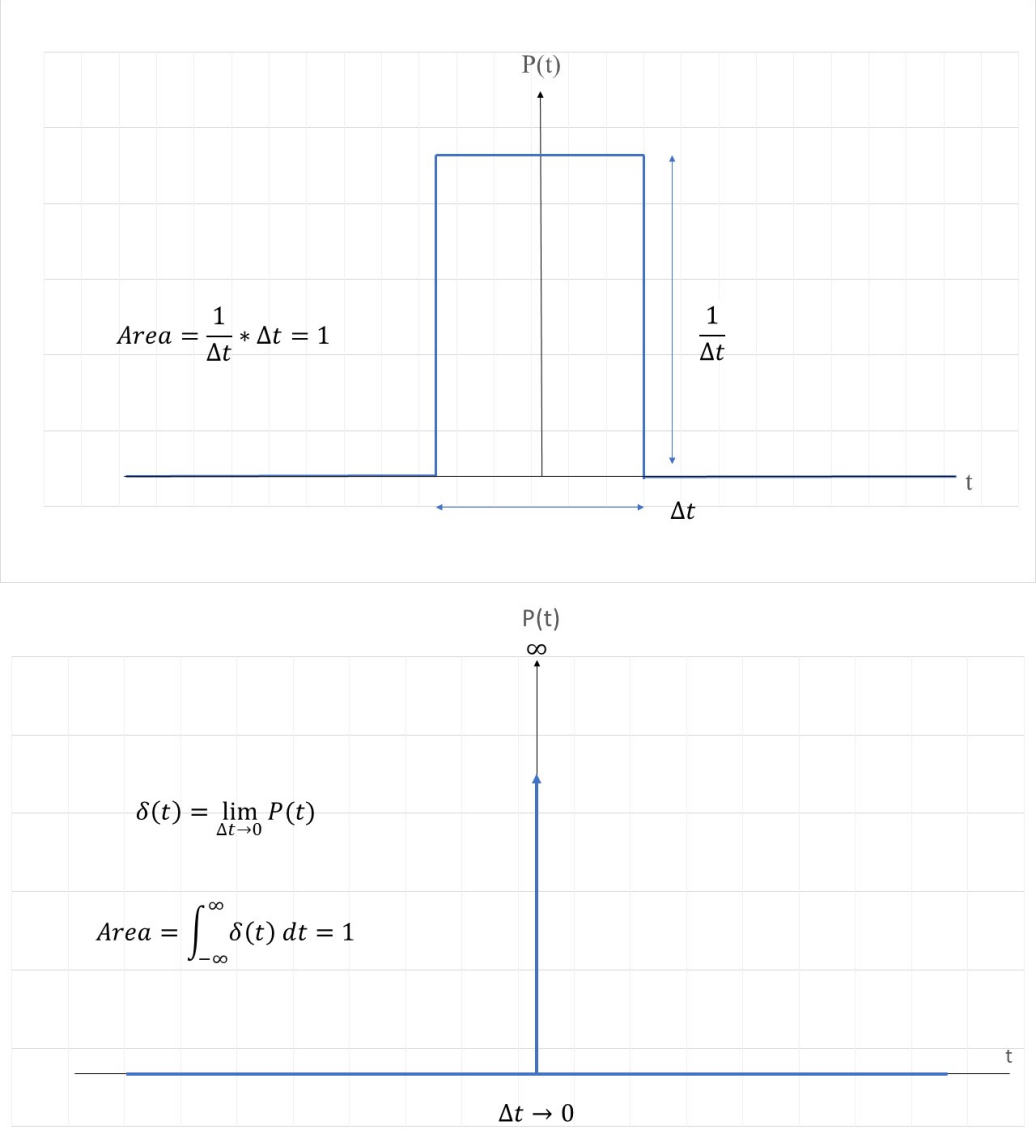

Figure 2.3: Schematic Representation of a continuous Impulse function (Dirac Delta Function)

Once input unit impulse $\delta(t)$ is applied on the LTI system and the impulse response $h(t)$ is known, the response $y(t)$ of the system to an arbitrary input, $x(t)$ is obtained through convolution with the impulse response as

$$y[t] = \int_{-\infty}^{\infty} x(\tau)h(t-\tau)\, d\tau \tag{2.3}$$

B-Spline Impulse Response Function(BIRF)

The B-Spline Impulse Response Function (BIRF) is the response of a dynamic system excited by a B-Spline polynomial of any order. The mathematical background is discussed in detail later in this thesis, since the concepts are used in this work within a System Identification and Damage Detection framework. When used in dynamic analysis of structures it has the advantage that it combines the continuity provided by Equation 2.3, and the efficiency of the discrete convolution shown in Equation 2.2. The first concepts of using B Spline polynomials in dynamic analysis appeared in 1993 in the work published by Rizos who developed a new generation of fundamental solutions for 3D elastodynamic analysis and wave propagation that employed the B-Spline family of polynomials as the impulse excitation [37][35][32]. The B-Spline Impulse Response Function (BIRF) concept has been further developed and implemented in different applications since then. In 2000, Rizos presented the BIRF of 3D rigid surface and embedded foundations of arbitrary shape [34]. In 2002 the B-spline family of polynomials and the BIRF functions were adapted in the development of a coupled the BEM-FEM methodology for 3D wave propagation and soil structure analysis in the direct time domain [36]. In 2005, BIRF was used to model the soil-tie system in a railroad track for simulation studied in high speed train research [30]. In 2006 BIRF functions used for representing the transient soil-structure interaction solutions in a closed form [47]. In 2011 BIRF were used to develop scalable models for the transient response of the sleepers in conventional and high-speed railway [24]. In 2012, BIRF were used in the development of a multi-solver, multi-domain methodology for the transient analysis of coupled systems [29]. In 2020 used BIRF functions for multi-body dynamics and vehicle structure interaction analysis[12].

Chapter 3

Mathematical Background

3.1 The B-Spline Polynomial

B-Spline polynomials belong to a family of basis functions used in data interpolation and approximation. The B-Spline functions are piece-wise smooth polynomials of order k derived based on a knot sequence $t_n, n = 1 \cdots N$. B-Spline polynomials of any order k are generated by the recursive formula,

$$B_n^k(t) = \begin{cases} 1, & t_n < t < t_{n+1} \\ 0, & \text{elsewhere} \end{cases} \qquad k = 1 \tag{3.1}$$

$$B_n^k(t) = (\frac{t - t_n}{t_{n+k-1} - t_n})B_n^{k-1}(t) + (\frac{tn + k - t}{t_{n+k} - t_{n+1}})B_{n+1}^{k-1}(t) \qquad k > 1 \tag{3.2}$$

The B_n^k Spline polynomials are of k-1 degree and have $k-2$ continuous derivatives. These polynomials are non-zero in a finite interval ΔT known as the B Spline support. For an equally spaced knot sequence, i.e., $t_n = n\Delta t, n = 1, 2 \cdots N$, the B Spline polynomials are known as Cardinal Splines. The spline support of Cardinal Splines depends on the order of the spline and is defined as $\Delta T = k\Delta t$. Cardinal Splines have an additional property according to which the B_n^k polynomials are translates of a representative one, i.e., $B_n^k(t) = B_0^k(t - t_n)$. Cardinal spline of order 1-4 are given below and depicted graphically in Figure 3.1:

- Constant

$$B_1^1(t) = \begin{cases} 1, & t_n < t < t_{n+1} \\ 0, & \text{elsewhere} \end{cases} \qquad k = 1 \qquad (3.3)$$

- Linear

$$B_0^2(t) = \begin{cases} 2\tau & 0 \le \tau < \frac{1}{2} \\ 2(1-\tau) & \frac{1}{2} \le \tau \le 1 \\ 0 & \text{elsewhere} \end{cases} \qquad k = 2 \qquad (3.4)$$

- Quadratic

$$B_0^3(t) = \begin{cases} \frac{9}{2}\tau^2 & 0 \le \tau < \frac{1}{3} \\ -9\tau^2 + 9\tau - \frac{3}{2} & \frac{1}{3} \le \tau < \frac{2}{3} \\ \frac{9}{2}\tau^2 - 9\tau + \frac{9}{2} & \frac{2}{3} \le \tau < 1 \\ 0 & \text{elsewhere} \end{cases} \qquad k = 3 \qquad (3.5)$$

- Cubic

$$B_0^4(t) = \begin{cases} \frac{32}{3}\tau & 0 \le \tau < \frac{1}{4} \\ -32\tau^3 + 32\tau^2 - 8\tau + \frac{2}{3} & \frac{1}{4} \le \tau < \frac{2}{4} \\ 32\tau^3 - 64\tau^2 + 40\tau + \frac{22}{3} & \frac{2}{4} \le \tau < \frac{3}{4} \\ \frac{-32}{3}\tau^3 + 32\tau^2 - 32\tau + \frac{32}{3} & \frac{3}{4} \le \tau < 1 \\ 0 & \text{elsewhere} \end{cases} \qquad k = 4 \qquad (3.6)$$

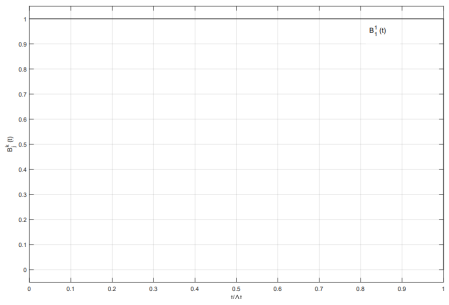

(a) Graphical Representation of Constant B-spline

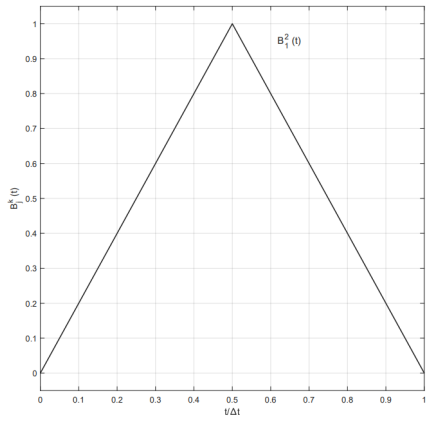

(b) Graphical Representation of Linear B-spline

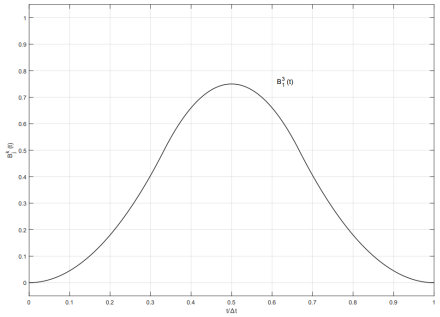

(c) Graphical Representation of Quadratic B-spline

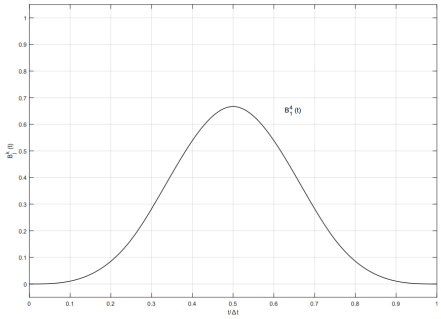

(d) Graphical Representation of Cubic B-spline

Figure 3.1: Graphical Representation of Cardinal B-Splines of order 1-4

The cubic (k=4) B_0^k Cardinal Spline is used in this work where $\tau = \frac{t}{\Delta T}$. The characteristic shape of the 4^{th} order Cardinal Spline is shown in Figure 3.1d. B Spline polynomials are commonly used in function interpolation and approximation. Hence, any function $g(t)$ can be represented as a linear combination of B-Spline polynomials [37, 13, 42, 41] as,

$$g(t) \approx \Sigma_{i=1}^{j} g(\tau_i) B_0^k(t - t_i), \qquad t \in [t_1, t_j], \qquad \tau_i = \frac{t_{i+1} + t_{i+2} + ... + t_{i+k-1}}{k-1}, \qquad k > 1 \tag{3.7}$$

Since the $B_0^k(t - t_n)$ is nonzero only within its support, ΔT, the summation appearing in Equation 3.7 involves a small number of terms that is equal to the

order of the B Spline. Details on the definition of B-Spline and associated function approximation schemes are discussed further in [37].

3.2 The B-Spline Impulse Response Function(BIRF)

A B-Spline Impulse Response Function (BIRF) is a continuous function in time that is defined between any two points q, the source, and p, the receiver, of the dynamic system. It represents the time history of the response of the receiver points due to an excitation with a B Spline modulation applied at the source point. The embodiment of an analytic BIRF in one example is the B Spline Fundamental Solution for an infinite, linear, homogeneous, elastodynamic 3D space expressed as [37]:

$$BIFR(\mathbf{p},\mathbf{q}) = U_{ij}^{B}(\mathbf{p}, t; \mathbf{q}|B_o^k(t)) =$$

$$(1/4\pi\rho)\{a_{ij}(r)F(t, r, c_1, c_2) + b_{ij}(r)B_o^k(t - \tfrac{r}{c_1}) + c_{ij}(r)B_o^k(t - \tfrac{r}{c_2})\} \tag{3.8}$$

where ρ, c_1,and c_2 are,respectively, the mass density, pressure wave and shear wave velocities of the medium and *i, j=1,2,3* are the principal directions of the cartesian coordinate system. In this case, the BIRF function, U_{ij}, represents the time history of the displacement response in the *"i"* direction at the receiver point $\mathbf{p}$ caused by a B-Spline, $B_o^k(t)$, force excitation applied at the source point $\mathbf{q}$ in the *"j"* direction. Coefficients a_{ij}, b_{ij}, c_{ij} and $F\,(t, r, c_1, c_2)$ depend on the distance, r, between the two points [37].The analytic BIRF functions have limited direct applicability to general dynamic systems. They are most useful in conjunction with numerical methods, e.g. the B Spline BEM [37]. However, the BIRF functions are very powerful and directly applicable to dynamic systems of arbitrary geometry and loading when represented in a discrete form. The discrete BIRFs can be obtained indirectly through numerical solutions. In such cases, the governing differential equations of a dynamic system are discretized, for instance in a Finite Element Method (FEM), Finite Difference Method (FED), or Boundary Element Method (BEM) sense, into a finite number of

degrees of freedom (DOF). One DOF at a time is excited by a B-Spline force and the response at all DOFs is computed numerically at discrete time instances through an appropriate time marching scheme. The resulting response is the fully discrete BIRF for each pair of DOF. An example of discrete BIRFs is shown in Figure 3.2. The dynamic system in this example consists of two rigid square foundations of side 2a resting on an elastic half space, as shown in the inset of the figure. The edge-to-edge distance between the footings is 2d. Since the footings are considered rigid, the motion of the foundation system is fully defined by 12 DOF, i.e., 3 translational and 3 rotational DOF at each footing center.The direct time domain BEM reported in rizos is used to compute the response of both foundations when a 4^{th} order B-Spline force is applied at the source footing on the left, as shown in the inset of the figure. The two BIRF curves shown in Figure 3.2 represent the normalized amplitude of the horizontal translation of the centers of each footing as a function of a nondimensional time parameter,τ_o.

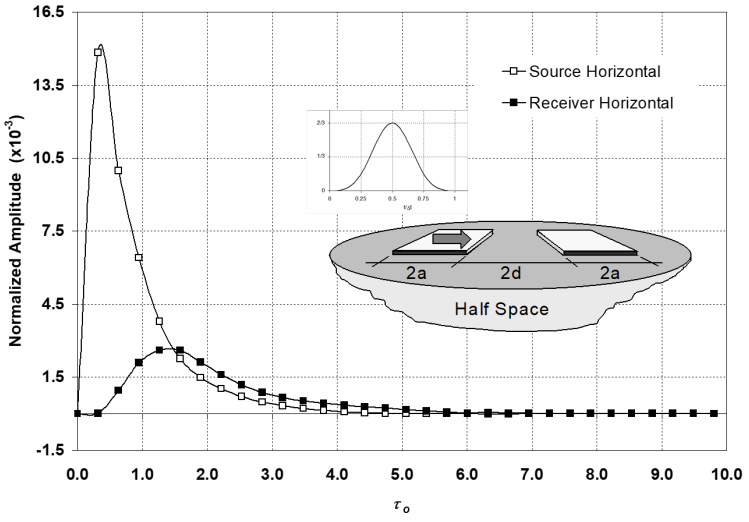

Figure 3.2: Example of Discrete BIRF Functions

The BIRFs for each pair of DOF can be collected in a matrix form at each time step, n, as:

$$\mathbf{B}_n = \begin{bmatrix} BIRF_{11} & \cdots & BIRF_{1q} \\ \vdots & \ddots & \vdots \\ BIRF_{p1} & \cdots & BIRF_{pq} \end{bmatrix}_n \tag{3.9}$$

In equation 3.9, the BIRF matrix $\mathbf{B}_n$ is evaluated at time step n, and subscripts **p** and **q** indicate, respectively, the source and receiver DOF. The following important points regarding the BIRF functions relate to this work and should be emphasized:

1. The BIRFs are independent of any external excitations. In fact, during loading of time invariant dynamic systems the BIRFs do not change and, therefore, are considered signature responses that capture the current state of the dynamic system.

2. In order to obtain the most general form of $\mathbf{B}_n$, the total number of degrees of freedom,*ndof*,of the system are considered in pairs. In this case, $p = q = ndof$ yields a square $\mathbf{B}_n$ matrix. The greatest advantages, however, are realized by recognizing that in most problems only a few points may be loaded during an event while the response at only a few points may be of interest. In such cases $p \neq q, p < ndof, q < ndof$ yields a rectangular $\mathbf{B}_n$ matrix of much smaller size. Furthermore, since the forced vibration phase of the system lasts for as long as the B-Spline support,ΔT, the system response will reach steady state, or attenuate significantly within a limited number of time steps.

3. While the BIRFs are computed efficiently in numerical models of the physical systems in a direct manner, it is almost impossible to measure the BIRFs directly in physical systems due to the difficulty of accurately reproducing the B-Spline loading with mechanical means.

3.3 BIRF Functions in Prediction of Dynamic Response to Arbitrary Excitation

The function interpolation scheme using B-Spline polynomials shown in Equation 3.7 indicates that if the BIRF of the system is known, then the response to an arbitrary excitation can be computed as a mere superposition of the BIRFs without further consideration of the system itself, as demonstrated in Figure 3.3

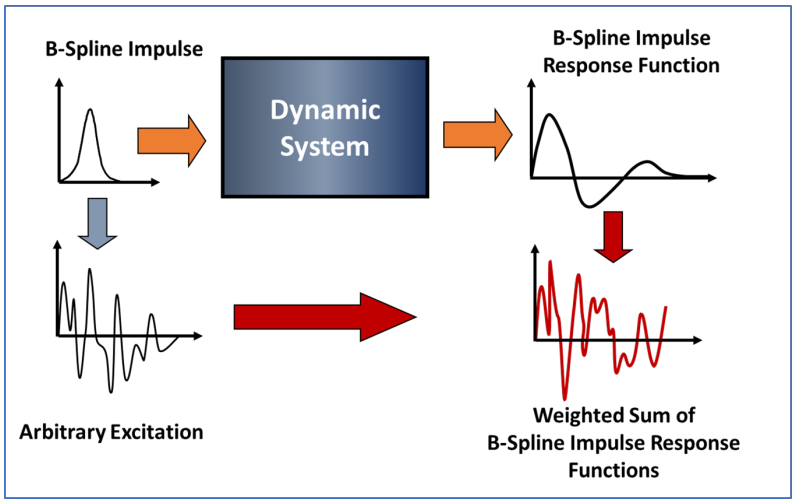

Figure 3.3: Response to Arbitrary Excitation Using BIRF Functions

To this end, the vector of arbitrary transient external excitations, $f(t)$, applied at the boundary nodes of the dynamic system is first evaluated at the time knots that define the B-Spline polynomial, i.e., $f(t = t_n) = f_n$. If R_n represents the unknown response of the dynamic system to the excitation $f(t)$, at time step N, then the superposition of the 4^{th} order BIRF is expressed as:

$$R_N = \Sigma_{n=1}^{\hat{N}} B_n f_{N-n+2}, \qquad \hat{N} = min(N, M) + 1 \tag{3.10}$$

where step M defines the time $t_M = M\Delta t$ after which $B_M = 0$ is considered negligible or zero.

Chapter 4

Identification of Dynamic Signature Response

4.1 The Inverse Problem and the B-DSR

Structural health monitoring and assessment procedures seek after the identification of the current state of the structure through load testing and simulations. In general, these methods identify structural properties and damage through signal processing of structural responses and/or model updating techniques. In view of the preceding discussion, the current state of the structure is captured in the B-Spline Impulse Response functions. Therefore, if the response time history $\mathbf{R}$ and the corresponding excitation $\mathbf{f}$ are known either through vibration test measurements or computer simulations, Equation 3.10 can be solved for the structural signature response, $\mathbf{B}$. To this end, Equation 3.10 is written at a step n as:

$$\begin{aligned}
\mathbf{R}_1 &= \mathbf{B}_1\mathbf{f}_2 + \mathbf{B}_2\mathbf{f}_1 \\
\mathbf{R}_2 &= \mathbf{B}_1\mathbf{f}_3 + \mathbf{B}_2\mathbf{f}_2 + \mathbf{B}_3\mathbf{f}_1 \\
\mathbf{R}_3 &= \mathbf{B}_1\mathbf{f}_4 + \mathbf{B}_2\mathbf{f}_3 + \mathbf{B}_3\mathbf{f}_2 + \mathbf{B}_4\mathbf{f}_1 \\
&\vdots \\
\mathbf{R}_N &= \mathbf{B}_1\mathbf{f}_{N+1} + \mathbf{B}_2\mathbf{f}_N + \cdots + \mathbf{B}_{N+1}\mathbf{f}_1
\end{aligned} \tag{4.1}$$

Equations 4.1 contain one more unknown than the number of equations and cannot be solved for $\mathbf{B}$ in this form. The additional needed equation is obtained by assuming a natural condition for the BIRF function $\mathbf{B}$ at any step, j, expressed in a central difference form as:

$$\ddot{\mathbf{B}}_j = \frac{\mathbf{B}_{j+1} - 2\mathbf{B}_j + \mathbf{B}_{j-1}}{\Delta \mathrm{t}^2} = \mathbf{0} \;\Rightarrow \mathbf{B}_{n+1} = 2\mathbf{B}_n - \mathbf{B}_{n-1} \tag{4.2}$$

Introducing Equation 4.2 into Equation 4.1 yields

$$\begin{aligned}
\mathbf{R}_1 &= \mathbf{B}_1\mathbf{f}_2 + (2\mathbf{B}_1 - \mathbf{B}_0)\,\mathbf{f}_1 \\
\mathbf{R}_2 &= \mathbf{B}_1\mathbf{f}_3 + \mathbf{B}_2\mathbf{f}_2 + (2\mathbf{B}_2 - \mathbf{B}_1)\,\mathbf{f}_1 \\
\mathbf{R}_3 &= \mathbf{B}_1\mathbf{f}_4 + \mathbf{B}_2\mathbf{f}_3 + \mathbf{B}_3\mathbf{f}_2 + (2\mathbf{B}_3 - \mathbf{B}_2)\,\mathbf{f}_1 \\
&\vdots \\
\mathbf{R}_N &= \mathbf{B}_1\mathbf{f}_{N+1} + \mathbf{B}_2\mathbf{f}_N + \cdots + (2\mathbf{B}_N - \mathbf{B}_{N-1})\,\mathbf{f}_1
\end{aligned} \tag{4.3}$$

which in compact form can be written as:

$$\begin{gathered}
\mathbf{R}_N = \hat{\mathbf{f}}_N\mathbf{B}_N + \mathbf{H}_N \\
\hat{\mathbf{f}}_N = (\mathbf{f}_2 + 2\mathbf{f}_1) \quad \textit{and} \quad \mathbf{H}_N = \textstyle\sum_{n=1}^{N-2} \mathbf{B}_n\mathbf{f}_{N-n+2} + \mathbf{B}_{N-1}\,(\mathbf{f}_3 - \mathbf{f}_1)
\end{gathered} \tag{4.4}$$

where $\hat{\mathbf{f}}_N$ is a modified force vector at step N,and $\mathbf{H}_N$ is a history vector representing the effects of past steps on the current step N and both are known at the current time step. Therefore, if the excitation and response of a system are determined experimentally, through in-situ measurements, or through computer simulations, the signature response of a system can be extracted by solving Equation 4.4 in a forward substitution manner as:

$$\mathbf{B}_N = \frac{\mathbf{R}_N - \mathbf{H}_N}{\hat{\mathbf{f}}_N} \tag{4.5}$$

4.2 Analytic Verification through Computer Simulations

The Benchmark Problem Using Displacement Based B-DSR

The proposed procedure for extracting the signature responses is verified first using simulated system responses. For demonstration purposes, and without loss of generality, a single degree of freedom system is considered. The stiffness of the system is

$k = 2,000$, the mass is $m = 500$, and the damping is $c = 50$ in consistent units. The system is subjected to two different excitation:

$$\begin{aligned} Load\ Case\ 1: &\quad f(t) = 100e^{-10t} \\ Load\ Case\ 2: &\quad f(t) = 100sin(10t) - 50cos(5t) \ + \ 50 \end{aligned} \tag{4.6}$$

The response in each case is computed using Newmark's algorithm. The loads and responses are shown in Figure 4.1

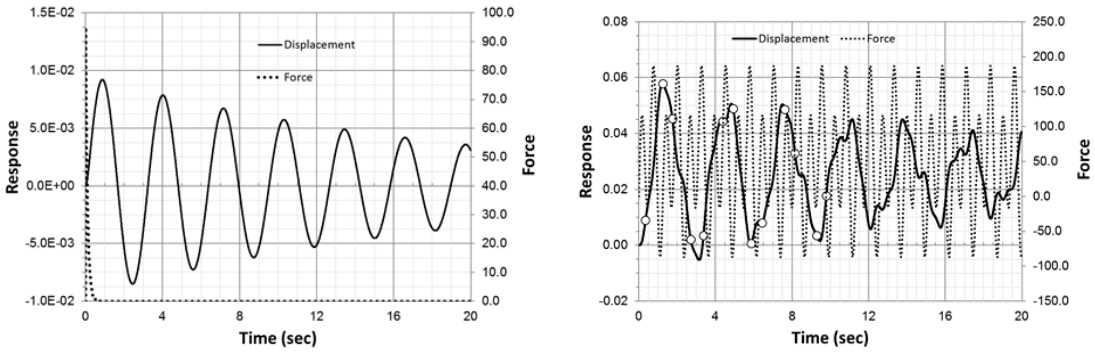

(a) Load Case 1 (b) Load Case 2

Figure 4.1: Two load cases and corresponding responses computed by the Newmark algorithm

These responses and the corresponding loads are used in Equation 4.5 to compute the signature response in each case. Since the system remains the same, it is expected that the two signature responses are identical as shown in Figure 4.2

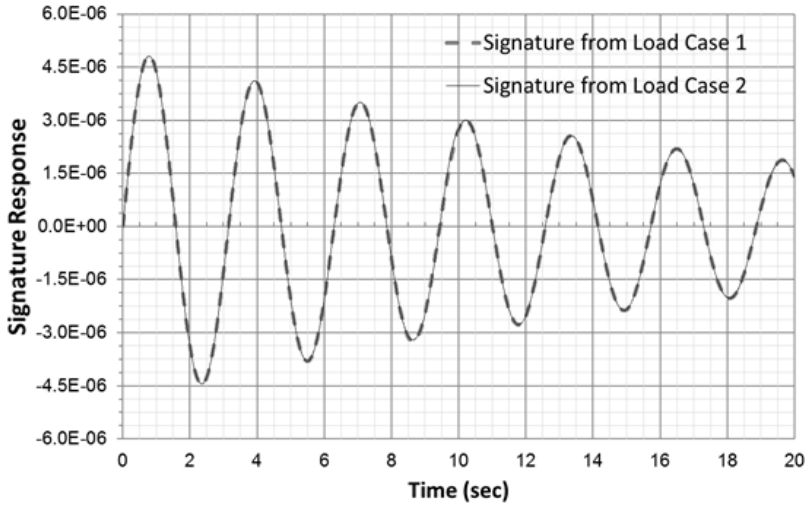

Figure 4.2: Signature Responses Extracted from two Different Load Cases

Subsequently, the system is subjected to an arbitrary excitation shown in Figure 4.3 and the response is computed using Newmark's method and the signature responses in Figure 4.2 along with Equation 3.10. Figure 4.3 shows the comparison between the two solutions. It is observed that the solutions are identical. The mean error is computed as 0.0049%.

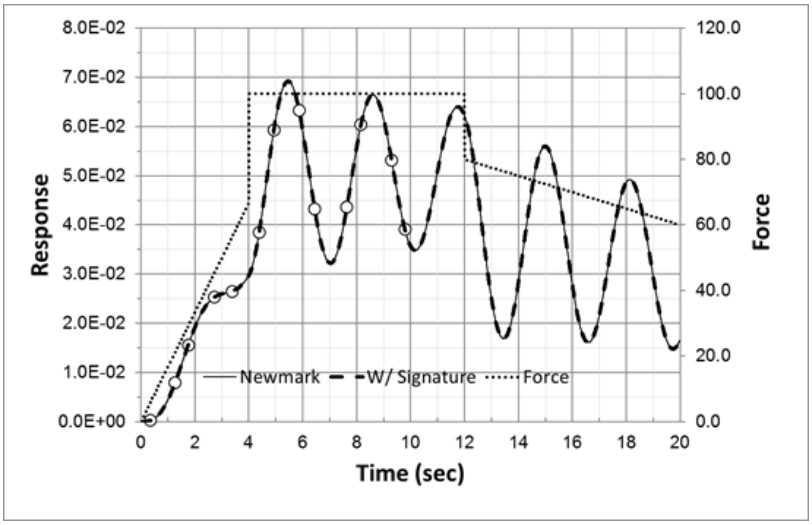

Figure 4.3: Response to Arbitrary Excitation - Verification Study

Multi-Degree of freedom Displacement Based B-DSR

A two degree of freedom system have been modeled as in Figure 4.4 . The mass and stiffens of the system are $m1 = m2 = 50, k1 = k2 = 2000$ consistent units. Damping of the system is calculated using Rayleigh damping where the damping ratio, $\zeta = 2.5\%$, is assumed the same for both modes. Six different load histories, shown in Figure 4.5, have been chosen randomly to apply forces.

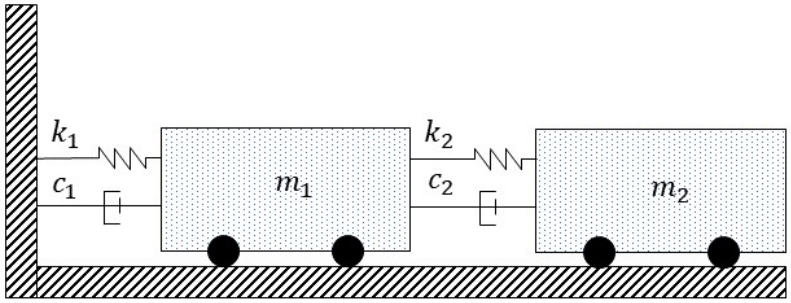

Figure 4.4: Multi-Degree of freedom system

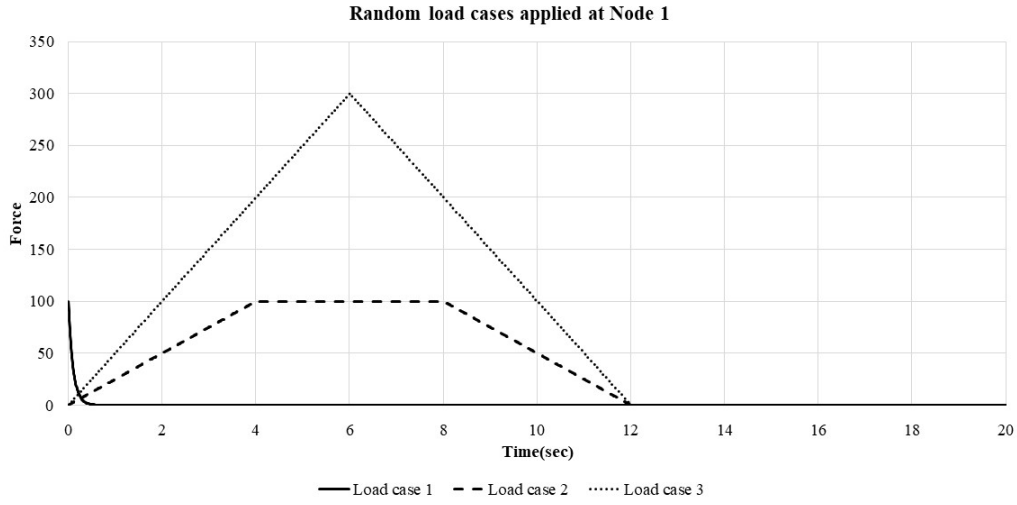

(a) Different Load Cases Applied at Node 1

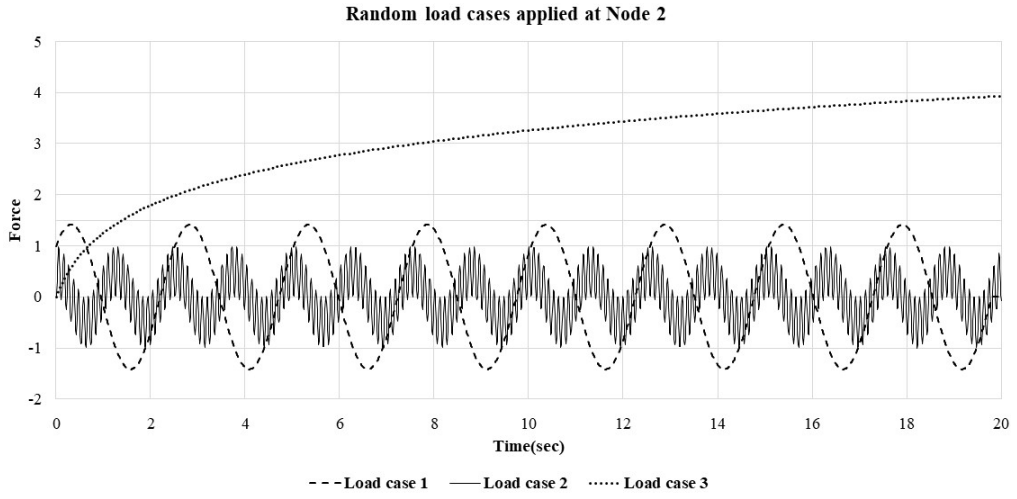

(b) Different Load Cases Applied at Node 2

Figure 4.5: Different Load Cases Applied at Node 1 and Node 2

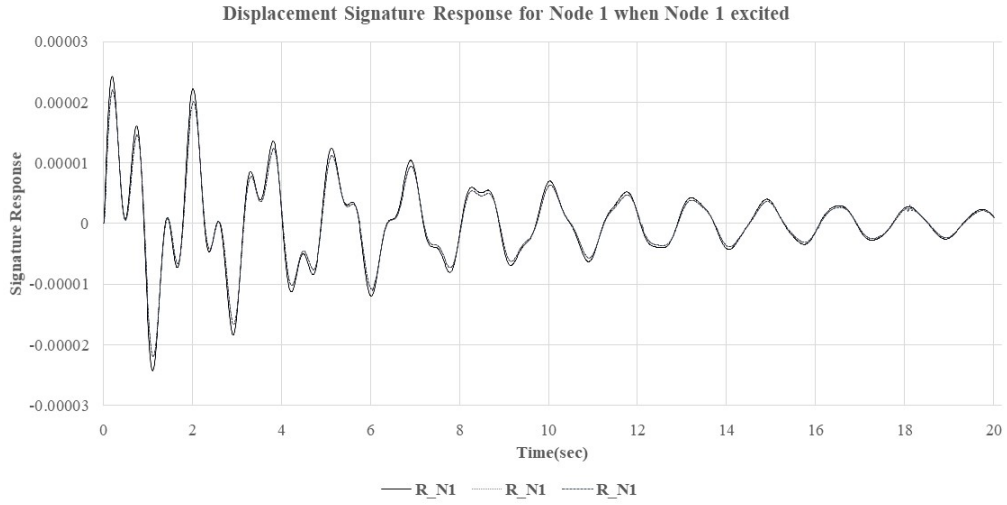

(a) B-DSR at Node 1

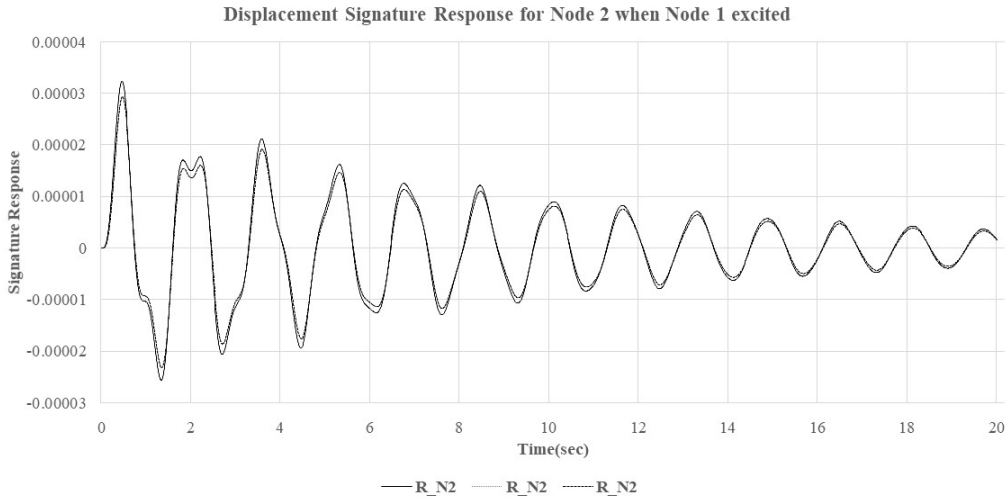

(b) B-DSR at Node 2

Figure 4.6: B-DSR For Node 1 and Node 2 when Node 1 is Excited

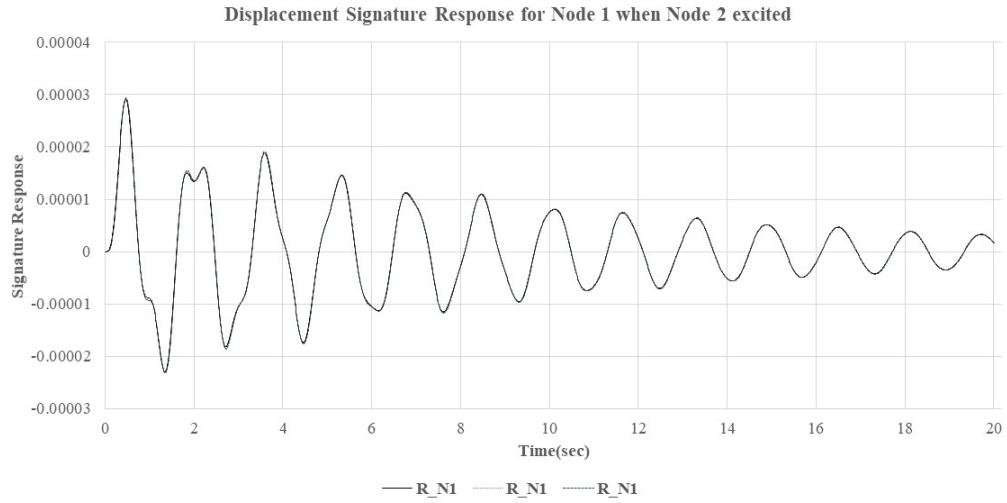

(a) B-DSR at Node 1

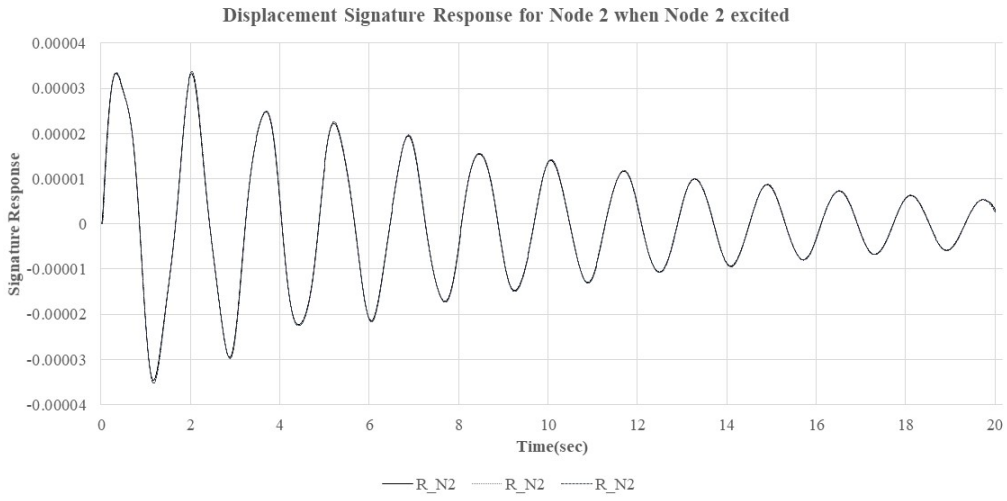

(b) B-DSR at Node 2

Figure 4.7: B-DSR For Node 1 and Node 2 when Node 2 is Excited

Figure 4.5 shows the load cases that have been selected and applied at one node at a time. As illustrated, extracting the B-DSR requires two sets of information, i.e., the applied force at the *sourcenode* and the associated response at all nodes *receivers*.

Figure 4.6 shows the extracted B-DSR of the structure due to the applied forces at *node*1 and using collocated displacement response data from *node*1 and *node*2. Similarly, Figure 4.7 shows the B-DSR for *node*1 and *node*2 when *node*2 is excited. It's been noted that the B-DSR for node 2 when node 1 is excited is similar to the B-DSR for node 1 when node 2 excited as shown in Figure 4.8.

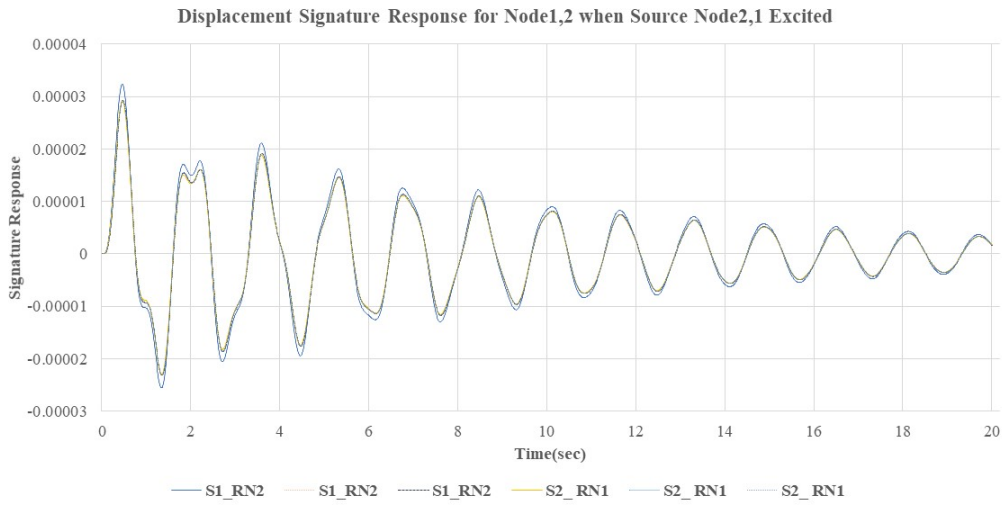

Figure 4.8: B-DSR For Node 1 and Node 2 when Node 2 and Node 1 Excited

4.3 Acceleration Based B-DSR

SDF

The B-DSR can be extracted using any type of response (displacement, velocity, and acceleration). Since acceleration measurements are more reliable and easier to implement on experiments, the same system used before has been used again here where $k = 2,000$, mass is $m = 500$, and the damping is $c = 50$ in consistent units. The system is subjected to the two load cases as represented in Eq 4.7.

$$\begin{aligned} Load\ Case\ 1: \quad & f(t) = \sin\left(\tfrac{t}{5}\right) - 3cos(t) + 1 \\ Load\ Case\ 2: \quad & f(t) = 100e^{-10t} \end{aligned} \tag{4.7}$$

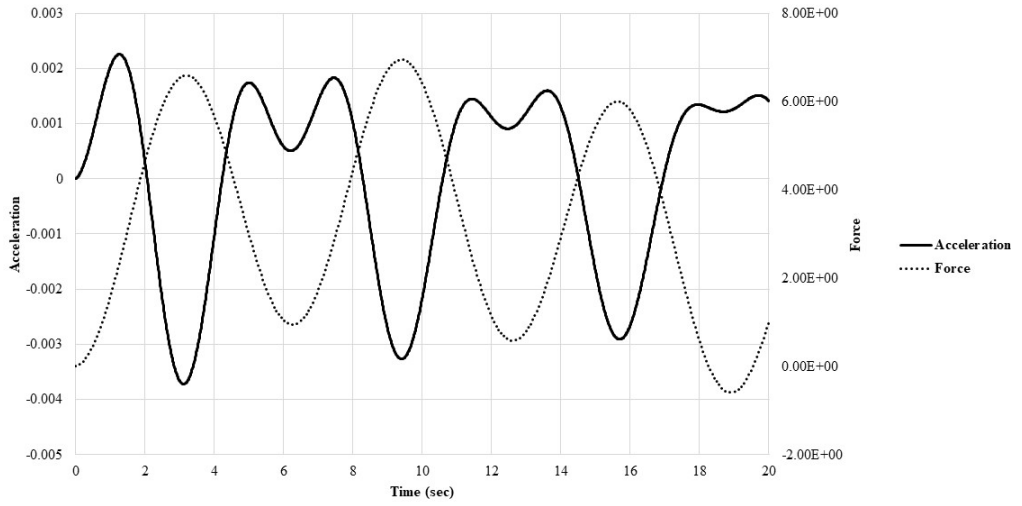

(a) Load case A

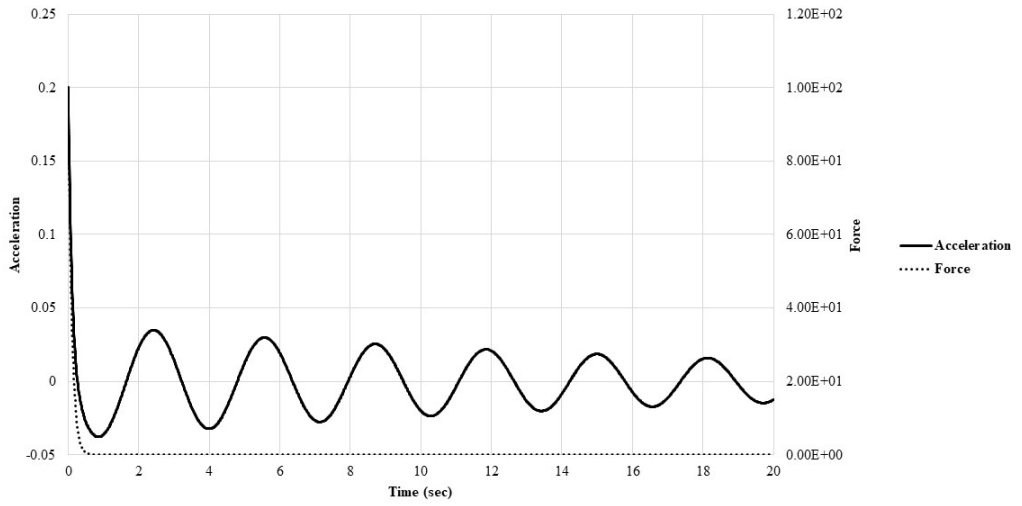

(b) Load case B

Figure 4.9: Two load cases and corresponding acceleration response computed by the Newmark algorithm

Figure 4.9 shows the acceleration response data that is used for extracting the B-DSR using the load case that presented in Eq 4.7. It's been noted that if the first

9 steps ignored, the correlation between the extracted B-DSR of those load cases are high as shown in Figure 4.10.

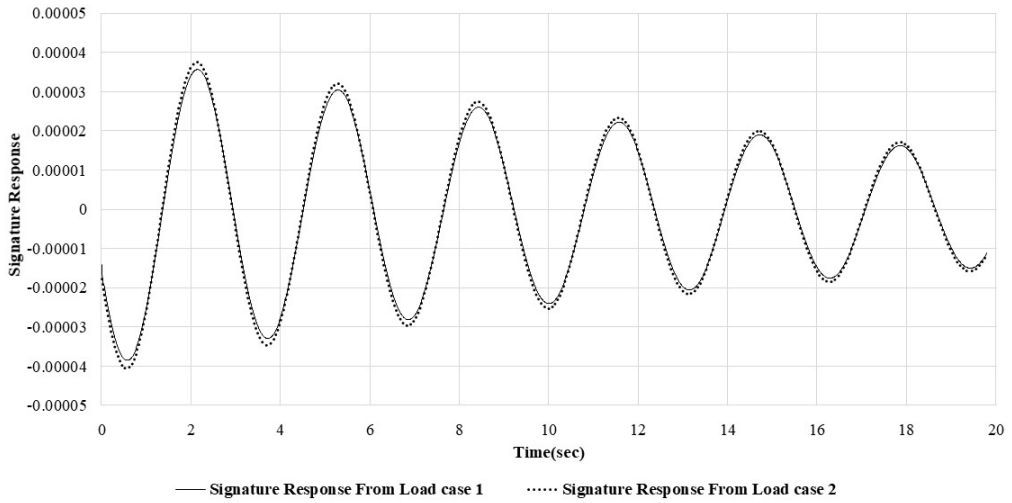

Figure 4.10: Using acceleration response for extracting B-DSR

MDF

For extracting the B-DSR of multi-degree of freedom system using the acceleration response, the system shown in Fig. 4.4 is used. The same load cases used in the verification of the displacement based B-DSR, and shown in Figure 4.5 are used to verify that we can use the acceleration response to extract B-DSR. The comparison with the solution obtained by the Newmark method is shown in Figure 4.11.

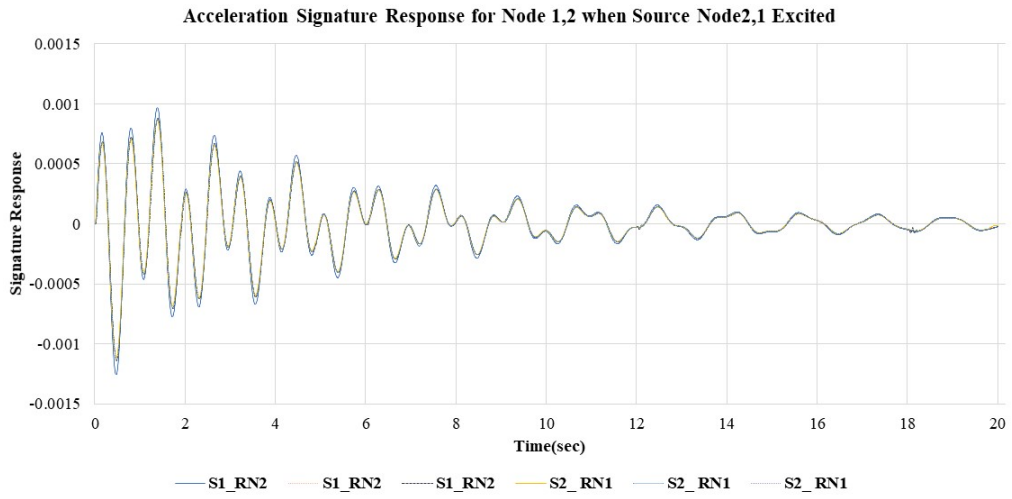

Figure 4.11: Using acceleration response for extracting B-DSR for MDF

Figure 4.11 shows that when any arbitrary force is applied at *node*1 the extracted B-DSR at *node*2 remain unchanged. The same is noted when *node*2 is extracted and *node*1 acceleration data is used for extracting the B-DSR. Moreover, the B-DSR are the same when *node*1 and 2 excited, and *node*2 and 1 are used, respectively, for extracting the B-DSR.

Chapter 5

Experimental Validation

5.1 Introduction

This section presents a series of laboratory experiments that were conducted to validate that the B-DSR can be extracted from experimental measurements. A cantilever structure has been excited at several points using a Modal hammer, and the time history of the accelerations are acquired through PCB accelerometers. The time history of the excitation force is also recorded. The force-response pairs are used to extract the B-DSR between the source and receiver points. The proposed approach is then validated by comparing measured and predicted acceleration histories to a known excitation. The laboratory setup and testing is discussed next along with the procedure to extract the B-DSR from measurements and its validation.

5.2 Laboratory Model Setup and Testing Sequence

Structure

The frame structure that was used for the validation study is shown in Figure 5.1. The overall dimensions of the frame are 455 inch X 64 inch and is made of rectangular hollow 5x4x3/16 structural steel shapes. The frame is considered fixed at one end and all connections are welded and considered rigid. At the free end of the frame, three concrete blocks are added to simulate a lumped mass at the end of the cantilever. The frame is a calibrated structure and its properties have been determined as mass, m =634 kg, natural frequency w_n=18.21 rad/sec , and damping ratio $\zeta = 0.6\%$.

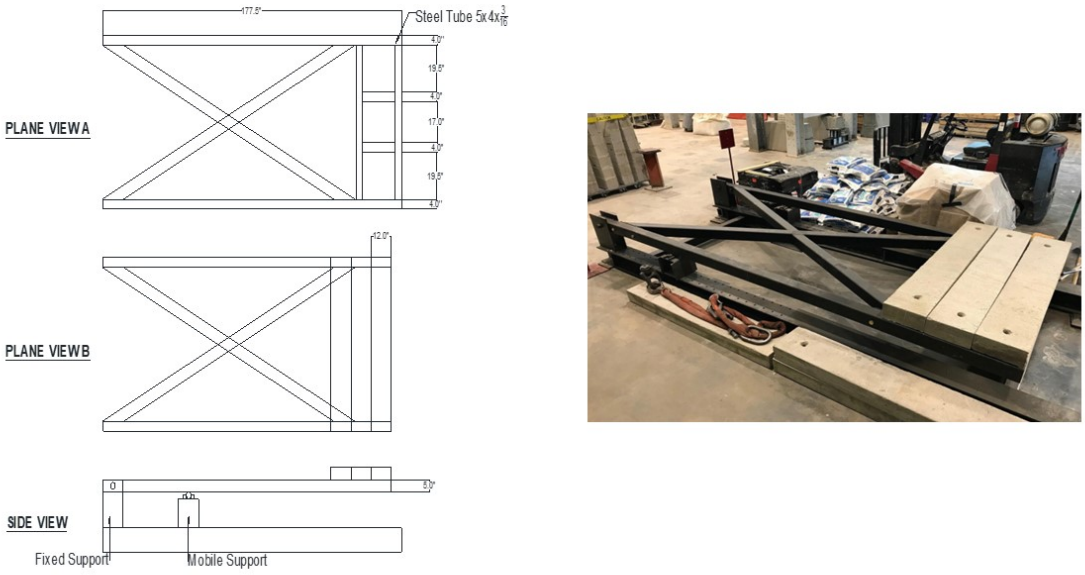

Figure 5.1: Laboratory frame structure

Instrumentation

with a sensitivity of 0.2305 mV/N , and is shown in Figure 5.2 .The maximum force that this hammer can record is ± 22240N. The force is applied at the eight different locations (source points P0-P7) shown in the frame diagram in Figure 5.3. The source points are marked by yellow dots on the picture of the frame shown in Figure 5.3. Acceleration measurements are recorded through an accelerometer and a data acquisition system. A single accelerometer is placed at the free end of the structure at location P0, as shown in Figure 5.3.The sensitivity of the accelerometer is 100 mVolts/g. The accelerometer and hammer are connected to a NI CompactDAQ data acquisition system with an NI9234 module, and LabVIEW for gathering data and controlling the experiment.

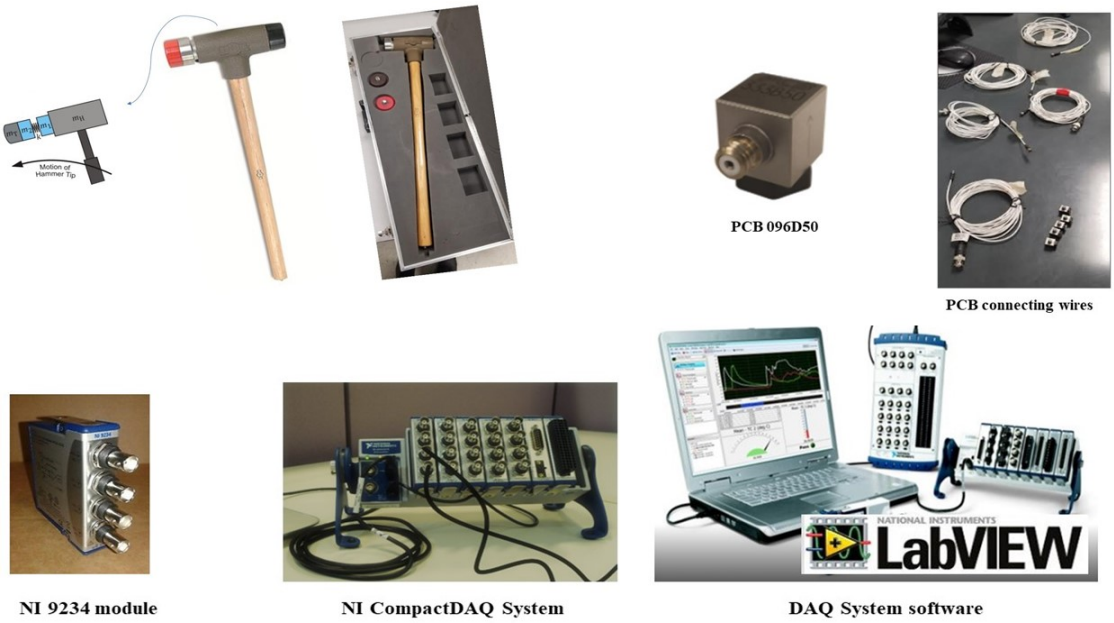

Figure 5.2: instrumentation and DAQ

Figure 5.3: instrumentation on Test Frame

Validation Test Procedure

Validation of the proposed concept is conducted through the following process. First, a pair of points is considered, i.e. the source point, P_s , and the receiver point, P_r. For each pair, two tests are conducted. In each test the source point is excited by a hammer blow and the force and acceleration time history at the source and receiver, respectively, is recorded. The first test provides the force and response records that are used to extract the B-DSR between P_s and P_r through Equation 4.5. The second test serves as the validation. To this end, the excitation force vector recorded in the second test and the B-DSR extracted in the first test are used in Equation 3.10 to predict the acceleration response which is then compared to the acceleration response as recorded in the second test. The validation is considered successful if the differences between the two are insignificant.

In this work, the sampling rate is set to s= 12800 samples/sec for both the force and acceleration records. The proposed method accommodates any B-Spline time step, $dt = \Delta T/4$, that is equal or greater to the sampling time step. To achieve this, the force and acceleration records are first filtered by a $n-$point rolling average as

$$\hat{r}_i = \sum_{j=i-n}^{i+n} r_i(2n+1) \tag{5.1}$$

where r_i is the value of the record at sample i, and the number of points, n, is defined as

$$n = 1/(s\ dt) \tag{5.2}$$

Subsequently, the records are resampled at a time step, $dt = \Delta T/4$, that defines the B-Spline. The initial segment of both records is trimmed up to the initial application of the load and the time axis shifted to zero to align the time with the initial

load value. In addition, the tail of each record is trimmed when the amplitude diminishes. The filtering and resampling tasks are performed using the in-house software "TRACE" developed for this purpose. The software interface is shown in Figure 5.4.

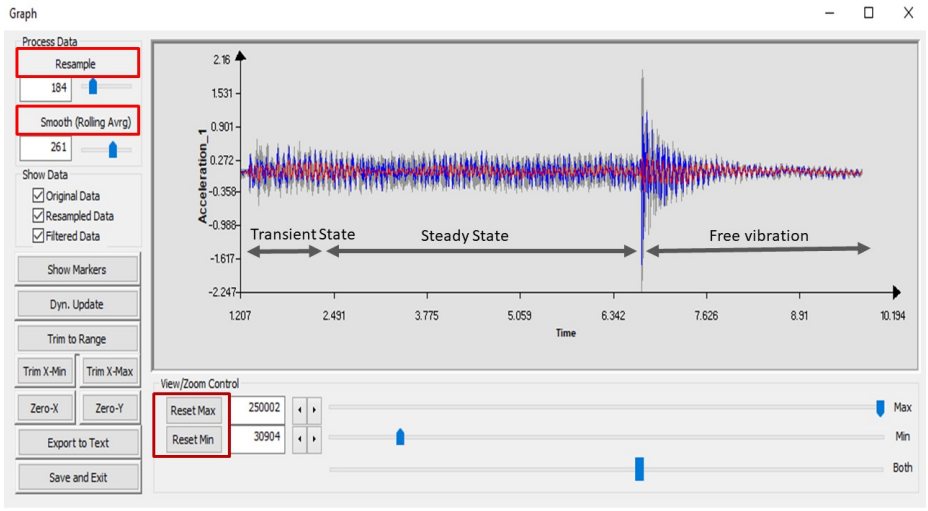

(a) Original Record

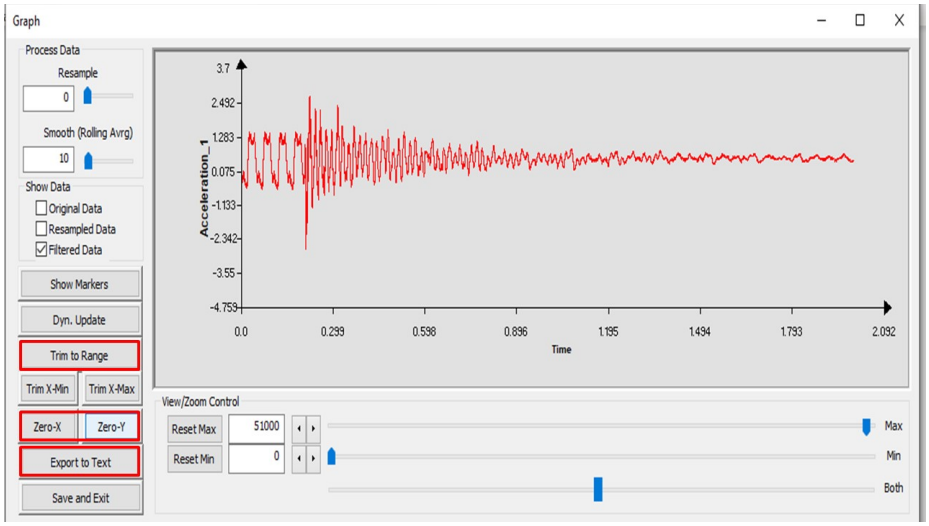

(b) After Filtering and Trimming

Figure 5.4: In-house software TRACE

Data Analysis and Results

For data analysis and in order to distinguish the B-DSR for each pair of points, the following convention is adopted. Each of the dynamic signature responses is denoted as $B - DSR_{ij}$ where i indicates the P_i receiver point and P_j indicates the

source point. For example, B-DSR01 corresponds to the dynamic signature response between P1 (source) and P0 (receiver). The B-DSR are expected to remain the same for each source-receiver pair. Figure5.5 shows the validation of B-DSR00. In particular, Figure 5.5a shows the experimental data of one test when P0 is excited by a hammer blow and the acceleration is recorded at P0. Figure 5.5b shows the B-DSR00 as extracted through Equation 4.5 from the measurement of this test. Subsequently, P0 is excited for a second time by a different hammer blow and the acceleration at P0 is recorded. The new recorded force time history is used with B-DSR00 to estimate the acceleration response at P0 and is compared in Figure 5.5c with the measured acceleration at the same point. The two curves are in excellent agreement. Similarly, Figures 5.5 - 5.12 show the validation of the B-DSR01 to B-DSR07 where it is also observed that the measured and predicted time histories are identical for all practical purposes.

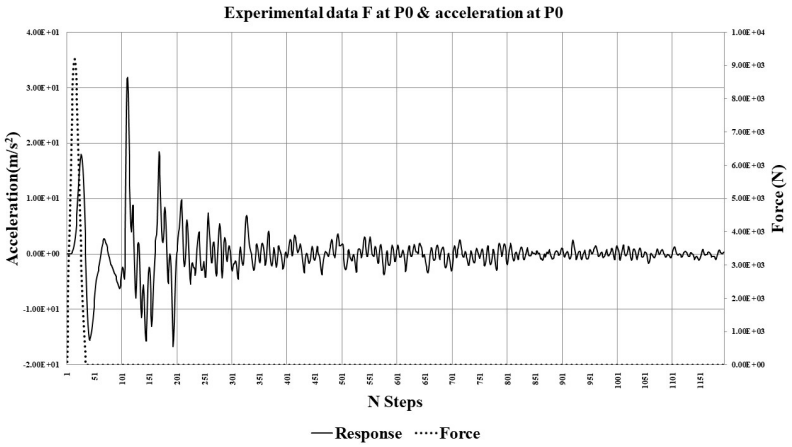

(a) Experimental Measurements

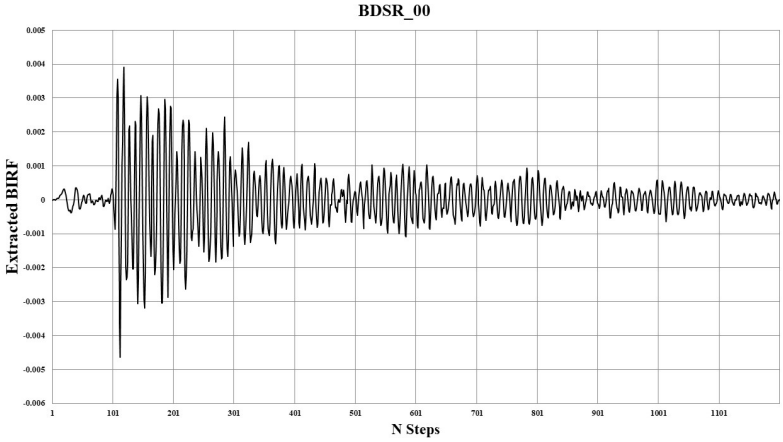

(b) Extracted B-DSR

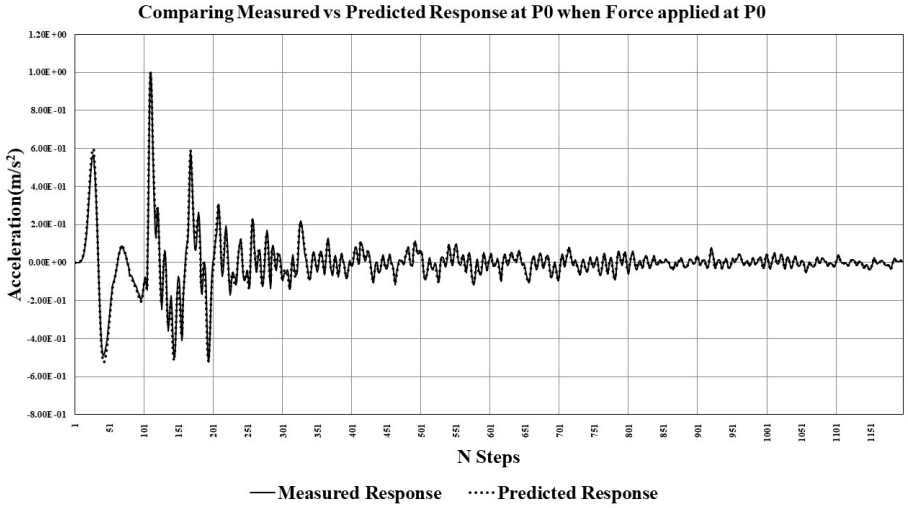

(c) Comparing Measured vs Predicted Response

Figure 5.5: Using Experimental data to Extract B-DSR_00 & Predict the Response at P0 when P0 is Excited.

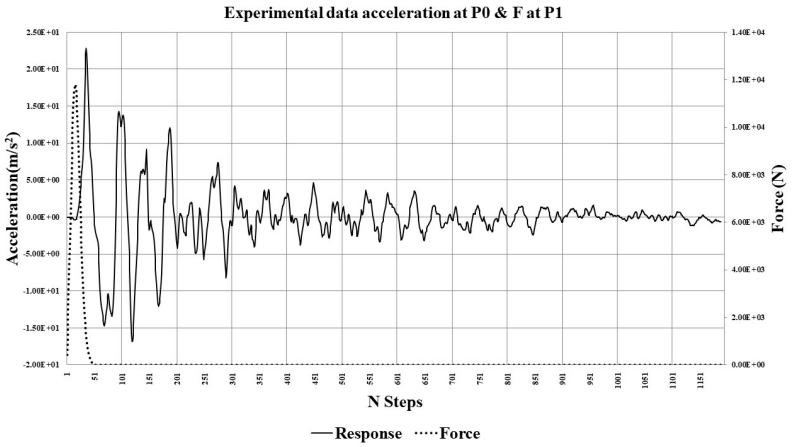

(a) Experimental Measurements

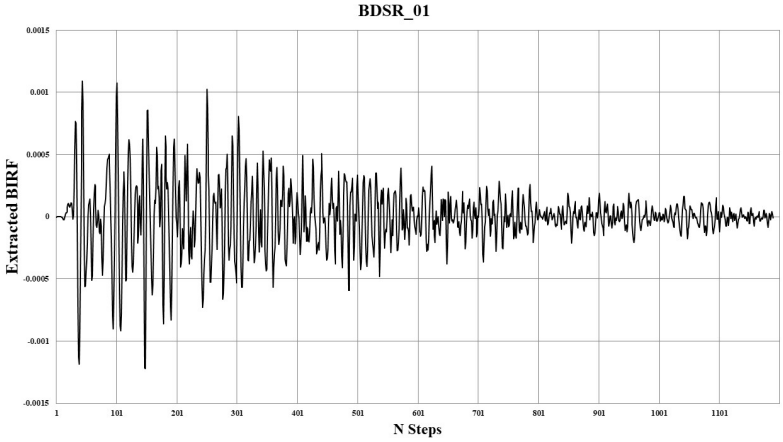

(b) Extracted B-DSR

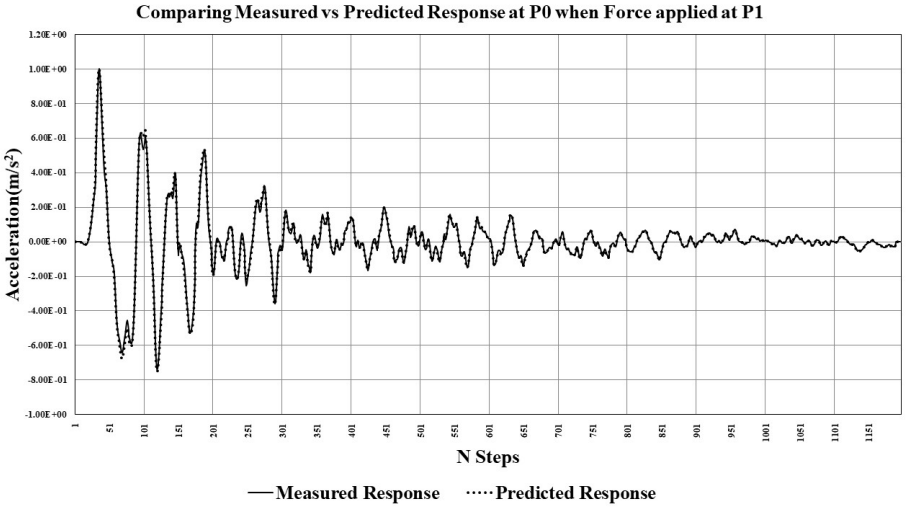

(c) Comparing Measured vs Predicted Response

Figure 5.6: Using Experimental data to Extract B-DSR_01 & Predict the Response at P0 when P1 is Excited.

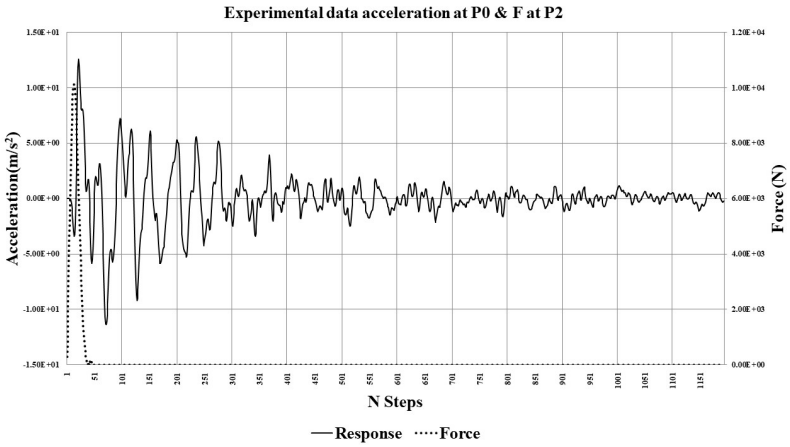

(a) Experimental Measurements

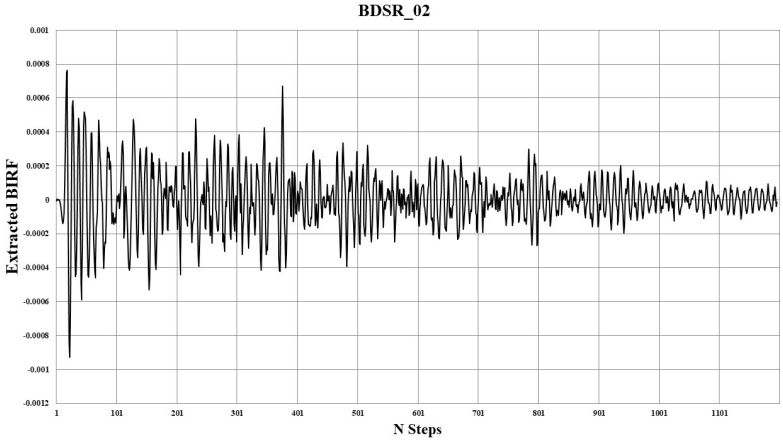

(b) Extracted B-DSR

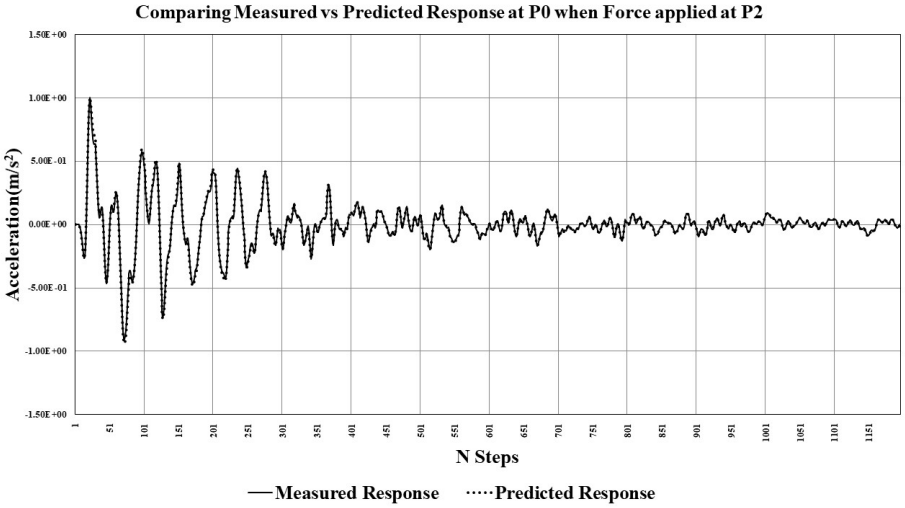

(c) Comparing Measured vs Predicted Response

Figure 5.7: Using Experimental data to Extract B-DSR_02 & Predict the Response at P0 when P2 is Excited.

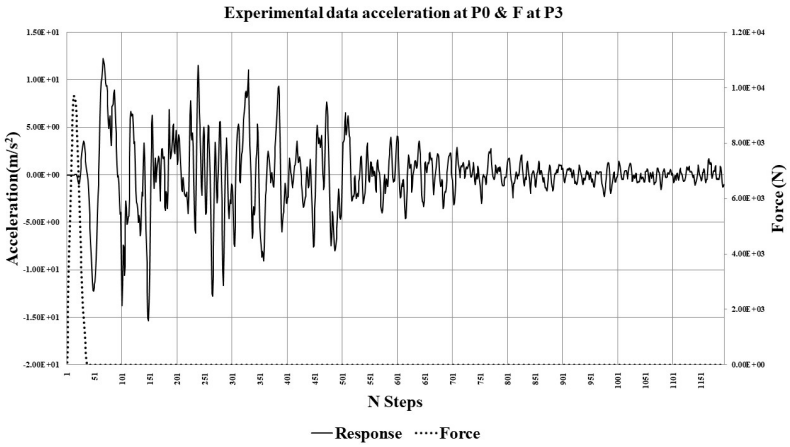

(a) Experimental Measurements

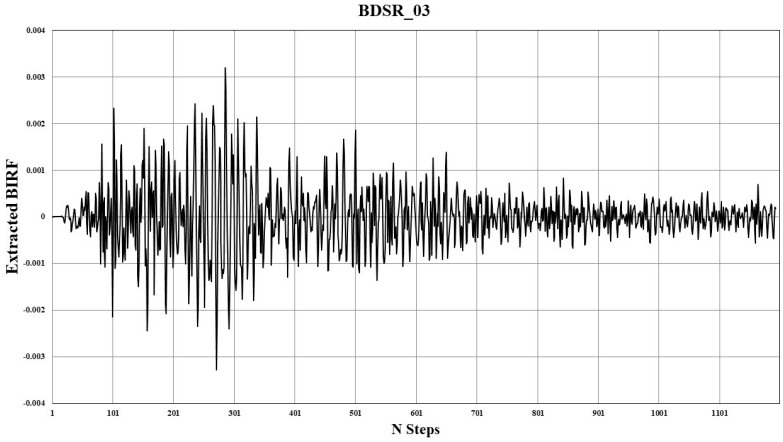

(b) Extracted B-DSR

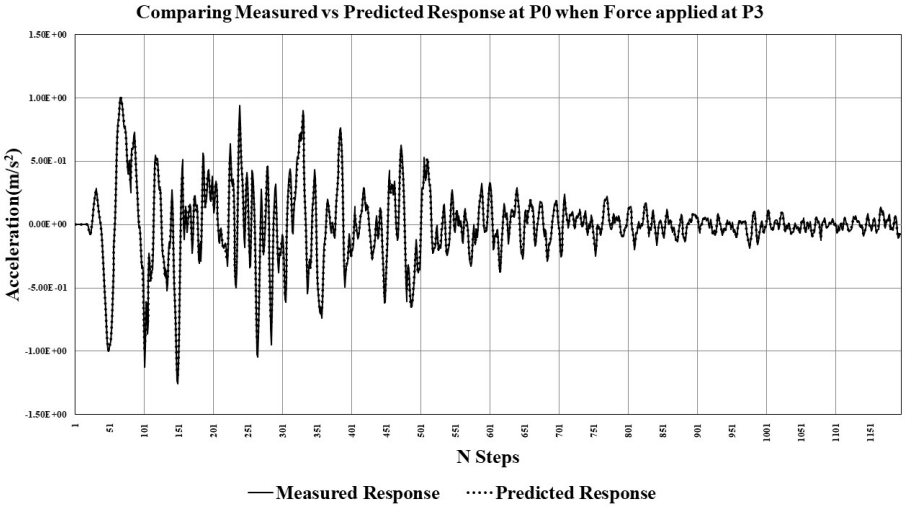

(c) Comparing Measured vs Predicted Response

Figure 5.8: Using Experimental data to Extract B-DSR_03 & Predict the Response at P0 when P3 is Excited.

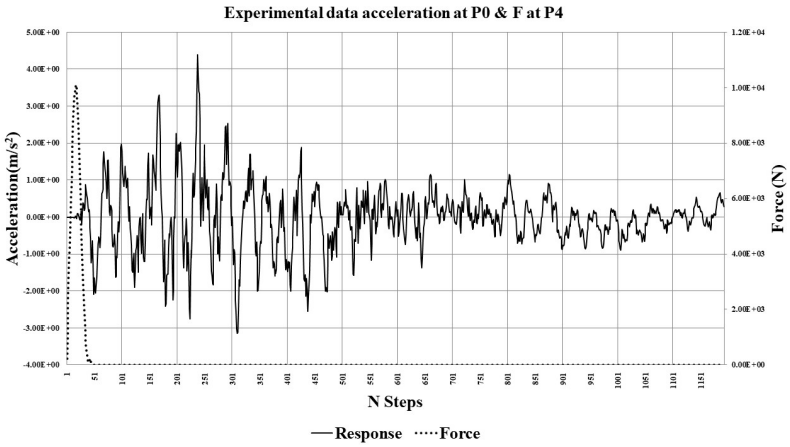

(a) Experimental Measurements

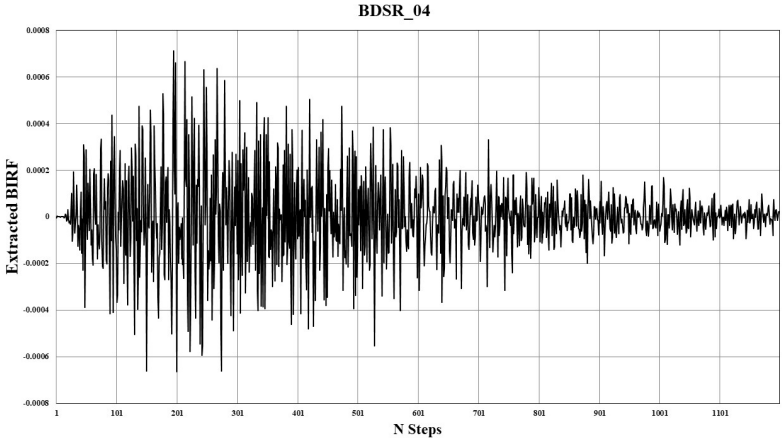

(b) Extracted B-DSR

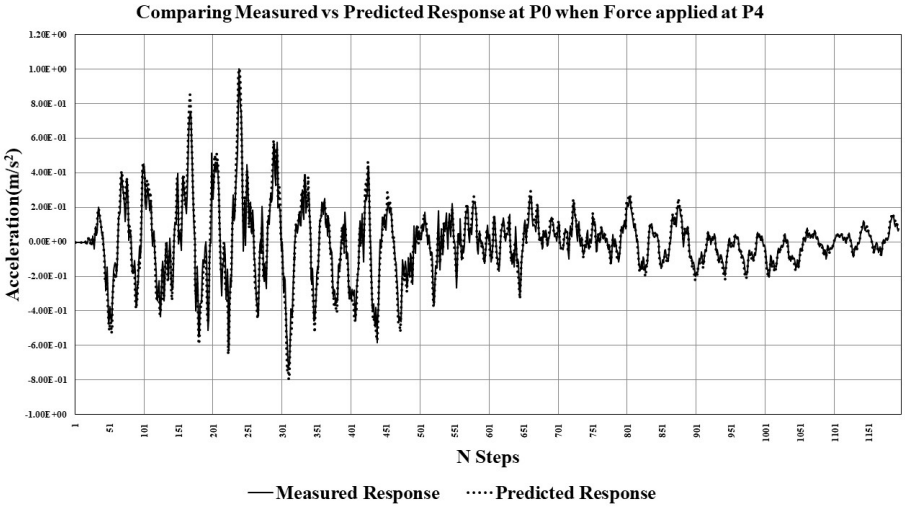

(c) Comparing Measured vs Predicted Response

Figure 5.9: Using Experimental data to Extract B-DSR_04 & Predict the Response at P0 when P4 is Excited.

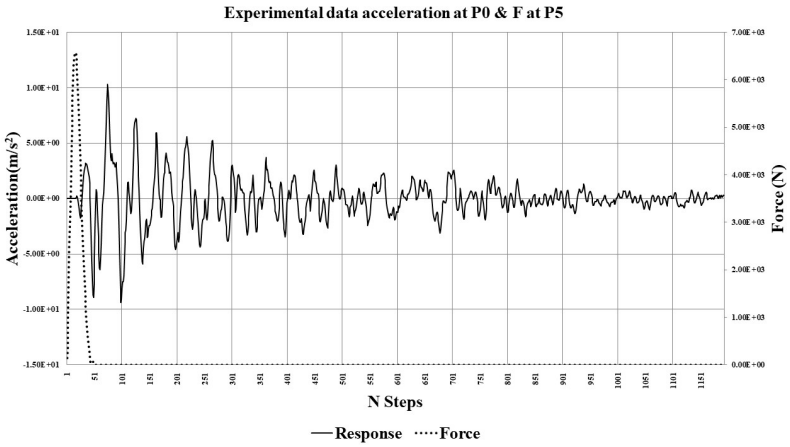

(a) Experimental Measurements

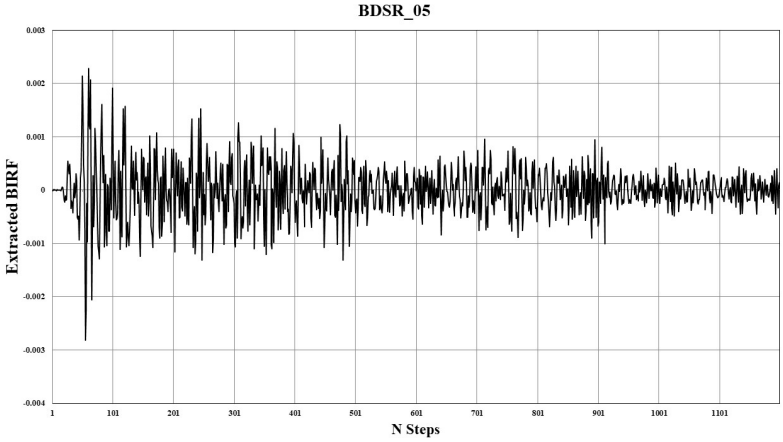

(b) Extracted B-DSR

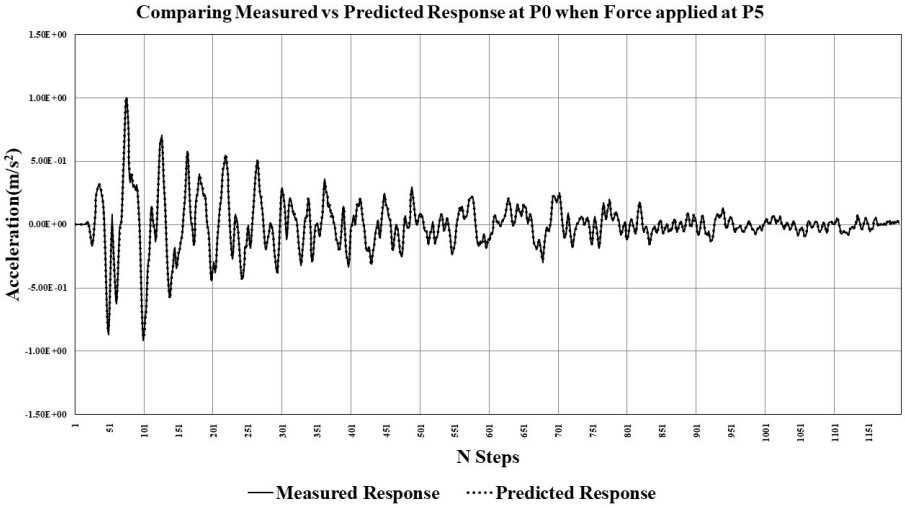

(c) Comparing Measured vs Predicted Response

Figure 5.10: Using Experimental data to Extract B-DSR_05 & Predict the Response at P0 when P5 is Excited.

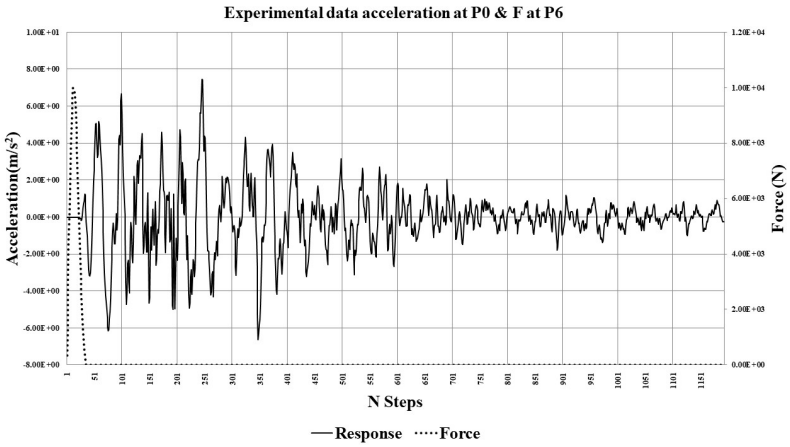

(a) Experimental Measurements

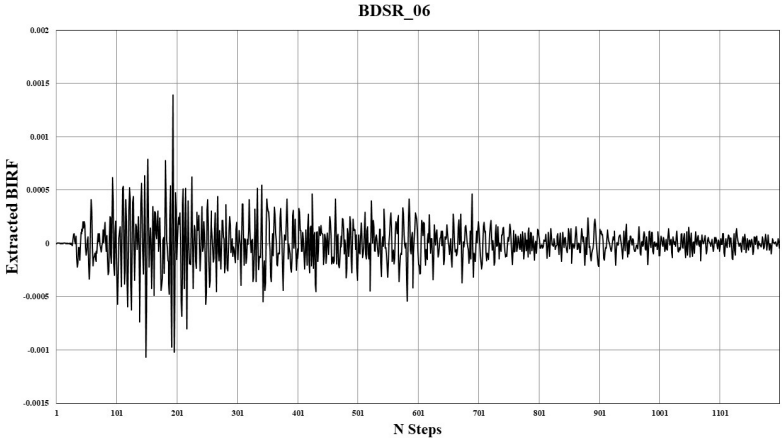

(b) Extracted B-DSR

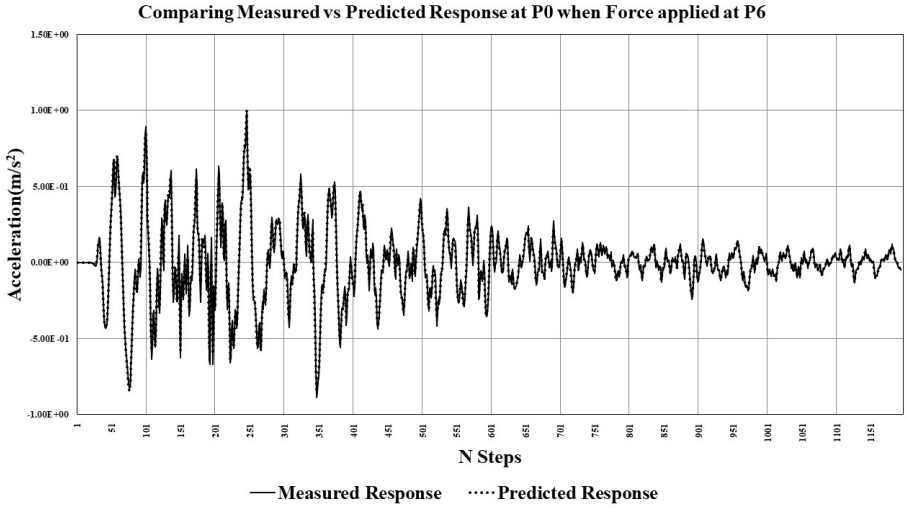

(c) Comparing Measured vs Predicted Response

Figure 5.11: Using Experimental data to Extract B-DSR_06 & Predict the Response at P0 when P6 is Excited.

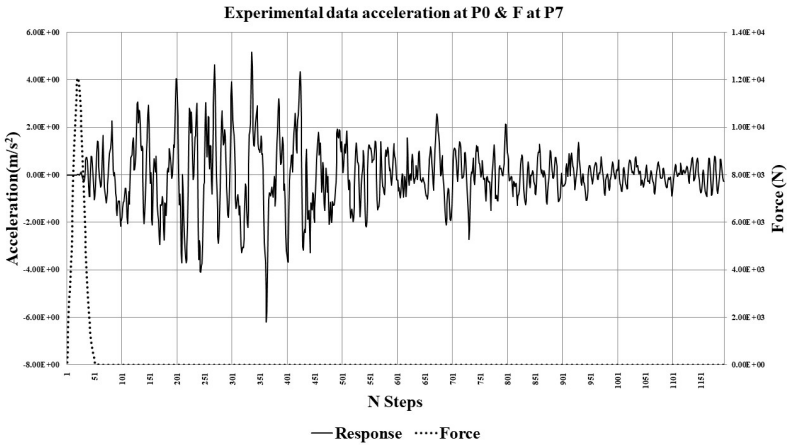

(a) Experimental Measurements

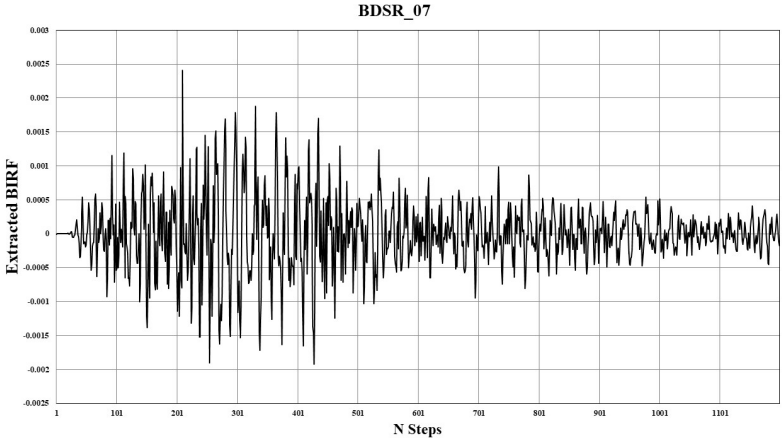

(b) Extracted B-DSR

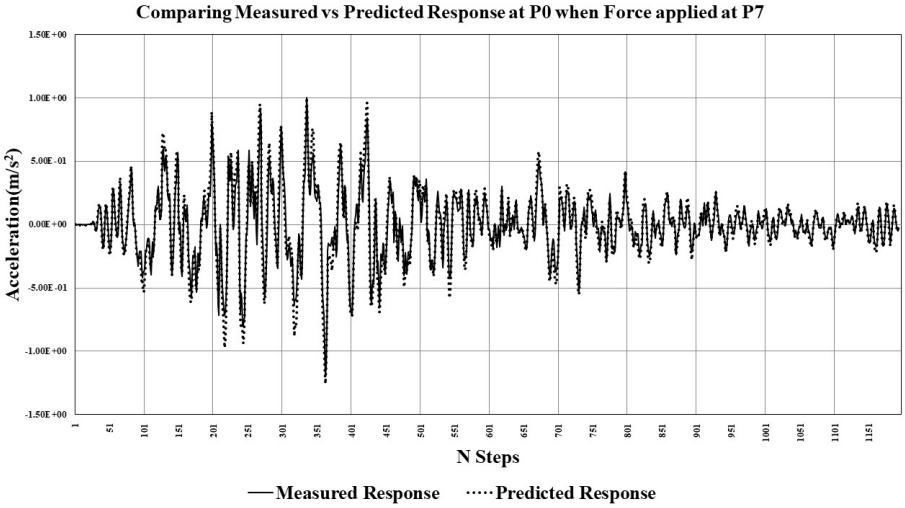

(c) Comparing Measured vs Predicted Response

Figure 5.12: Using Experimental data to Extract B-DSR_07 & Predict the Response at P0 when P7 is Excited.

Chapter 6

Implementation to Damage Detection

This chapter presents an implementation of the B-DSR to a damage detection procedure that was developed at the University of South Carolina. The damage detection integrates three technologies, i.e., wireless sensors that acquire vibration measurements, Unmanned Aircraft Systems (UAS) that deliver and install the sensor package to the bridge, or other structures and the proposed B-DSR that uses the vibration measurements to detect presence of damage within a change detection framework. Details of this initiative have been reported by the author of this thesis and his collaborators in [6]. The following sections discuss the implementation of the B-DSR in damage detection, as developed for integration with the other two technologies. Details on the sensor development, and drone operations and controls are beyond the scope of this thesis and can be found in [6].

6.1 Laboratory Model Setup and Testing Procedure

The laboratory model structure that was used in this study is the steel frame shown in Figure 6.1a. The frame is 6.5 feet wide, 6.5 feet tall and 2 feet deep. It consists of steel columns and beams and a 2ftx4ft steel plate is bolted on the beams at the story level. The arrangement of the bolts is shown in Figure 6.1b. A liner actuator equipped with a load cell is installed at the center on the top side of the plate, directly above accelerometer a2. A function generator drives the actuator at prescribed waveforms. All instrumentation is connected to a NI data acquisition system and controlled through LabVIEW.

The plate is excited by two harmonic excitations at 7 and 14 Hz. The loading at each frequency is repeated three times. It is noted that the natural frequency of the out-of-plane vibration mode of the steel plate is estimated at 12 Hz. Subsequently damage is introduced in the structure by removing 3 bolts that attach the plate to the frame, as shown in Figure 6.1b and another set of loadings is applied. In each loading case before and after damage the time history of the force and the accelerations are acquired at a 25.6 kHz sampling rate.

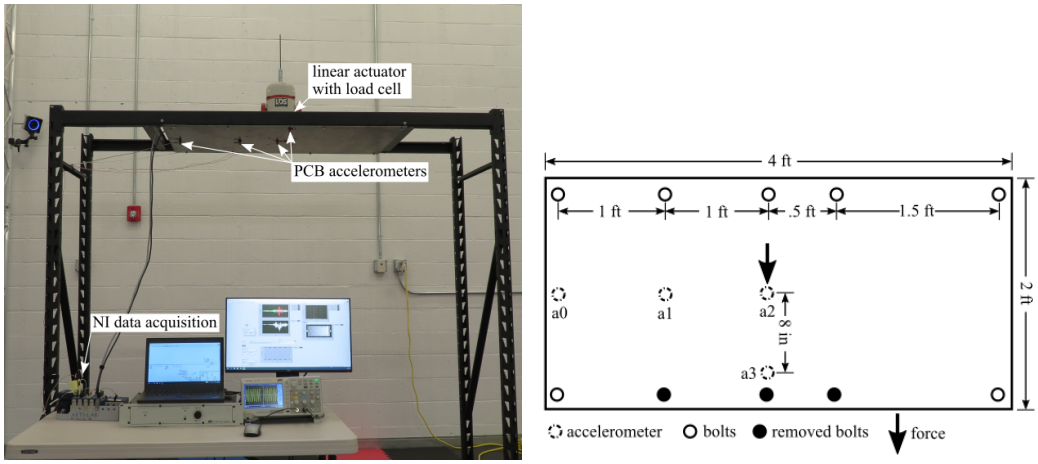

(a) Test Apparatus with Key Components Annotated

(b) Accelerometer Locations

Figure 6.1: Overview of the Test Setup and Experiment Tools

6.2 B-DSR EXTRACTION AND DAMAGE DETECTION

It is expected that any physical changes in the structure's configuration alter the B-DSR and, thus, the B-DSR is extracted for the "Before Damage" and "After Damage" cases. To this end, the acquired data were first pretreated and resampled as discussed in Chapter 5. The B-DSR in each case is then extracted using Equation 4.5. Figure 6.2a shows the B-DSR for the "Before Damage" case for each of the three tests. The high correlation coefficient shown in Figure 6.2b, demonstrates that the B-DSR remains essential the same. Figure 6.3a shows the B-DSR for the "After Damage" case for each of the three load tests. The high correlation coefficient shown in Figure

6.3b, demonstrates that the B-DSR also remains essential the same after damage has occurred. However, the correlation between the Before Damage and After Damage B-DSR is significantly reduced as demonstrated in Figure 6.4 The loss of correlation indicates presence of damage in the structure.

A similar process has been conducted for a test frame loaded with the 14 Hz Cyclic load. The B-DSR is extracted for all cases and similar conclusions were reached. Table 6.1 presents the correlation coefficient for all source-receiver excitation pairs before and after damage, the two excitation frequencies and between any two tests. It is demonstrated the B-DSR does not depend on the external load but is highly affected by the change in the physical structure. The analysis results for all other tests are included in the Appendices. Appendix A shows the results of the B-DSR extracted from the force vibration stage when voltage force used for extracting the B-DSR. Appendix B shows the the results of the B-DSR extracted from the force vibration stage using the recorded load cell force for extracting the B-DSR. Similarly Appendix C and D shows the results on the B-DSR extracted from the free vibration stage using voltage and load cell.

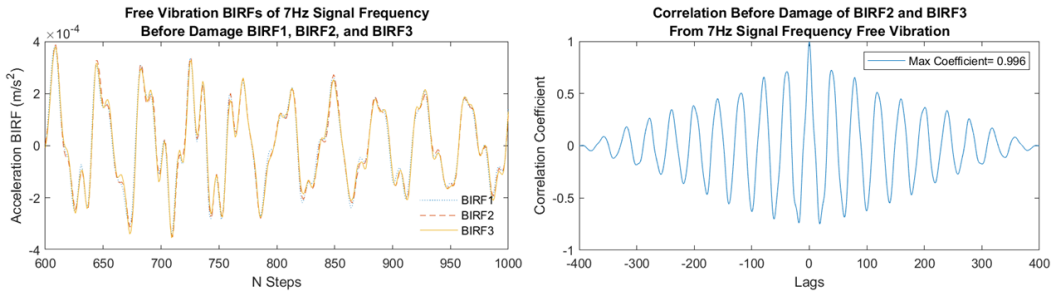

(a) (b)

Figure 6.2: Comparison of B-DSR Before Damage and Correlation

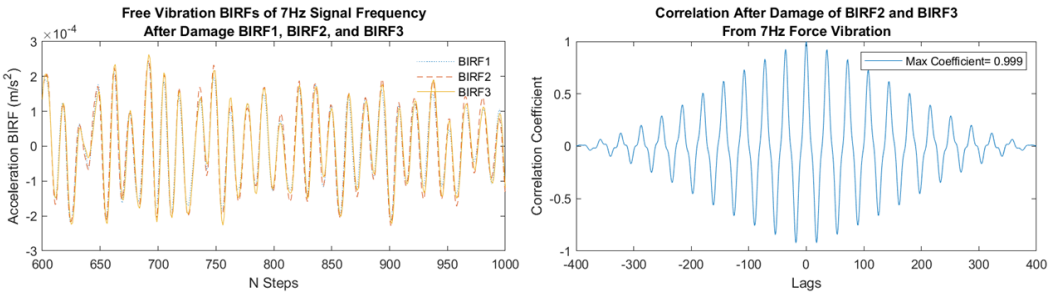

(a) (b)

Figure 6.3: Comparison of B-DSR After Damage and Correlation

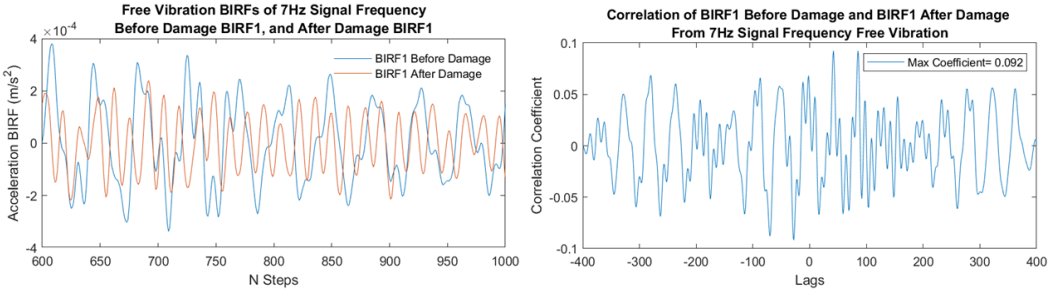

(a) (b)

Figure 6.4: Comparison of B-DSR Before and After Damage and Correlation

Table 6.1: Summary of The Results

			Before Damage						After Damage					
			7 Hz			14 Hz			7 Hz			14 Hz		
		Test	1	2	3	1	2	3	1	2	3	1	2	3
Before Damage	7 Hz	1	1	0.991	0.99	0.897	0.885	0.883	0.092	0.079	0.092	0.077	0.076	0.067
		2		1	0.996	0.902	0.886	0.885	0.093	0.085	0.094	0.067	0.065	0.057
		3			1	0.898	0.878	0.878	0.096	0.091	0.085	0.061	0.06	0.051
	14 Hz	1				1	0.939	0.94	0.07	0.065	0.067	0.053	0.055	0.05
		2					1	1	0.08	0.07	0.076	0.067	0.054	0.054
		3						1	0.08	0.069	0.076	0.066	0.053	0.052
After Damage	7 Hz	1							1	0.99	0.972	0.86	0.873	0.863
		2								1	0.977	0.875	0.876	0.876
		3									1	0.867	0.873	0.873
	14 Hz	1										1	0.99	0.995
		2											1	0.993
		3												1

Chapter 7

Conclusion and Future Work

This paper presents a methodology for extracting dynamic signature response using B-spline impulse response function. The B-DSR verified using numerical and experimental approaches. Form the numerical approach, using different load cases to extract the B-DSR was feasible. Experimentally, it was challenging to extract the B-DSR using the force vibration response of the structure, however, the free vibration was practical to extract the B-DSR. The proposed method implemented in drone-based vibration monitoring and assessment of structures, a normalized cross correlation for quantifying the similarities of the signals used. The method successfully captured the damage and gave a clear indication that the dynamic signature state has changed once damage introduced. Below are some improvements that can be addressed for future work;

Chapter 4: Identification of Dynamic Signature Response

Using displacement as a response was more favorable instead of using acceleration as a response based on the numerical approach when damping is low or there is no damping.

Chapter 5: Experimental Validation

Shorter path between the source and the receiver gives better quality of B-DSR because stronger signal and easier to synchronization. Also, for future work, Trace,in-house program, can be adjusted to filter all data for all nodes and force at the same

time. Moreover, Trace can include algorithm to extract B-DSR directly.

Chapter 6: Implementation to Damage Detection

Using free vibration instead of the force vibration provides higher correlation values. The method should be expanded to compute the BIRF without the forcing function. Future work, should focus on how B-DSR can be used for quantifying and localizing damage(Level 2 and 3).

Bibliography

[1] M Abdo. "Structural health monitoring, history, applications and future". In: *A review book. Open Science* (2014).

[2] M.A.-B. Abdo. "Structural Health Monitoring, History, Applications and Future". en. In: *A Reviw Book* (2014).

[3] A.Furukawa Aiko and J. Kiyono. "Identification of Structural Damage Based on Vibration Responses". en. In: *13 WCEE CANADA 2004*. Vancouver, 2004.

[4] Randall J Allemang. "The modal assurance criterion–twenty years of use and abuse". In: *Sound and vibration* 37.8 (2003), pp. 14–23.

[5] A Alvandi and C Cremona. "Assessment of vibration-based damage identification techniques". In: *Journal of sound and vibration* 292.1-2 (2006), pp. 179–202.

[6] Sabrina Carroll et al. "Drone-Based Vibration Monitoring and Assessment of Structures". In: *Applied Sciences* 11.18 (2021), p. 8560.

[7] F.R. Charles and D.W. Scott. "An Overview of Modal-Based Damage Identification Methods". en. In: *Proceedings of DAMAS conference*. 1997.

[8] Phillip Cornwell, Scott W Doebling, and Charles R Farrar. "Application of the strain energy damage detection method to plate-like structures". In: *Journal of sound and vibration* 224.2 (1999), pp. 359–374.

[9] RO Curadelli et al. "Damage detection by means of structural damping identification". In: *Engineering Structures* 30.12 (2008), pp. 3497–3504.

[10] Ulrike Dackermann. "Vibration-based damage identification methods for civil engineering structures using artificial neural networks". PhD thesis. 2009.

[11] Swagato Das, P Saha, and SK Patro. "Vibration-based damage detection techniques used for health monitoring of structures: a review". In: *Journal of Civil Structural Health Monitoring* 6.3 (2016), pp. 477–507.

[12] Arya Datta et al. “A robust non-iterative algorithm for multi-body dynamics and vehicle–structure interaction analysis”. In: *Vehicle System Dynamics* (2020), pp. 1–19.

[13] Carl. De Boor. *A practical guide to splines / Carl de Boor*. English. Springer-Verlag New York, 1978, xxiv, 392 p. : ISBN: 0387903569 3540903569.

[14] S.W. Doebling, C.R. Farrar, and M.B. Prime. “A summary review of vibration-based damage identification methods”. en. In: *The Shock and Vibration Digest* 30 (1998), pp. 91–105.

[15] Anjan Dutta and S Talukdar. “Damage detection in bridges using accurate modal parameters”. In: *Finite Elements in Analysis and Design* 40.3 (2004), pp. 287–304.

[16] David J Ewins. *Modal testing: theory, practice and application*. John Wiley & Sons, 2009.

[17] Charles R Farrar and Scott W Doebling. “An overview of modal-based damage identification methods”. In: (1997).

[18] C.-P. Fritzen and P. Kraemer. “Self-diagnosis of smart structures based on dynamical properties”. In: *Mechanical Systems and Signal Processing* 23.6 (2009). Special Issue: Inverse Problems, pp. 1830–1845. ISSN: 0888-3270. DOI: https://doi.org/10.1016/j.ymssp.2009.01.006. URL: https://www.sciencedirect.com/science/article/pii/S0888327009000119.

[19] N Hallermann and G Morgenthal. “The application of unmanned aerial vehicles for the inspection of structures”. In: *Proc. of PLSE* (2012), pp. 1085–1095.

[20] Vanessa Mary Heckman. “Damage Detection in Civil Structures using High-Frequency Seismograms”. en. In: *Dissertation (Ph.D.), California Institute of Technology*. 2014. DOI: 10.7907/NVKN-8D47..

[21] Siti Nadia Jamian. “Application video borescope in building inspection”. In: (2014).

[22] S Graham Kelly. *Mechanical vibrations: theory and applications*. Cengage learning, 2012.

[23] Seth S Kessler et al. “Damage detection in composite materials using frequency response methods”. In: *Composites Part B: Engineering* 33.1 (2002), pp. 87–95.

[24] L. Leon, D.C. Rizos, and L.M. Caicedo. “A Procedure to Develop Scalable Models for the Transient Response of Sleepers in Conventional and High-Speed

Railway Lines and Implementation to the Vertical Vibration Mode". en. In: *Soil Dynamics and Earthquake Engineering* 31 (2011), pp. 506–511.

[25] Hao Li, Zhongrong Lu, and Jike Liu. "Structural damage identification based on residual force vector and response sensitivity analysis". In: *Journal of Vibration and Control* 22.11 (2016), pp. 2759–2770.

[26] Zakriya Mohammed, Ibrahim Abe M Elfadel, and Mahmoud Rasras. "Monolithic multi degree of freedom (MDoF) capacitive MEMS accelerometers". In: *Micromachines* 9.11 (2018), p. 602.

[27] Subhajit Mondal et al. "Damage detection in beams using frequency response function curvatures near resonating frequencies". In: *Advances in Structural Engineering*. Springer, 2015, pp. 1563–1573.

[28] John J. Moughty and Joan R. Casas. "A State of the Art Review of Modal-Based Damage Detection in Bridges: Development, Challenges, and Solutions". In: *Applied Sciences* 7.5 (2017). ISSN: 2076-3417. DOI: 10.3390/app7050510. URL: https://www.mdpi.com/2076-3417/7/5/510.

[29] J Mulliken and DC Rizos. "A coupled computational method for multi-solver, multi-domain transient problems in elastodynamics". In: *Soil Dynamics and Earthquake Engineering* 34.1 (2012), pp. 78–88.

[30] J O'brien and DC Rizos. "A 3D BEM-FEM methodology for simulation of high speed train induced vibrations". In: *Soil Dynamics and Earthquake Engineering* 25.4 (2005), pp. 289–301.

[31] H Abdul Razak and FC Choi. "The effect of corrosion on the natural frequency and modal damping of reinforced concrete beams". In: *Engineering structures* 23.9 (2001), pp. 1126–1133.

[32] D.C. Rizos and D.L. Karabalis. "A Time Domain BEM for 3-D Elastodynamic Analysis using the B Spline Fundamental Solutions". et. In: *Soil Dynamics and Earthquake Engineering* 22 (1998), pp. 108–115.

[33] D.C. Rizos and K. Loya. "Dynamic and Seismic Analysis of Foundations Based on Free Field B-Spline Characteristic Response Histories". en. In: *ASCE Journal of Engineering mechanics* 128.4 (2002), pp. 438–447.

[34] DC Rizos. "A rigid surface boundary element for soil-structure interaction analysis in the direct time domain". In: *Computational Mechanics* 26.6 (2000), pp. 582–591.

[35] DC Rizos and DL Karabalis. “An advanced direct time domain BEM formulation for general 3-D elastodynamic problems”. In: *Computational Mechanics* 15.3 (1994), pp. 249–269.

[36] DC Rizos and Z Wang. “Coupled BEM–FEM solutions for direct time domain soil–structure interaction analysis”. In: *Engineering Analysis with Boundary Elements* 26.10 (2002), pp. 877–888.

[37] Dimitrios C. Rizos. “Advanced time domain boundary element method for general three-dimensional elastodynamic problems”. English. Copyright - Database copyright ProQuest LLC; ProQuest does not claim copyright in the individual underlying works; Last updated - 2021-04-21. PhD thesis. 1993, p. 165. URL: https://login.pallas2.tcl.sc.edu/login?url=https://www-proquest-com.pallas2.tcl.sc.edu/dissertations-theses/advanced-time-domain-boundary-element-method/docview/304057762/se-2?accountid=13965.

[38] A. Sabamehr, C. Lim, and A. Bagchi. “System identification and model updating of highway bridges using ambient vibration tests”. en. In: *Journal of Civil Structural Health Monitoring* 8.5 (Nov. 2018), pp. 755–771.

[39] S Sankarasrinivasan et al. “Health monitoring of civil structures with integrated UAV and image processing system”. In: *Procedia Computer Science* 54 (2015), pp. 508–515.

[40] Edward Sazonov and Powsiri Klinkhachorn. “Optimal spatial sampling interval for damage detection by curvature or strain energy mode shapes”. In: *Journal of Sound and Vibration* 285.4 (2005), pp. 783–801. ISSN: 0022-460X. DOI: https://doi.org/10.1016/j.jsv.2004.08.021. URL: https://www.sciencedirect.com/science/article/pii/S0022460X04007023.

[41] I. J. SCHOENBERG. “CONTRIBUTIONS TO THE PROBLEM OF APPROXIMATION OF EQUIDISTANT DATA BY ANALYTIC FUNCTIONS: PART A.—ON THE PROBLEM OF SMOOTHING OR GRADUATION. A FIRST CLASS OF ANALYTIC APPROXIMATION FORMULAE”. In: *Quarterly of Applied Mathematics* 4.1 (1946), pp. 45–99. ISSN: 0033569X, 15524485. URL: http://www.jstor.org/stable/43633538.

[42] I. J. SCHOENBERG. “CONTRIBUTIONS TO THE PROBLEM OF APPROXIMATION OF EQUIDISTANT DATA BY ANALYTIC FUNCTIONS: PART B—ON THE PROBLEM OF OSCULATORY INTERPOLATION. A SECOND CLASS OF ANALYTIC APPROXIMATION FORMULAE”. In: *Quarterly of Applied Mathematics* 4.2 (1946), pp. 112–141. ISSN: 0033569X, 15524485. URL: http://www.jstor.org/stable/43633544.

[43] SM Seyedpoor, A Ahmadi, and N Pahnabi. "Structural damage detection using time domain responses and an optimization method". In: *Inverse Problems in Science and Engineering* 27.5 (2019), pp. 669–688.

[44] Jean-Jacques Sinou. "A review of damage detection and health monitoring of mechanical systems from changes in the measurement of linear and non-linear vibrations". In: *Mechanical Vibrations: Measurement, Effects and Control*. Ed. by Robert C. Sapri. Nova Science Publishers, Inc., 2009, pp. 643–702. URL: https://hal.archives-ouvertes.fr/hal-00779322.

[45] Sandeep Sony, Shea Laventure, and Ayan Sadhu. "A literature review of next-generation smart sensing technology in structural health monitoring". In: *Structural Control and Health Monitoring* 26.3 (2019), e2321.

[46] W.J. Staszewski, C. Boller, and G.R. Tomlinson. *Health Monitoring of Aerospace Structure, West Sussex*. en. John Wiley Sons Ltd, 2004.

[47] E. Stehmeyer and D.C. Rizos. "B-Spline Impulse Response Function (BIRF) Model for the Transient SSI Analysis of Rigid Foundations". en. In: *Soil Dynamics and Earthquake Engineering* 26.5 (2006), pp. 421–434.

[48] Tadeusz Stepinski, Tadeusz Uhl, and W. J. Staszewski. *Advanced structural damage detection: from theory to engineering applications*. John Wiley amp; Sons Inc., 2013.

[49] Tadeusz Stepinski, Tadeusz Uhl, and Wieslaw Staszewski. "Advanced structural damage detection: from theory to engineering applications". In: (2013).

[50] Norris Stubbs, Jeong-Tae Kim, and Charles R Farrar. "Field verification of a nondestructive damage localization and severity estimation algorithm". In: *Proceedings-SPIE the international society for optical engineering*. SPIE International Society for Optical. 1995, pp. 210–210.

[51] Thomas Vetterlein and S Georgi. "Application of magnetic particle inspection in the field of the automotive industry". In: (2006).

[52] M.S.C. W. Ostachowicz. "Structural damage identification using damping: a compendium of uses and features". en. In: *Smart Materials and Structures* 26.4 (2017), p. 043001.

[53] Guirong Yan et al. "Structural damage detection using residual forces based on wavelet transform". In: *Mechanical Systems and Signal Processing* 24.1 (2010), pp. 224–239.

[54] Q.W. Yang and J.K. Liu. "Structural damage identification based on residual force vector". In: *Journal of Sound and Vibration* 305.1 (2007), pp. 298–307. ISSN: 0022-460X. DOI: https://doi.org/10.1016/j.jsv.2007.03.033. URL: https://www.sciencedirect.com/science/article/pii/S0022460X07002039.

[55] VD Zimin and DC Zimmerman. "Structural damage detection using time domain periodogram analysis". In: *Structural Health Monitoring* 8.2 (2009), pp. 125–135.

Appendix A

Force Vibration Results Using Voltage Data

Table A.1: Summary of Results Using force vibration 'Voltage'

Force Vibration results Using Voltage Data

			Before Damage						After Damage					
			7 Hz			14 Hz			7 Hz			14 Hz		
		Test	BD1	BD2	BD3	BD1	BD2	BD3	AD1	AD2	AD3	AD1	AD2	AD3
Before Damage	7 Hz	BD1	1.000	0.983	0.983	0.209	0.245	0.244	0.400	0.406	0.407	0.485	0.506	0.490
		BD2		1.000	0.995	0.215	0.252	0.242	0.394	0.404	0.400	0.487	0.511	0.491
		BD3			1.000	0.221	0.256	0.248	0.396	0.405	0.402	0.483	0.507	0.486
	14 Hz	BD1				1.000	0.964	0.962	0.148	0.150	0.149	0.494	0.486	0.475
		BD2					1.000	0.951	0.150	0.151	0.149	0.497	0.492	0.484
		BD3						1.000	0.158	0.157	0.158	0.518	0.511	0.502
After Damage	7 Hz	AD1							1.000	0.999	1.000	0.390	0.391	0.407
		AD2								1.000	0.999	0.390	0.392	0.402
		AD3									1.000	0.390	0.391	0.406
	14 Hz	AD1										1.000	0.988	0.988
		AD2											1.000	0.985
		AD3												1.000

A.1 7 Hz Before Damage

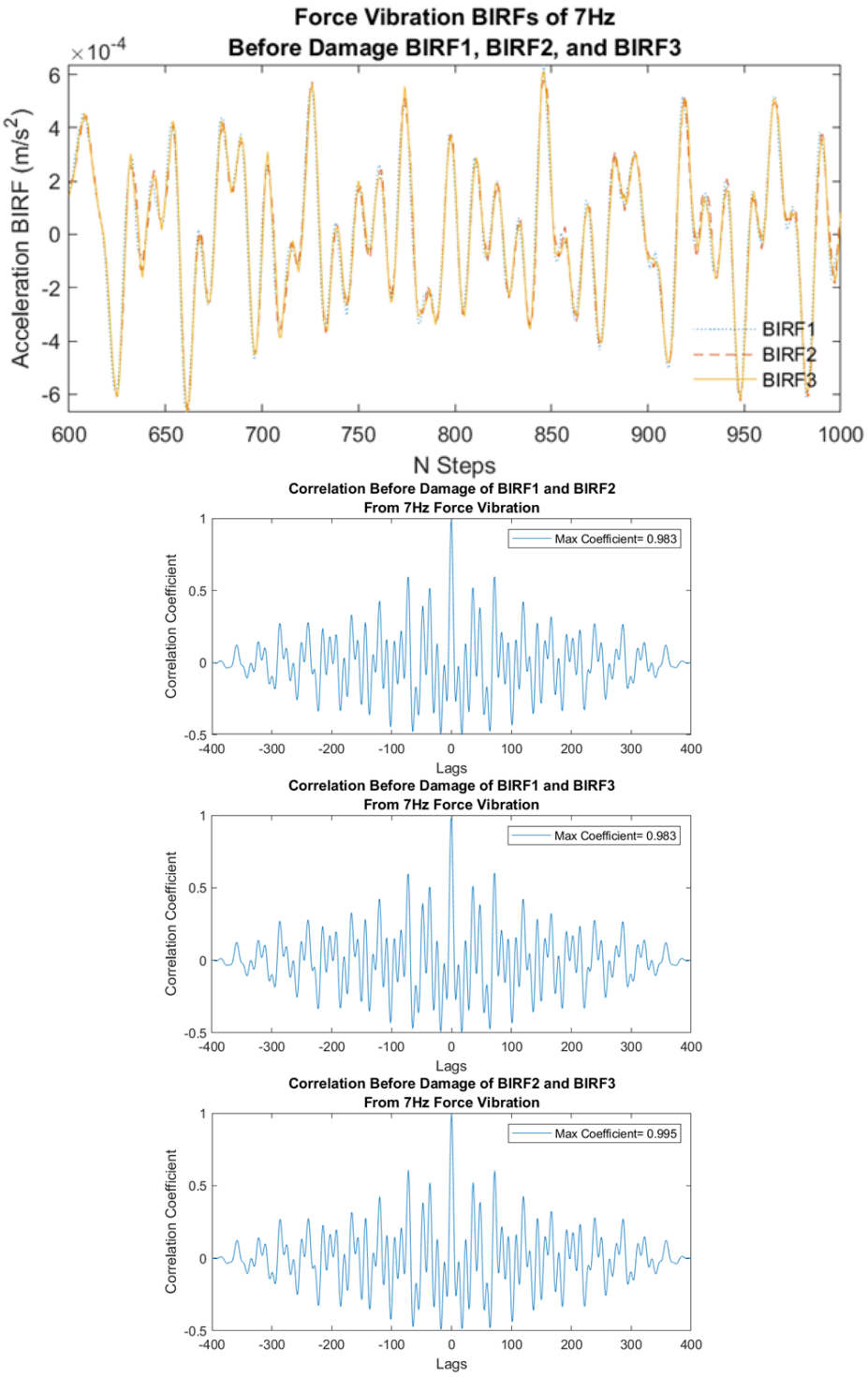

Figure A.1: 7Hz force vibration BIRFs before damage using voltage data

A.2 7 Hz After Damage

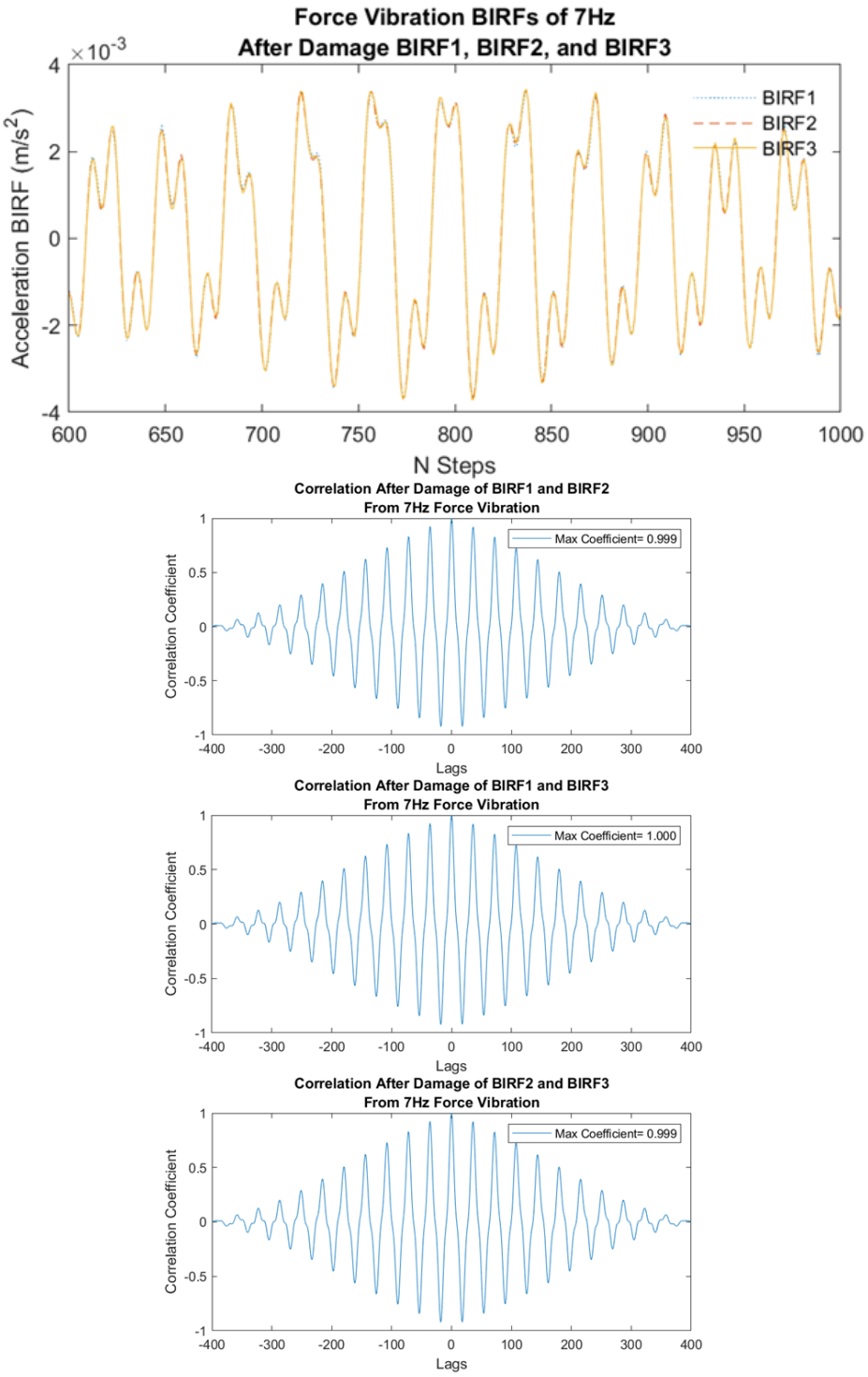

Figure A.2: 7Hz force vibration BIRFs after damage using voltage data

A.3 7 and 14 Hz Before Damage

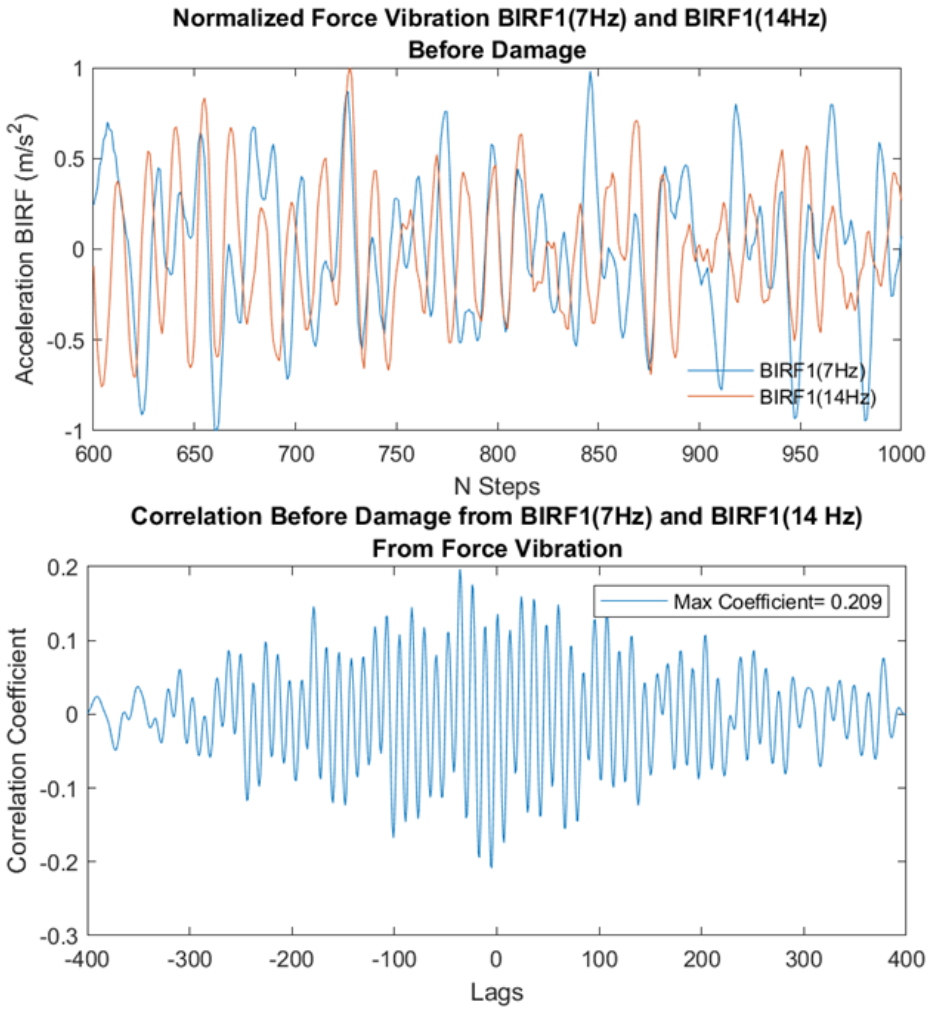

Figure A.3: 7 and 14Hz force vibration BIRFs before damage using voltage data

A.4 7 and 14 Hz After Damage

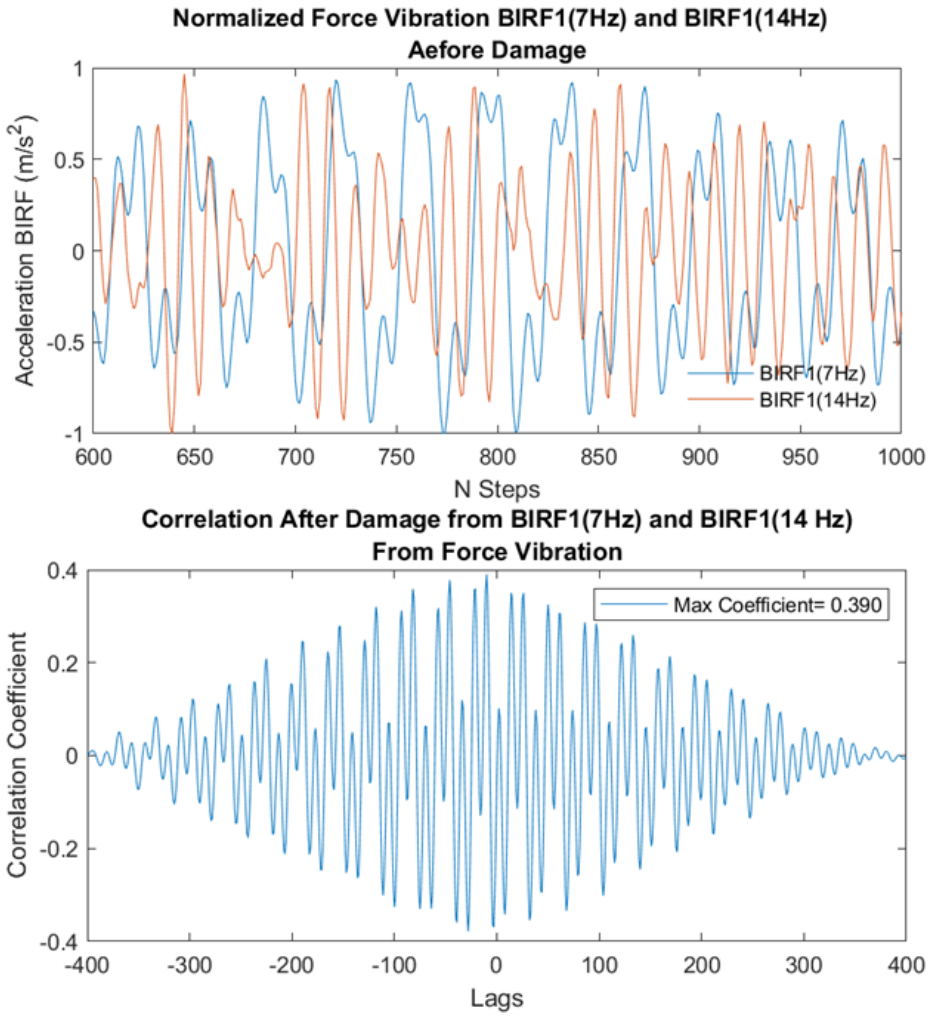

Figure A.4: 7 and 14Hz force vibration BIRFs after damage using voltage data

A.5 7Hz Before and After Damage

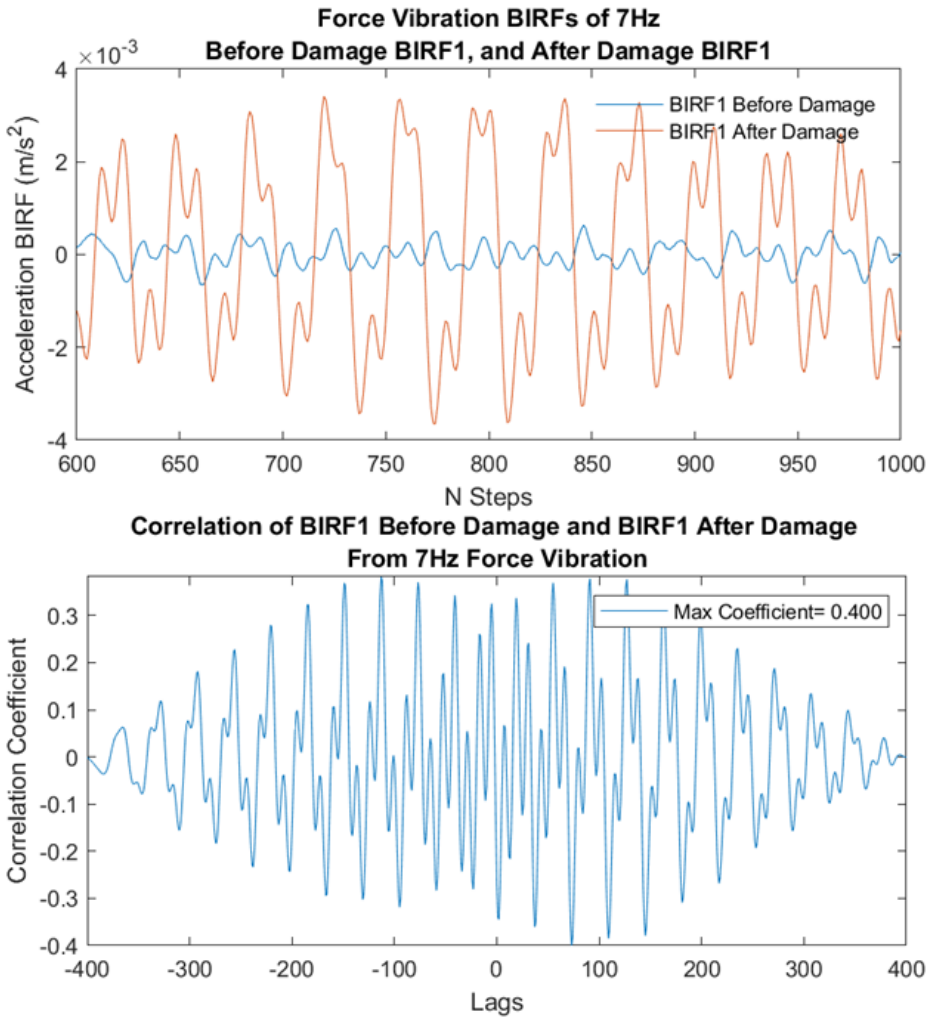

Figure A.5: 7Hz force vibration BIRFs before and after damage using voltage data

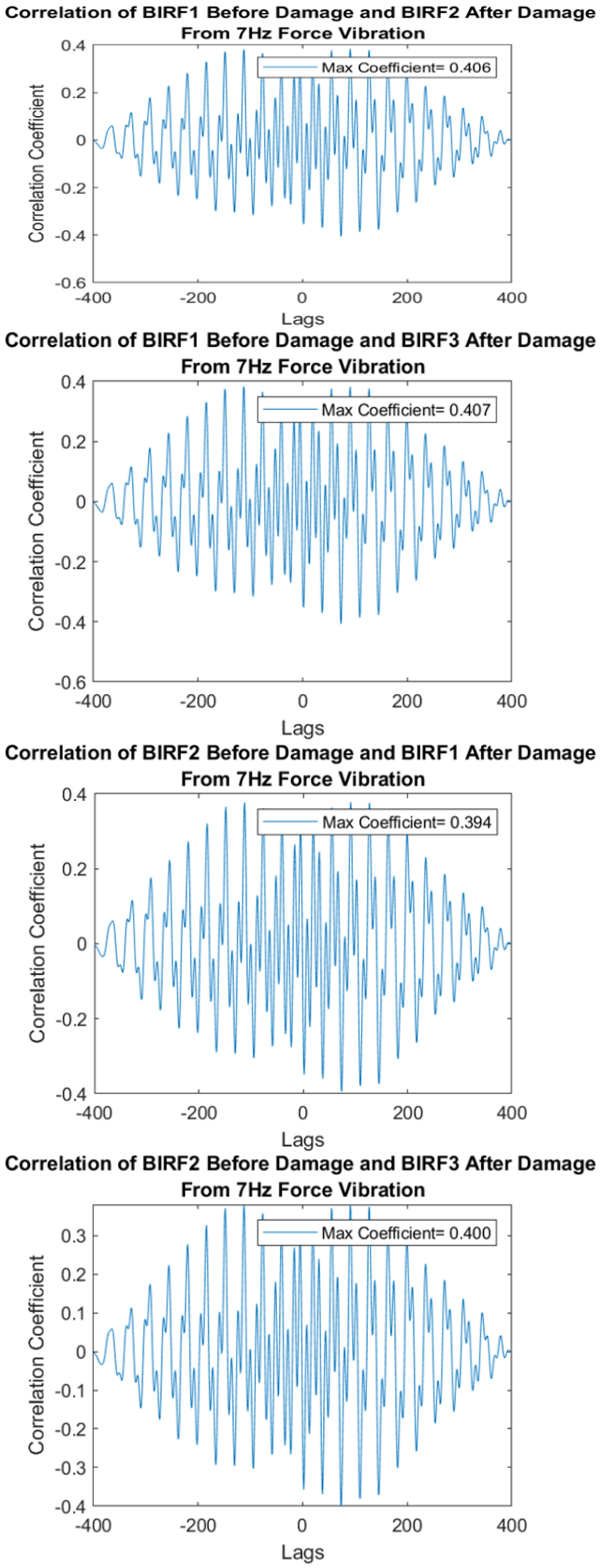

Figure A.6: Correlation values of 7Hz force vibration BIRFs before and after damage using voltage data 1

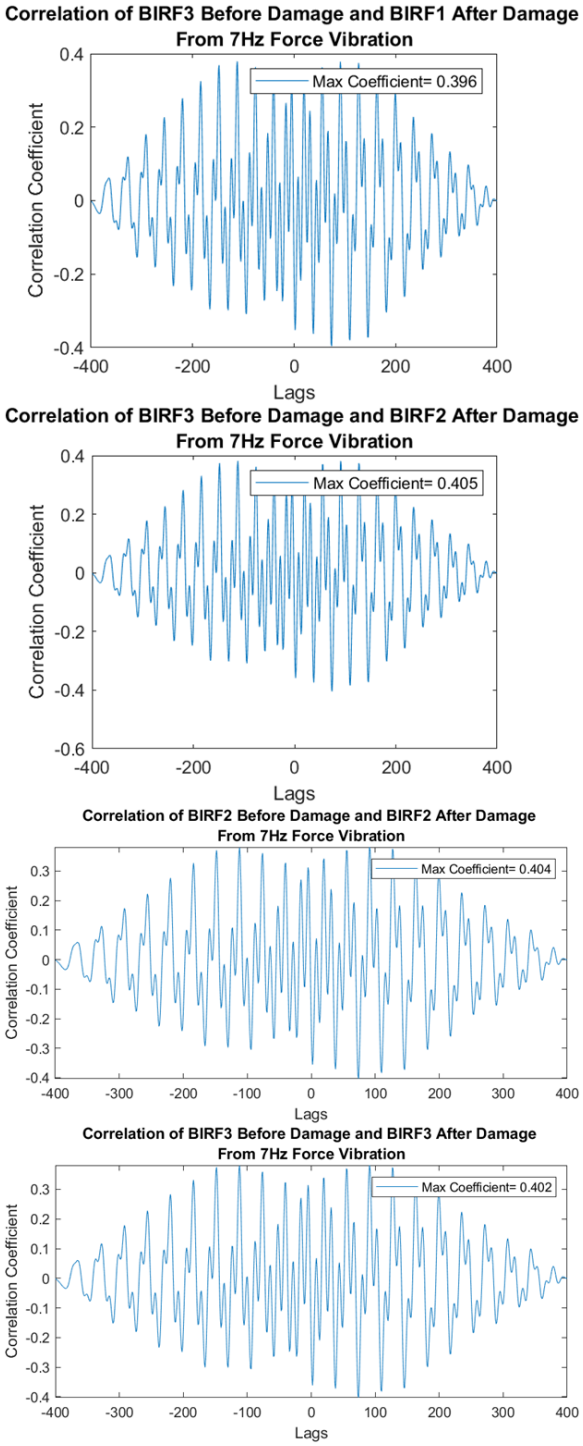

Figure A.7: Correlation values of 7Hz force vibration BIRFs before and after damage using voltage data 2

Appendix B

Force Vibration Results Using Load Cell Data

Table B.1: Summary of Results Using force vibration 'Load Cell'

Force Vibration Results Using Load Cell Data

			Before Damage						After Damage					
			7 Hz			14 Hz			7 Hz			14 Hz		
		Test	BD1	BD2	BD3	BD1	BD2	BD3	AD1	AD2	AD3	AD1	AD2	AD3
Before Damage	7 Hz	BD1	1.000	0.979	0.981	0.288	0.271	0.285	0.358	0.356	0.357	0.623	0.629	0.625
		BD2		1.000	0.994	0.294	0.280	0.282	0.368	0.364	0.367	0.624	0.627	0.628
		BD3			1.000	0.279	0.270	0.269	0.357	0.354	0.356	0.614	0.615	0.618
	14 Hz	BD1				1.000	0.971	0.967	0.137	0.135	0.137	0.472	0.474	0.481
		BD2					1.000	0.962	0.149	0.148	0.149	0.472	0.471	0.481
		BD3						1.000	0.125	0.123	0.126	0.454	0.453	0.464
After Damage	7 Hz	AD1							1.000	0.999	1.000	0.467	0.471	0.470
		AD2								1.000	0.999	0.459	0.463	0.462
		AD3									1.000	0.468	0.473	0.471
	14 Hz	AD1										1.000	0.993	0.990
		AD2											1.000	0.988
		AD3												1.000

B.1 7 Hz Before Damage

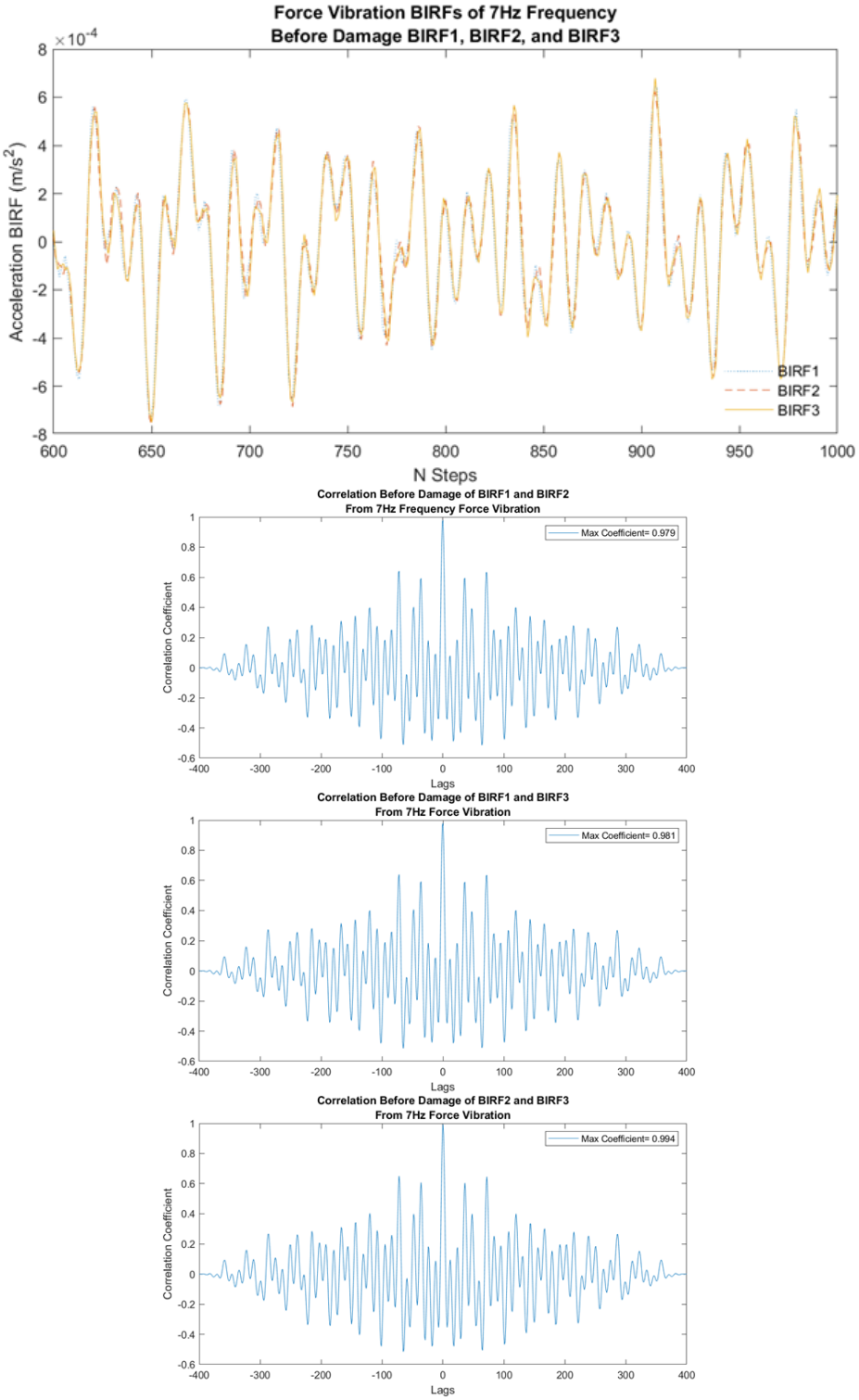

Figure B.1: 7Hz force vibration BIRFs before damage using load cell data

B.2 7 Hz After Damage

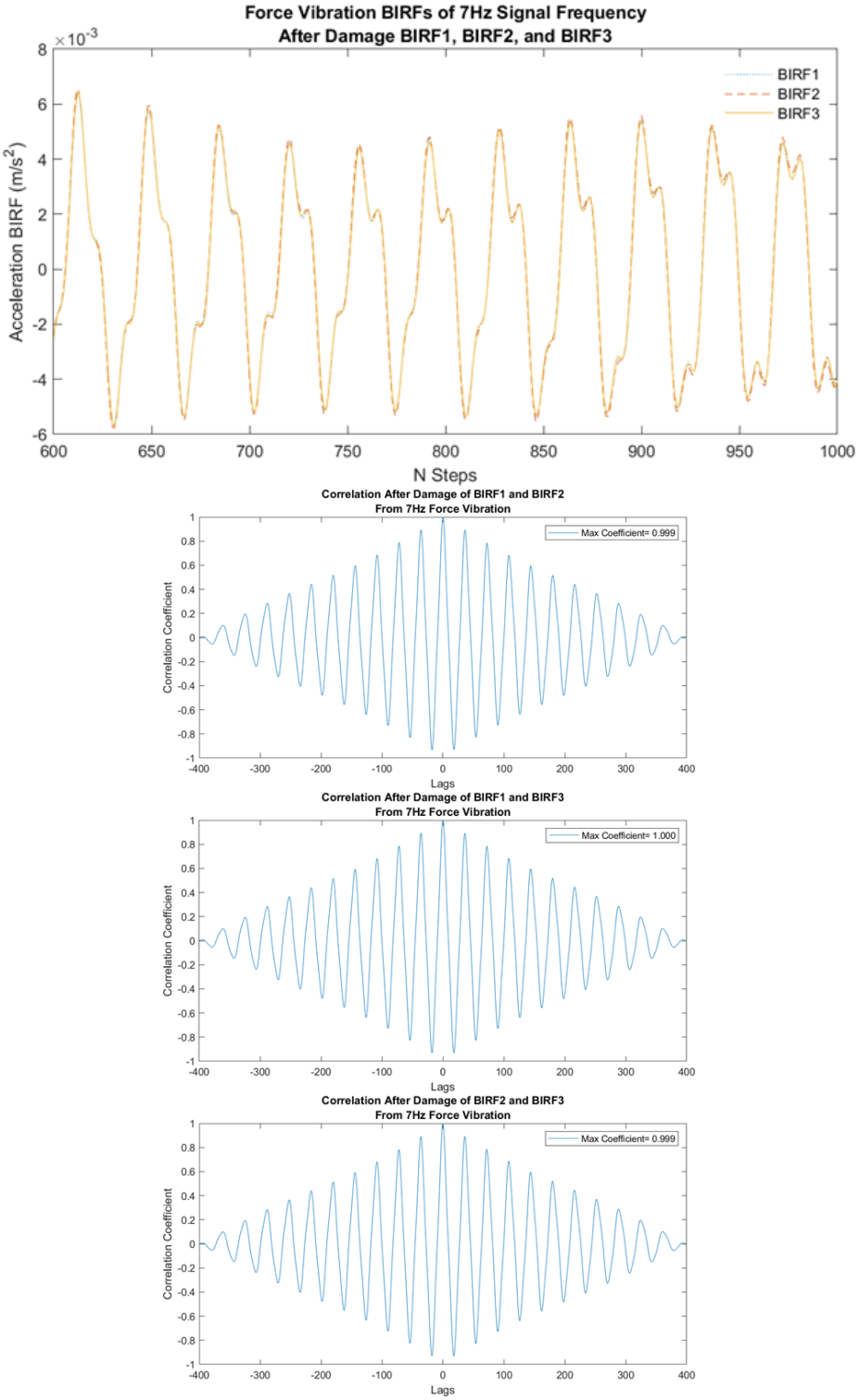

Figure B.2: 7Hz force vibration BIRFs after damage using load cell data

B.3 7 and 14 Hz Before Damage

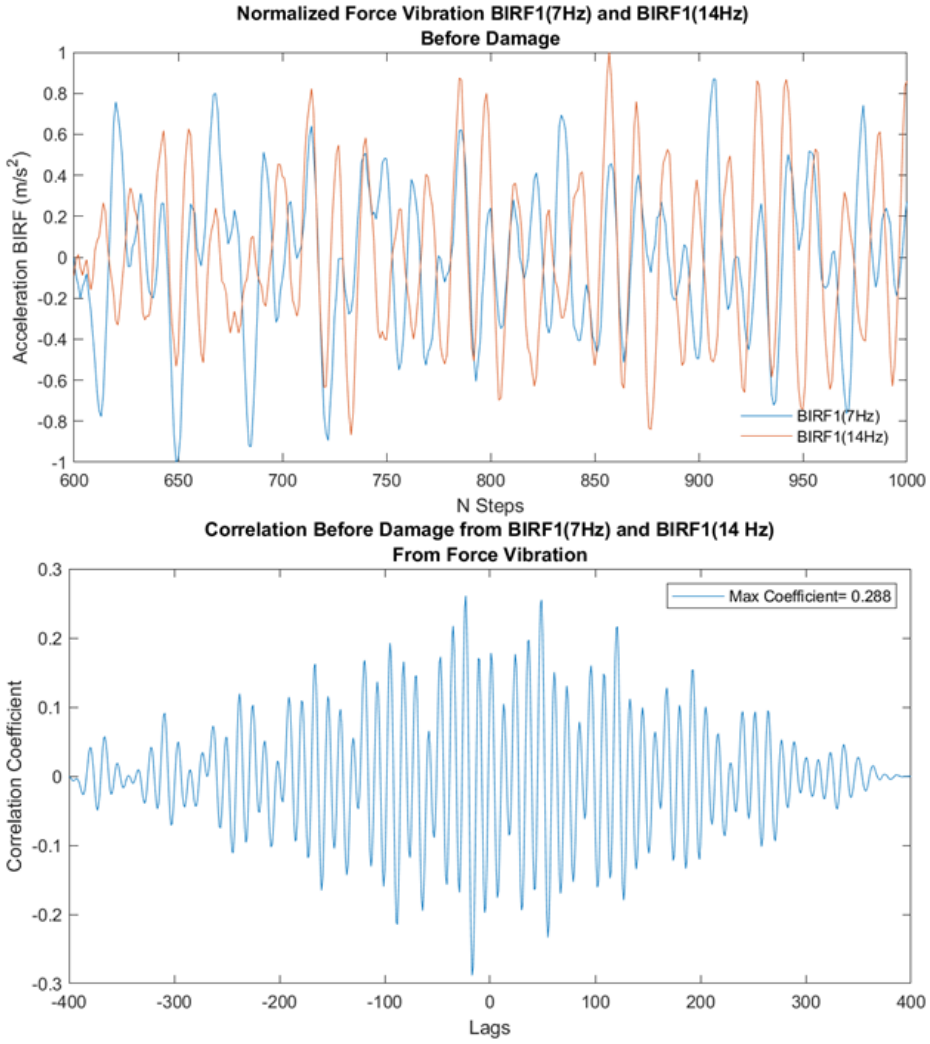

Figure B.3: 7 and 14Hz force vibration BIRFs before damage using load cell data

B.4 7 and 14 Hz After Damage

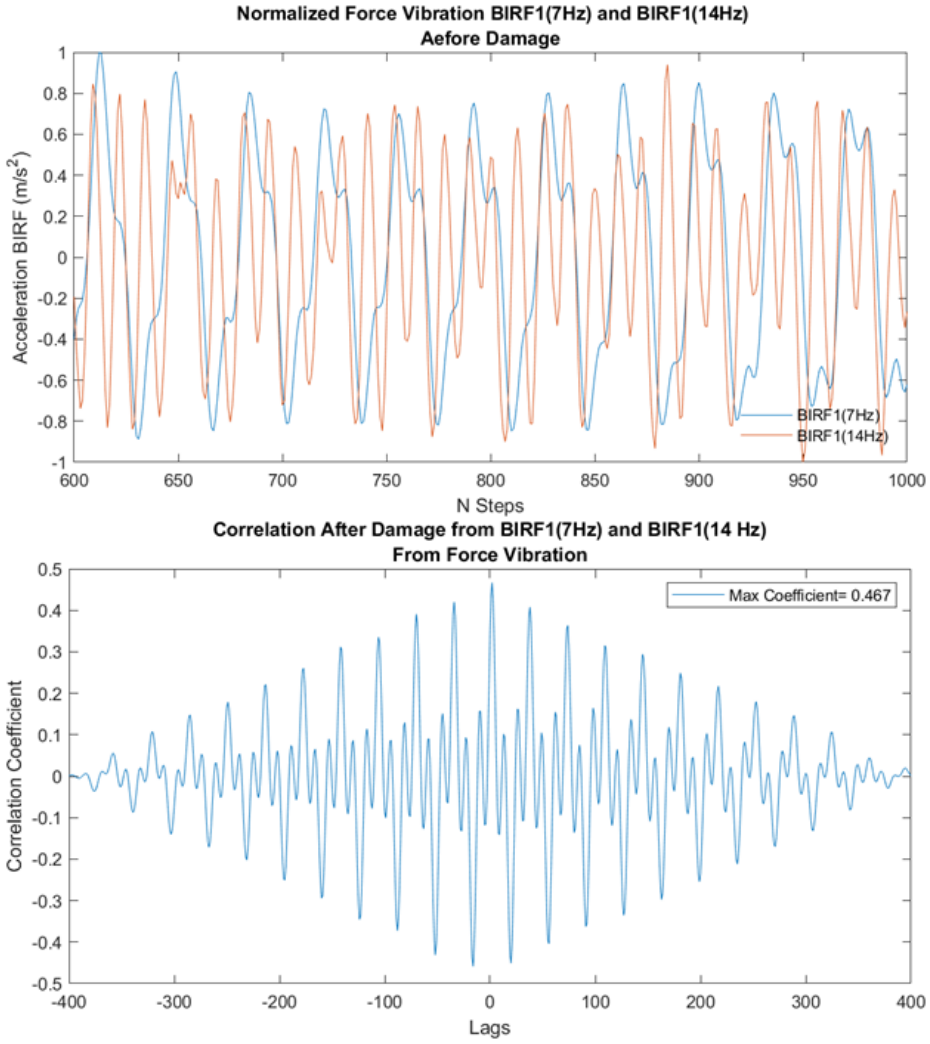

Figure B.4: 7 and 14Hz force vibration BIRFs after damage using voltage data

B.5 7Hz Before and After Damage

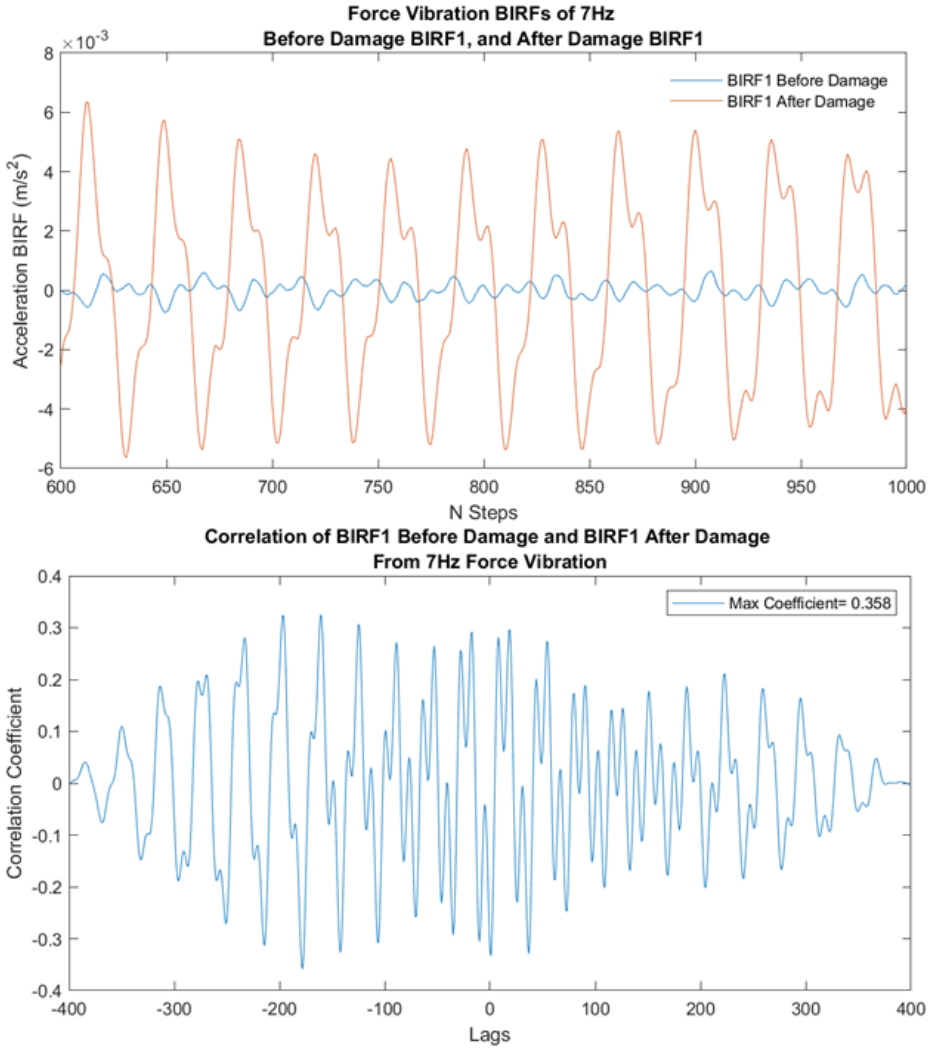

Figure B.5: 7Hz force vibration BIRFs before and after damage using load cell data

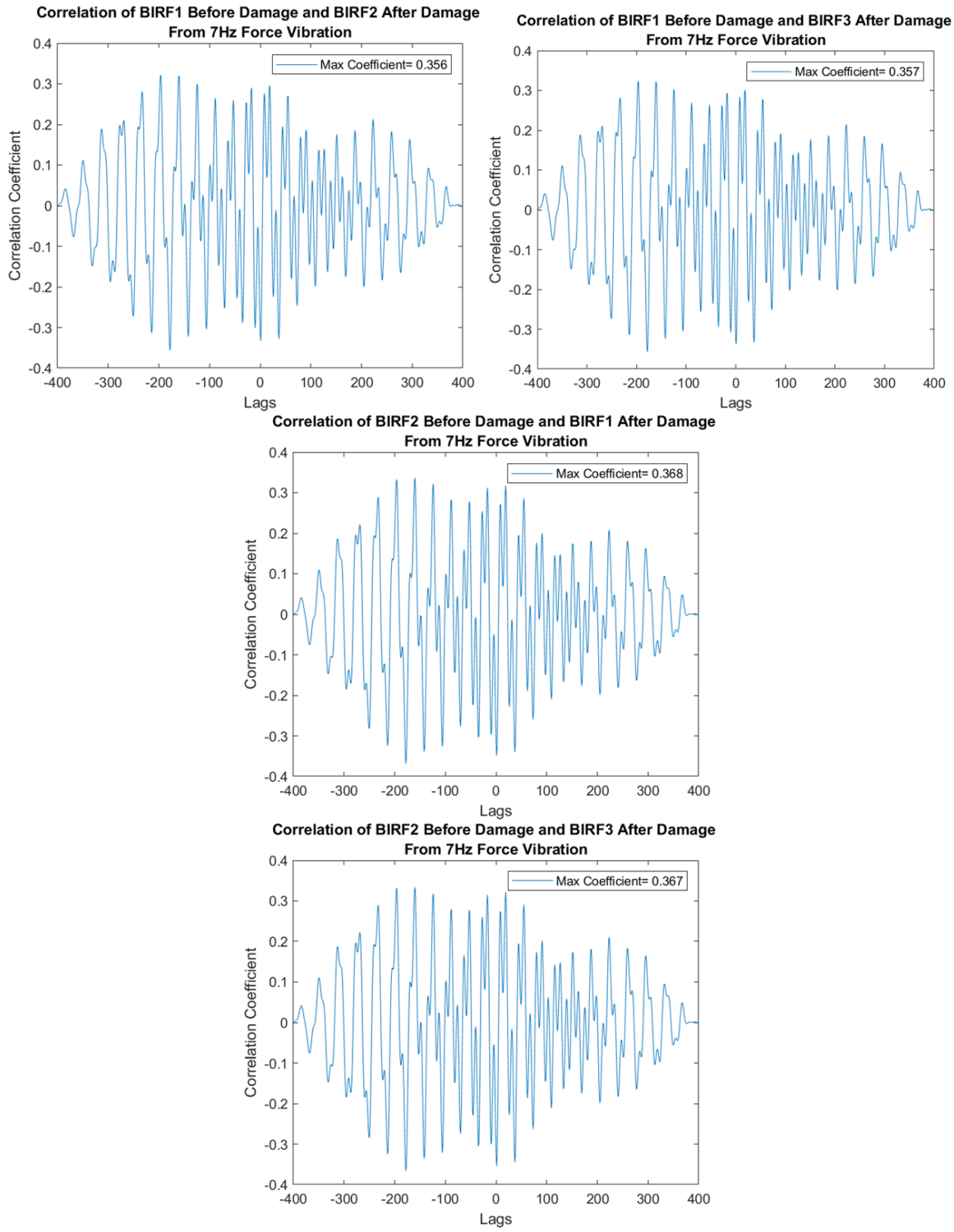

Figure B.6: Correlation values of 7Hz force vibration BIRFs before and after damage using load cell data 1

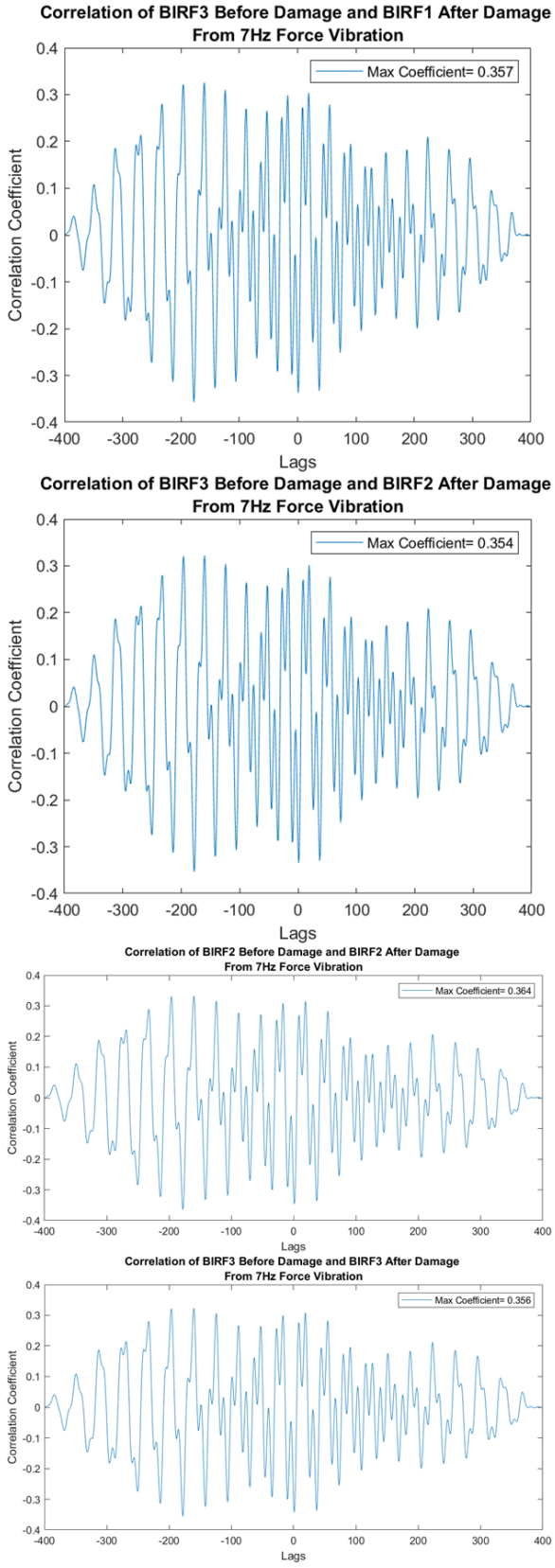

Figure B.7: Correlation values of 7Hz force vibration BIRFs before and after damage using load cell data 2

Appendix C

Free Vibration Results Using Voltage Data

Table C.1: Summary of Results Using free vibration 'Voltage'

Free Vibration Results Using Voltage Data

			Before Damage						After Damage					
			7 Hz			14 Hz			7 Hz			14 Hz		
		Test	BD1	BD2	BD3	BD1	BD2	BD3	AD1	AD2	AD3	AD1	AD2	AD3
Before Damage	7 Hz	BD1	1.000	0.992	0.991	0.893	0.894	0.892	0.087	0.075	0.086	0.063	0.063	0.053
		BD2		1.000	0.997	0.894	0.894	0.894	0.088	0.082	0.087	0.054	0.054	0.047
		BD3			1.000	0.889	0.889	0.888	0.091	0.088	0.080	0.049	0.051	0.043
	14 Hz	BD1				1.000	0.999	1.000	0.081	0.068	0.076	0.058	0.047	0.045
		BD2					1.000	1.000	0.080	0.070	0.075	0.061	0.049	0.047
		BD3						1.000	0.080	0.069	0.075	0.060	0.048	0.046
After Damage	7 Hz	AD1							1.000	0.990	0.972	0.869	0.874	0.867
		AD2								1.000	0.977	0.878	0.876	0.878
		AD3									1.000	0.871	0.876	0.875
	14 Hz	AD1										1.000	0.991	0.995
		AD2											1.000	0.993
		AD3												1.000

C.1 7 Hz Before Damage

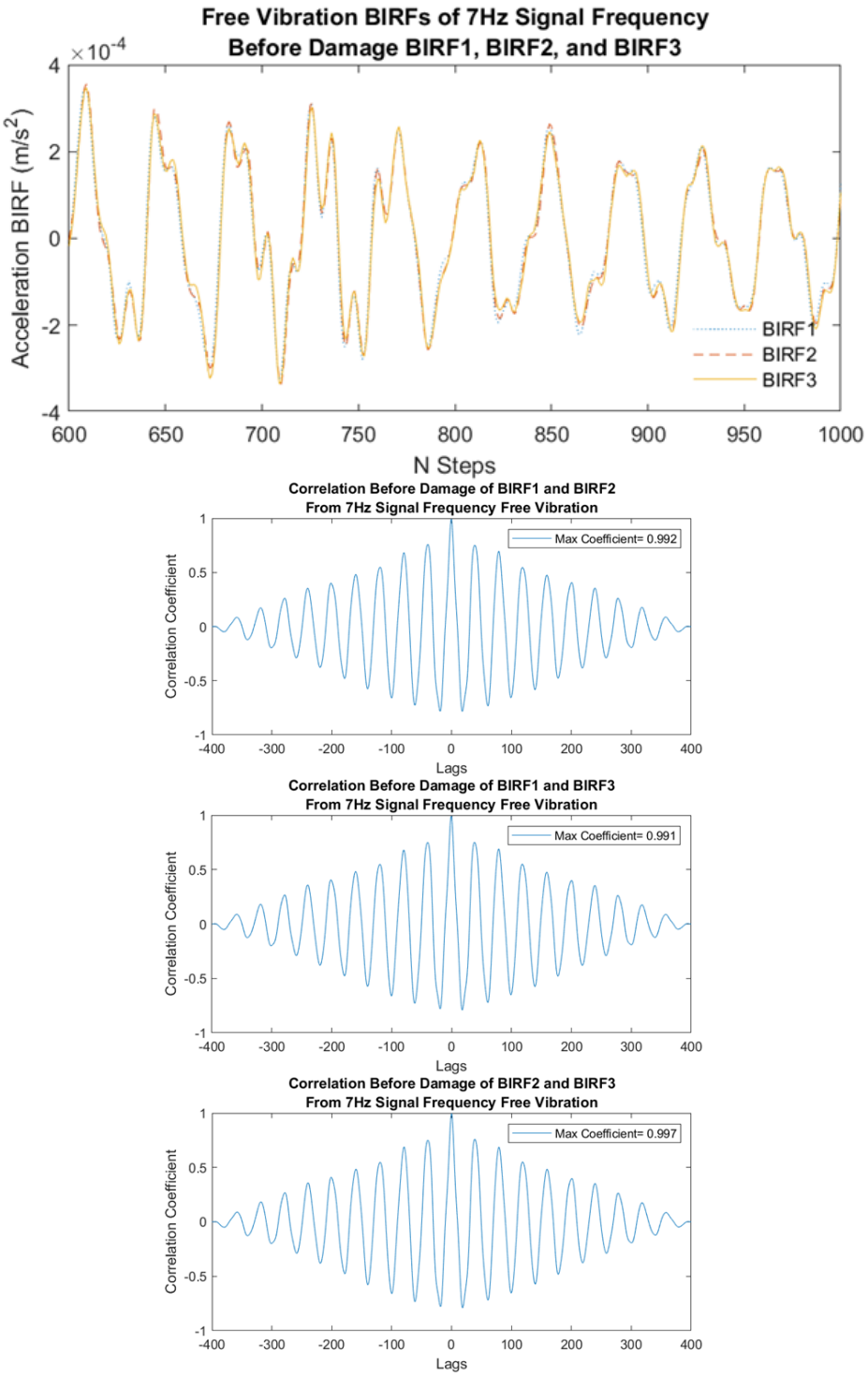

Figure C.1: 7Hz free vibration BIRFs before damage using voltage data

C.2 7 Hz After Damage

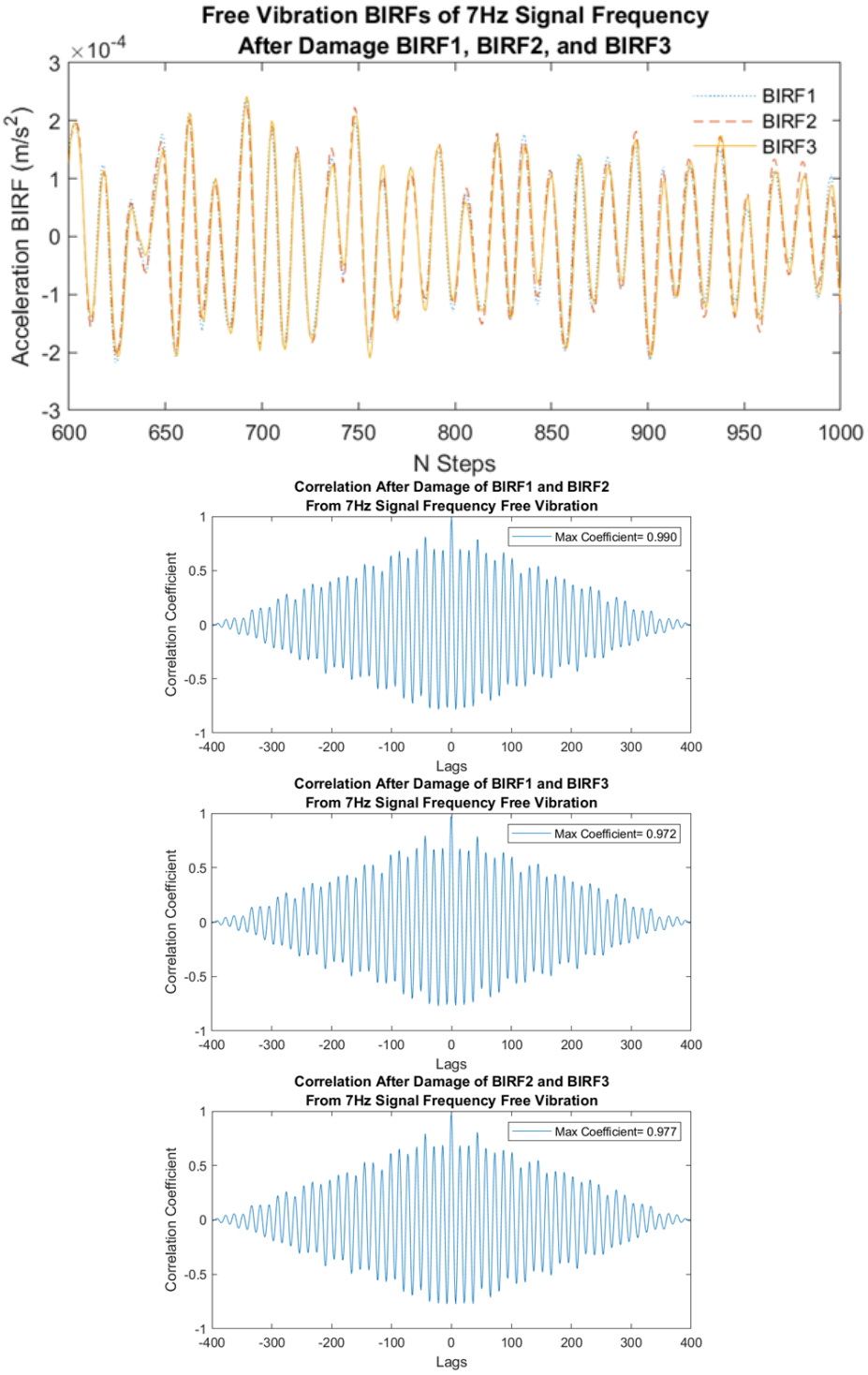

Figure C.2: 7Hz free vibration BIRFs after damage using voltage data

C.3 7 and 14 Hz Before Damage

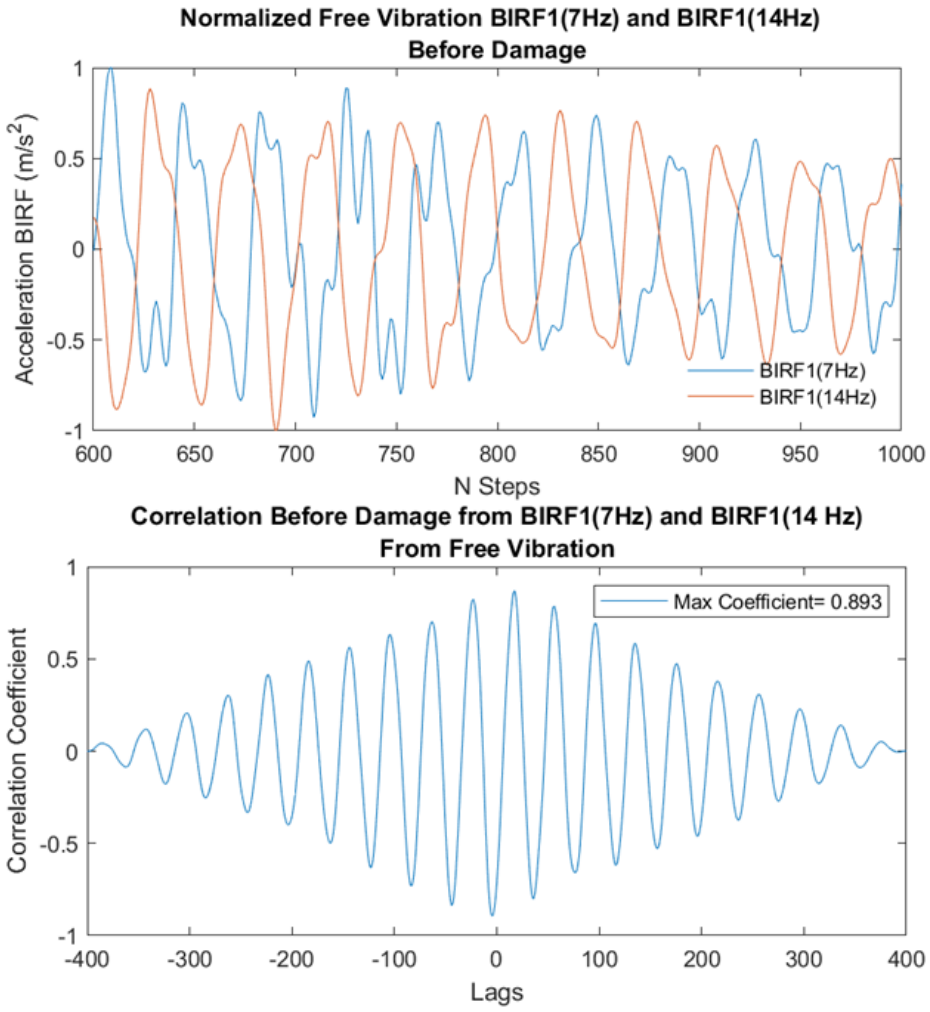

Figure C.3: 7 and 14Hz free vibration BIRFs before damage using voltage data

C.4 7 and 14 Hz After Damage

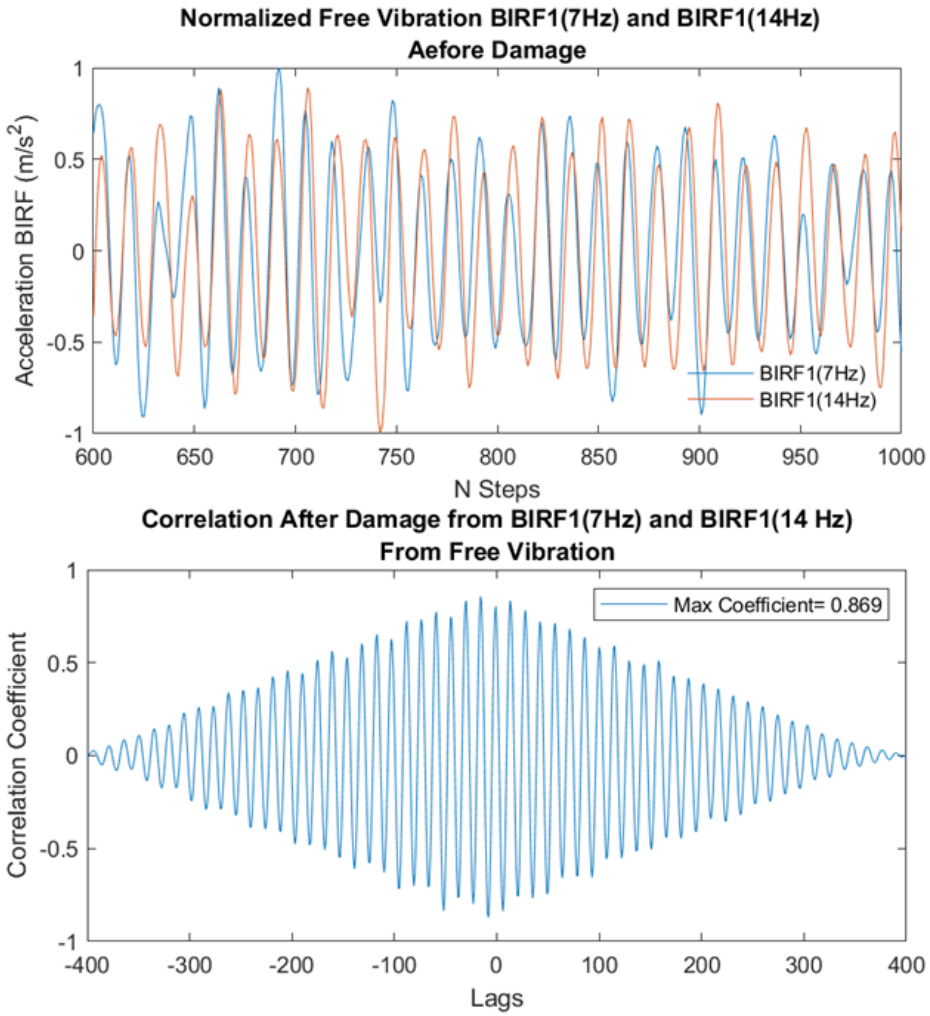

Figure C.4: 7 and 14Hz free vibration BIRFs after damage using voltage data

C.5 7 Hz Before and After Damage

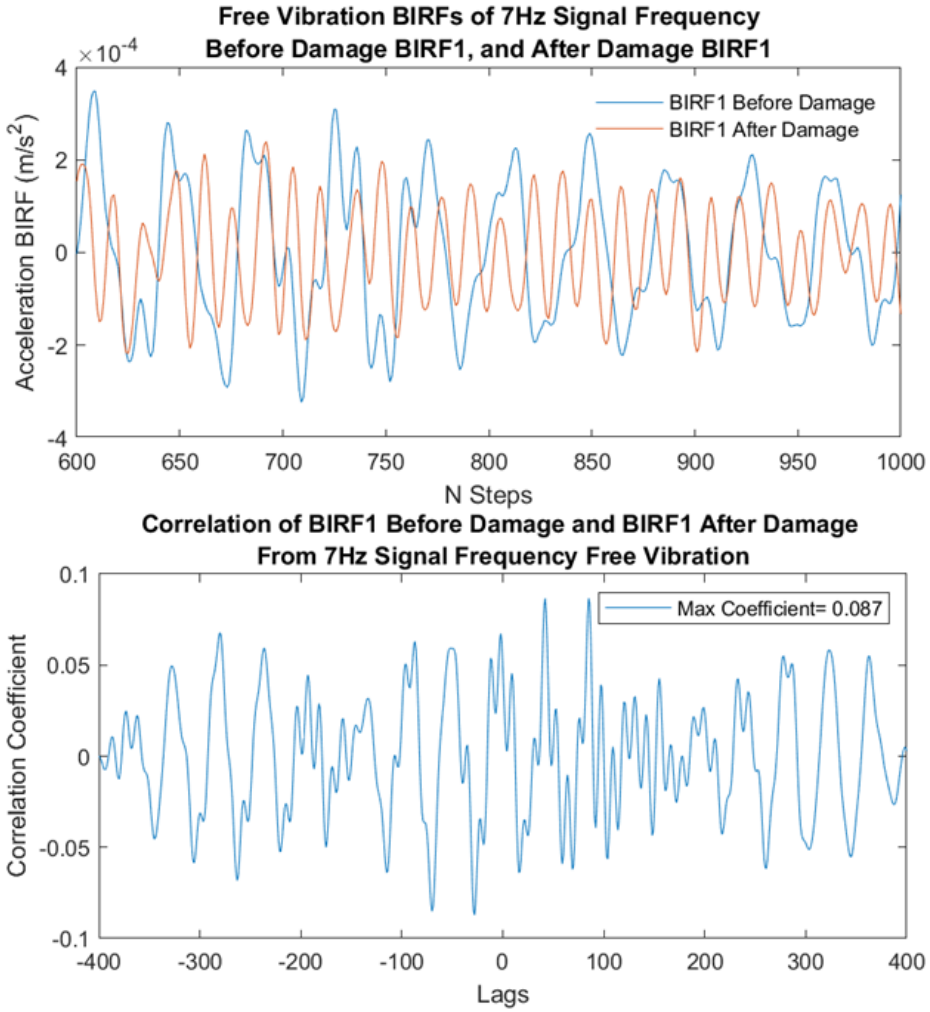

Figure C.5: 7Hz free vibration BIRFs before and after damage using voltage data

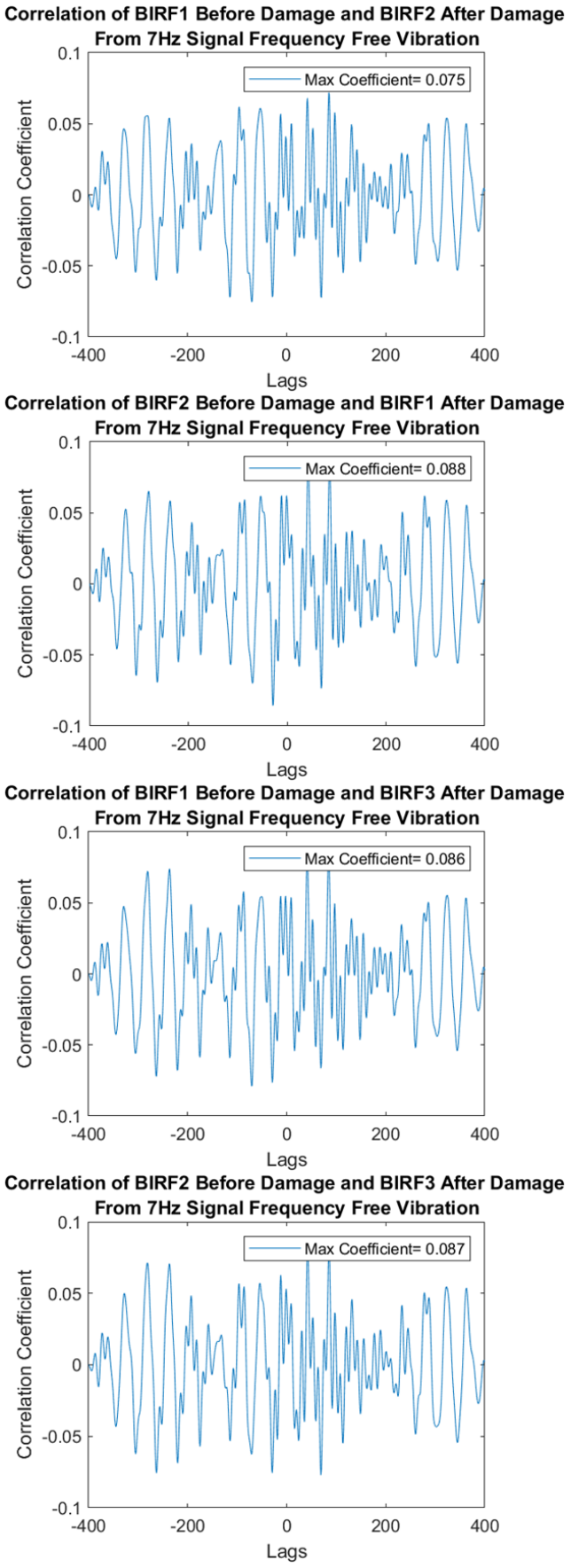

Figure C.6: Correlation values of 7Hz free vibration BIRFs before and after damage using voltage data 1

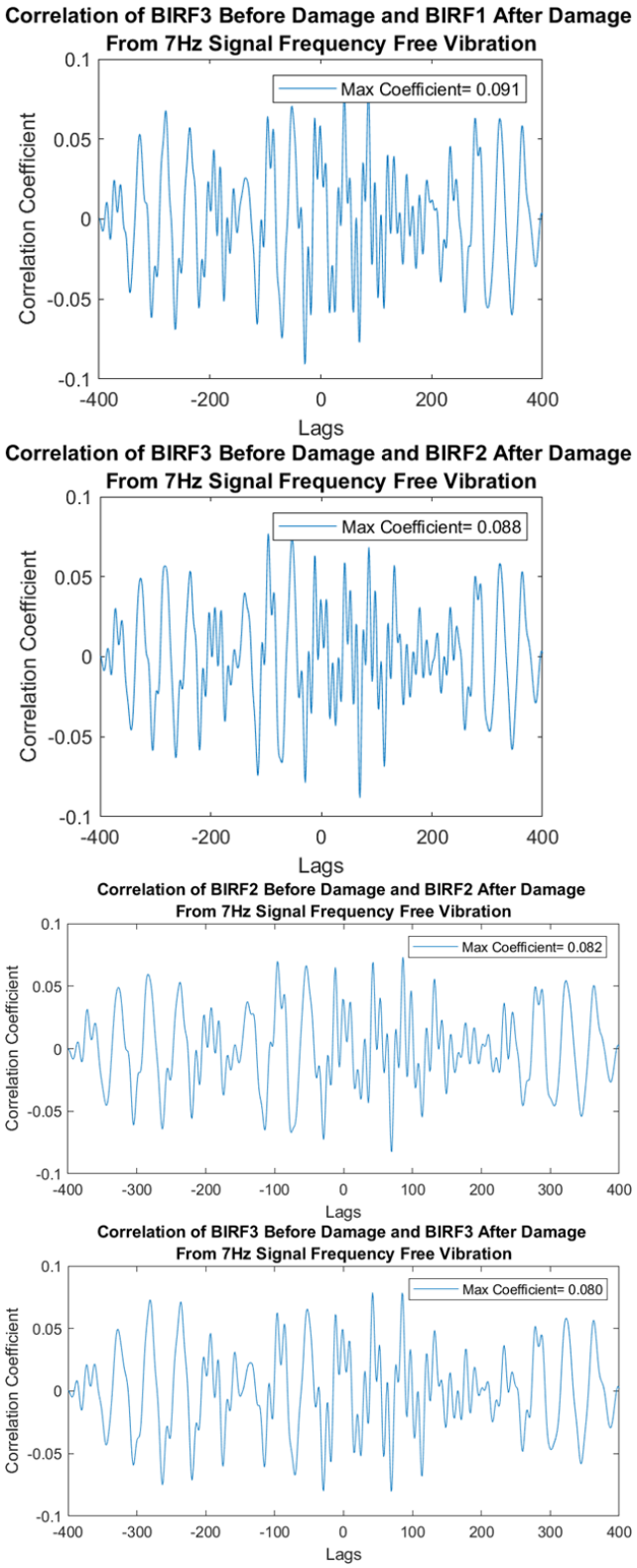

Figure C.7: Correlation values of 7Hz free vibration BIRFs before and after damage using voltage data 2

Appendix D

Free Vibration Results Using Load Cell Data

Table D.1: Summary of Results Using free vibration 'Load Cell'

Free Vibration Results Using Loadcell Data

			Before Damage						After Damage					
			7 Hz			14 Hz			7 Hz			14 Hz		
		Test	BD1	BD2	BD3	BD1	BD2	BD3	AD1	AD2	AD3	AD1	AD2	AD3
Before Damage	7 Hz	BD1	1.000	0.991	0.990	0.897	0.885	0.883	0.092	0.079	0.092	0.077	0.076	0.067
		BD2		1.000	0.996	0.902	0.886	0.885	0.093	0.085	0.094	0.067	0.065	0.057
		BD3			1.000	0.898	0.878	0.878	0.096	0.091	0.085	0.061	0.060	0.051
	14 Hz	BD1				1.000	0.939	0.940	0.070	0.065	0.067	0.053	0.055	0.050
		BD2					1.000	1.000	0.080	0.070	0.076	0.067	0.054	0.054
		BD3						1.000	0.080	0.069	0.076	0.066	0.053	0.052
After Damage	7 Hz	AD1							1.000	0.990	0.972	0.860	0.873	0.863
		AD2								1.000	0.977	0.875	0.876	0.876
		AD3									1.000	0.867	0.873	0.873
	14 Hz	AD1										1.000	0.990	0.995
		AD2											1.000	0.993
		AD3												1.000

D.1 7 Hz Before Damage

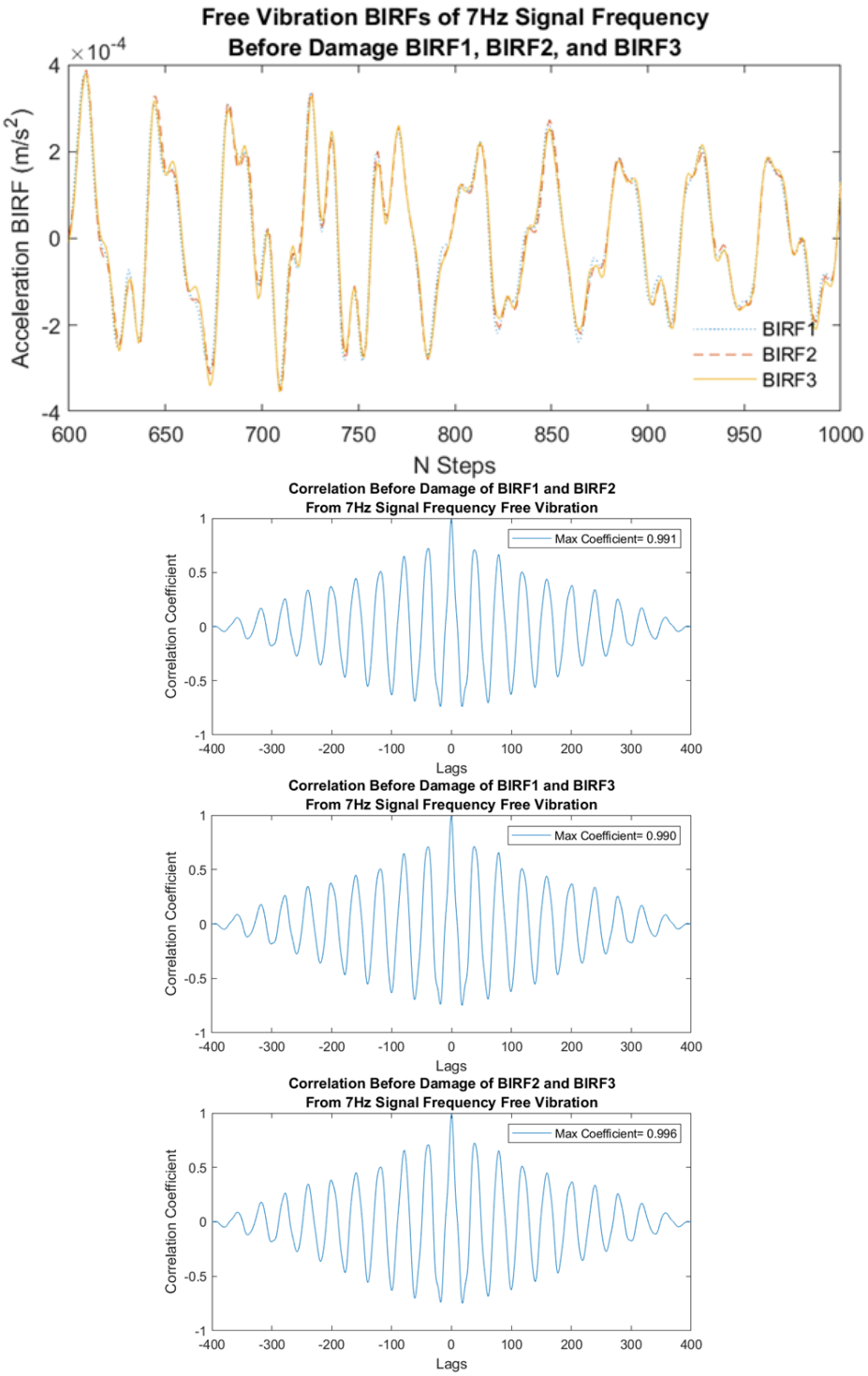

Figure D.1: 7Hz free vibration BIRFs before damage using load cell data

D.2 7 Hz After Damage

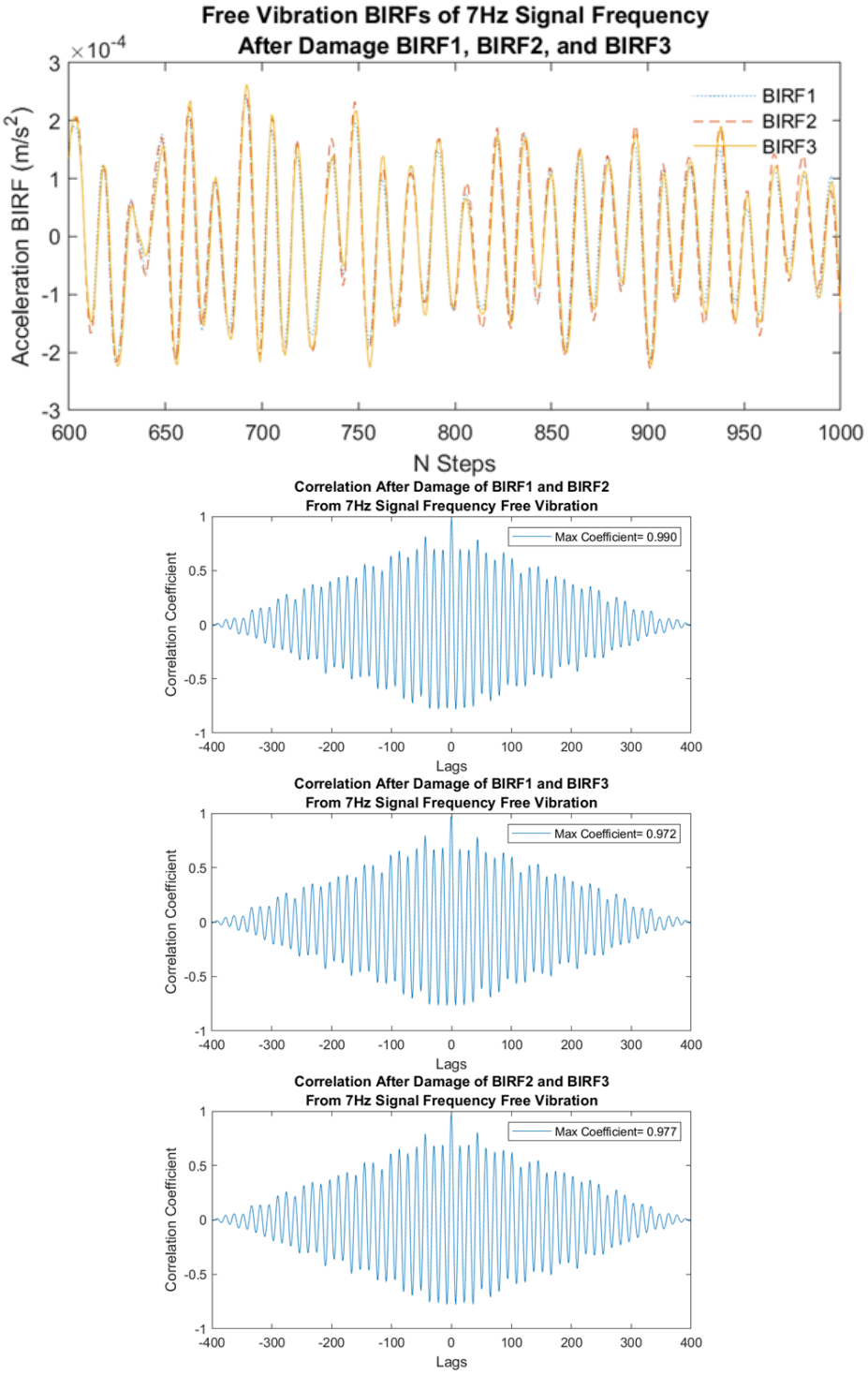

Figure D.2: 7Hz free vibration BIRFs after damage using load cell data

D.3 7 and 14 Hz Before Damage

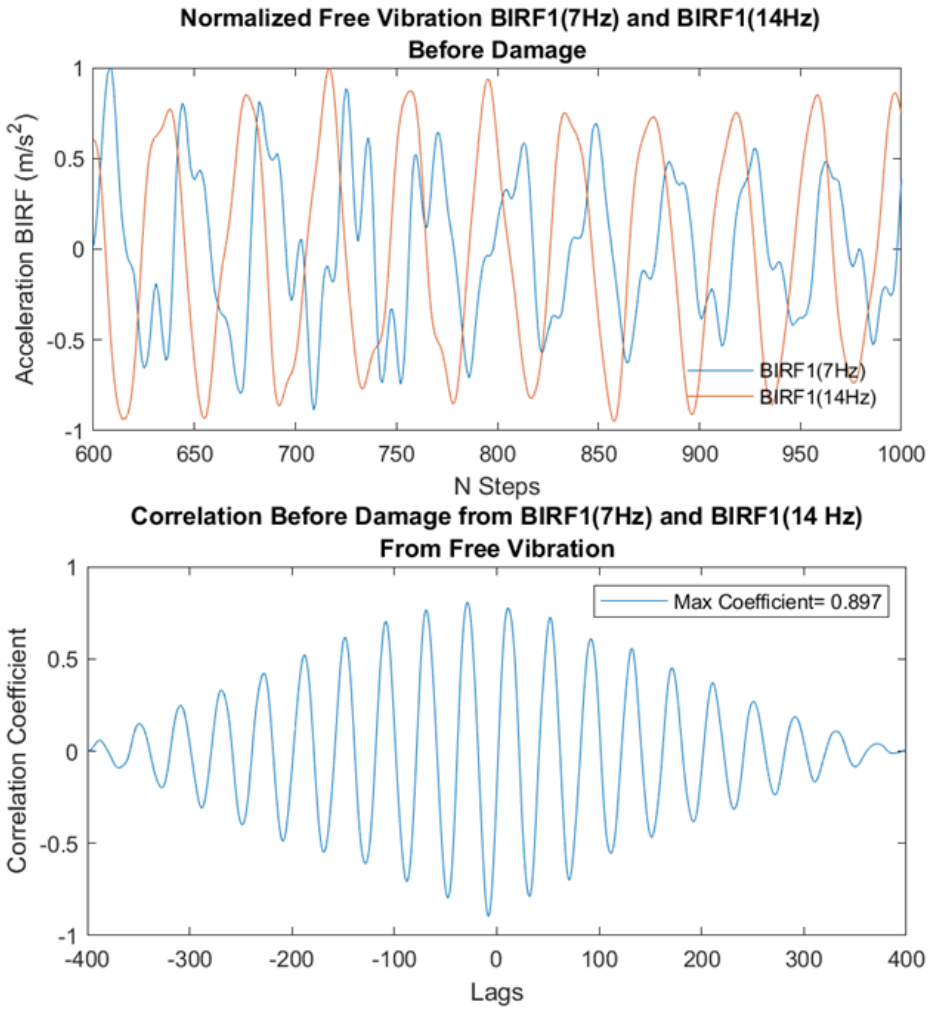

Figure D.3: 7 and 14Hz free vibration BIRFs before damage using load cell data

D.4 7 and 14 Hz After Damage

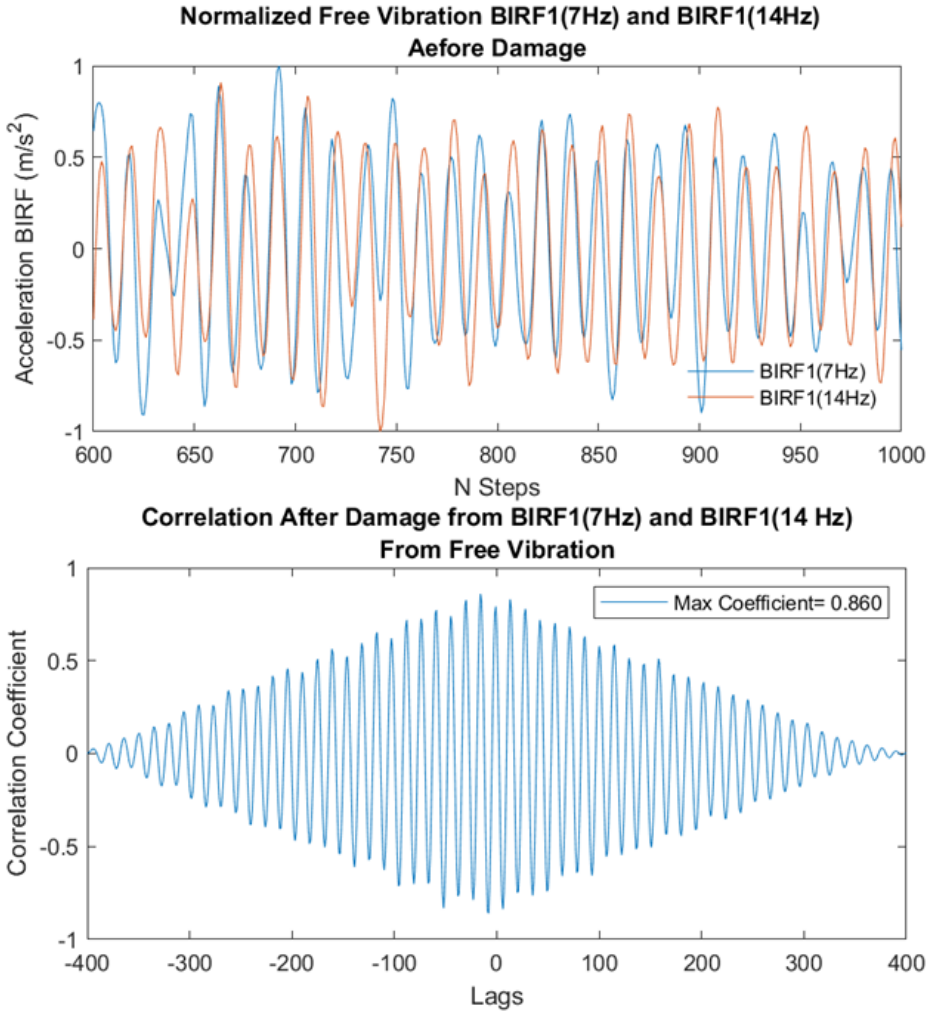

Figure D.4: 7 and 14Hz free vibration BIRFs after damage using voltage data

D.5 7Hz Before and After Damage

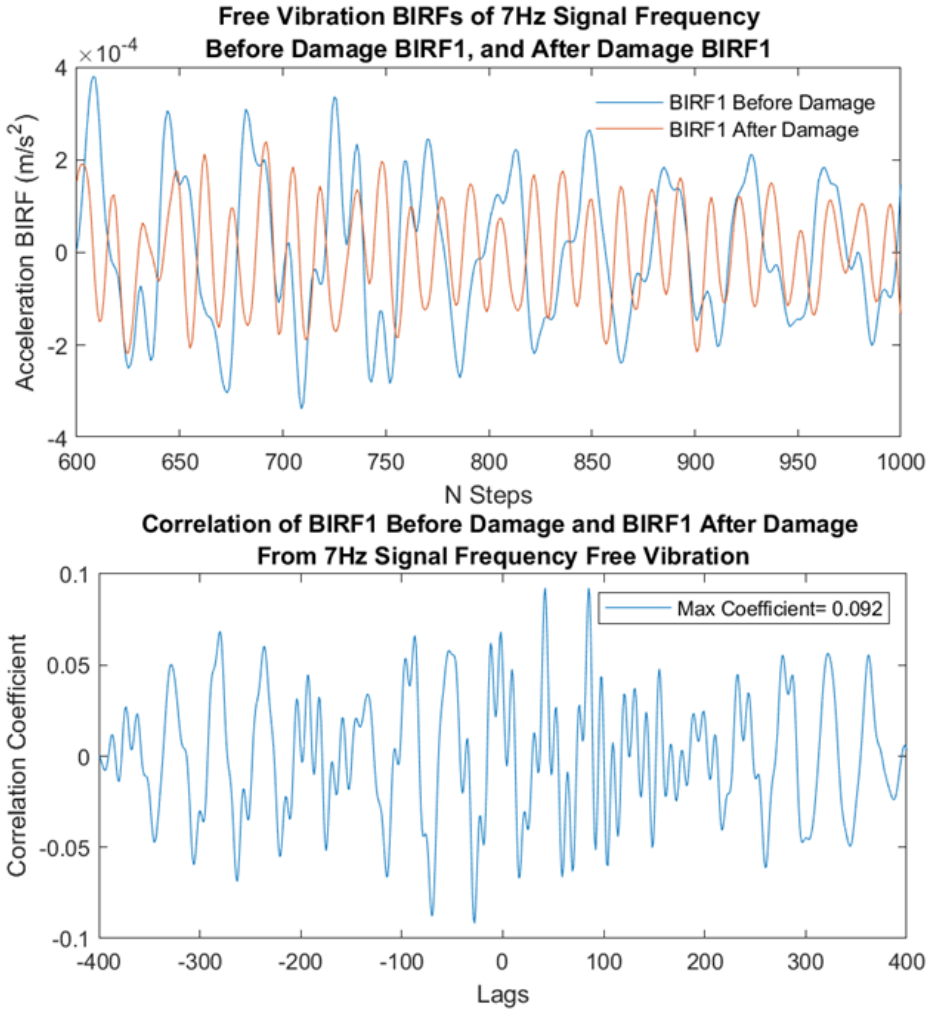

Figure D.5: 7Hz free vibration BIRFs before and after damage using load cell data

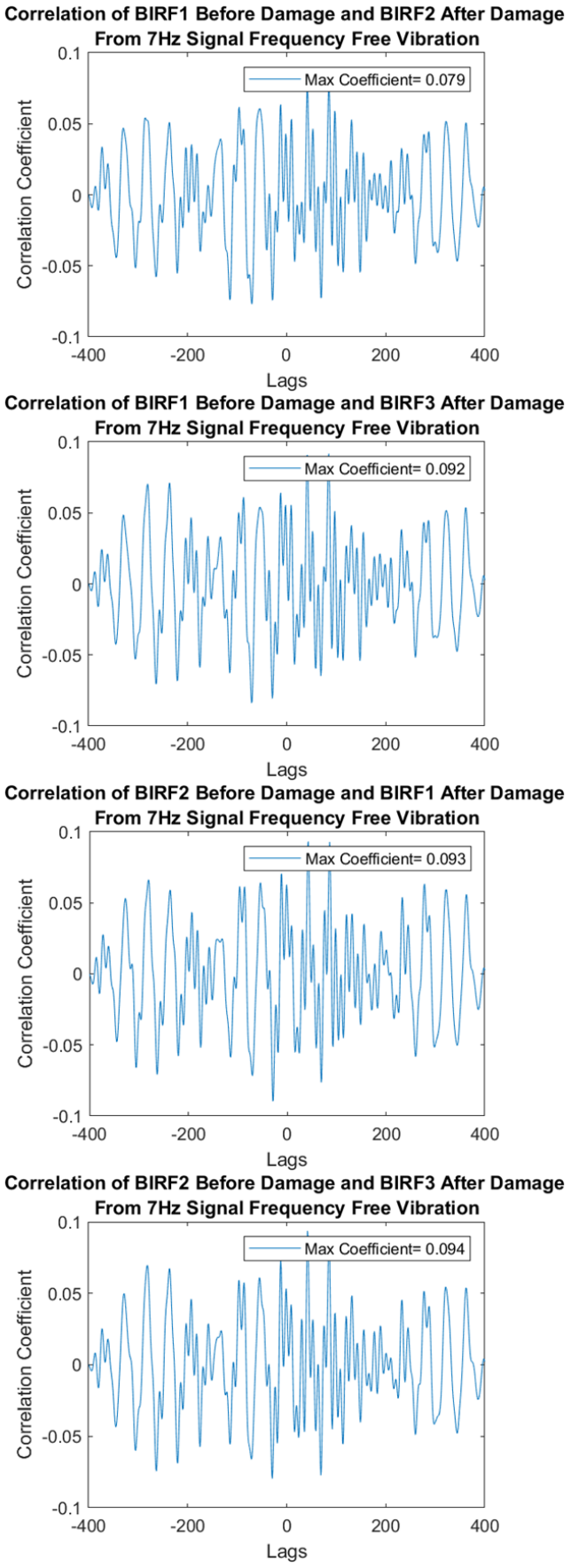

Figure D.6: Correlation values of 7Hz free vibration BIRFs before and after damage using load cell data 1

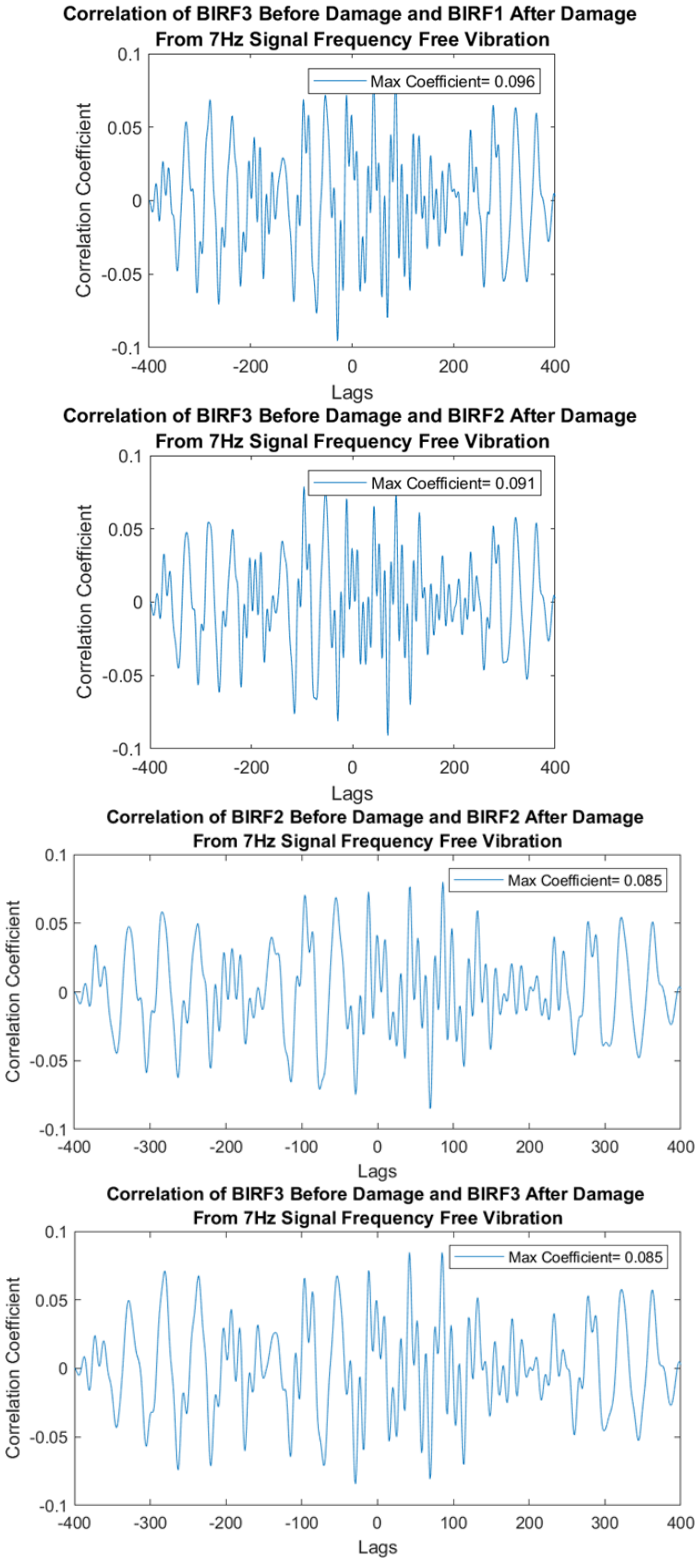

Figure D.7: Correlation values of 7Hz free vibration BIRFs before and after damage using load cell data 2